STRUCTURAL STUDIES OF PARKIN ACTIVATION

Marjan Seirafi

Department of Biochemistry
McGill University, Montreal
December 2017

A thesis submitted to McGill University in partial fulfillment of the requirements of the degree of Doctor of Philosophy

Dedication

I dedicate this work to my amazing parents, my biggest supporters of all time, and to my beloved sister and brother. Their sincere love means a lot to me; I love you so much and you are always with me even though distance keeps us apart.

I dedicate this work to my husband for encouragement and support. His advice gave me confidence on my way.

Finally, I dedicate this work to my little blessing, Liam. You have made me stronger, better and more fulfilled than I could have ever imagined.

Abstract

Parkinson's disease (PD) is the second most common neurodegenerative disease after Alzheimer's disease. It affects more than 5 million people worldwide, yet no disease modifying treatment is available for patients. In 5-10 % of the cases, PD is inherited in a typical Mendelian manner. It is through the study of the hereditary forms that we have improved our understanding of the disease.

Mutations in the *PARK2* or *PINK1* genes are the leading causes of the autosomal recessive form of PD. The gene products, the E3 ubiquitin ligase parkin and the kinase PINK1, are neuroprotective proteins, which act together in a mitochondrial quality control pathway. Parkin is a basally inactive protein in the cytosol and is activated by PINK1 on the mitochondria upon damage. PINK1 phosphorylates parkin and ubiquitin, both of which bring full parkin activation. Upon activation by PINK1, parkin attaches ubiquitin molecules to the impaired organelle and leads to their degradation by autophagy, a process termed mitophagy.

I carried out structural studies to gain insight into the mechanism of parkin autoinhibition. Crystal structures of parkin uncovered the compact rearrangement of domains, stabilized by multiple hydrophobic interactions. Biophysical studies revealed the mechanism of parkin recruitment and activation on mitochondria in a feed-forward mechanism. This model explains why parkin activity is required for mitochondrial translocation. Using nuclear magnetic resonance titrations and pull-down assays, I found that parkin binding to the brain-specific presynapse-enriched protein endophilin A1 is dependent on parkin activation and requires either phospho-ubiquitin binding or parkin phosphorylation. Parkin binding to endophilin A1 modestly inhibits parkin phosphorylation by PINK1 and attenuates parkin ubiquitin ligases activity; further work is required to identify the potential role of endophilin A1 in regulating mitophagy in neurons. In summary, these studies illustrate the mechanism of parkin autoinhibition and activation and show how parkin activity is attenuated by endophilin A1.

Résumé

La maladie de Parkinson est la deuxième maladie neurodégénérative la plus fréquente après la maladie d'Alzheimer. Elle touche plus de 5 millions de personnes dans le monde, mais aucun traitement n'est encore disponible. Dans 5 à 10% des cas, la maladie de Parkinson est héritée de façon mendélienne. C'est grâce à l'étude de ses formes héréditaires que nous avions amélioré notre compréhension de la maladie.

Les mutations dans les gènes PARK2 ou PINK1 sont les principales causes de la forme autosomique récessive du Parkinson. Les produits géniques, soit l'ubiquitine ligase E3 parkine et la kinase PINK1, sont des protéines neuroprotectrices qui agissent ensemble dans une voie de gestion de la qualité mitochondriale. Parkine est une protéine fondamentalement inactive dans le cytosol et est activée par PINK1 sur les mitochondries lorsque celles-ci subissent des dommages. PINK1 phosphoryle parkine et l'ubiquitine, menant à son activation totale, d'où celle-ci attache des molécules d'ubiquitine à l'organelle endommagée et mène à sa dégradation par l'autophagie. Ce processus se nomme la mitophagie.

J'ai effectué des études structurales pour mieux comprendre le mécanisme de l'auto-inhibition de pakine. Les structures cristallines de parkine m'ont permis de découvrir l'arrangement compact des domaines, qui d'ailleurs étaient stabilisés par plusieurs interactions hydrophobes. De plus, les études biophysiques réalisées sur la protéine révèlent un mécanisme auto-amplificateur qui permet son recrutement ainsi que son activation sur la surface des mitochondries. Ce modèle démontre pourquoi l'activité de parkine est requise pour la translocation mitochondriale. En réalisant des titrages de résonance magnétique nucléaire et des analyses déroulantes, j'ai constaté que la liaison par parkine à la protéine endophiline A1 présynaptique dépend de l'activation de parkine, et nécessite soit une liaison à la phospho-ubiquitine ou une phosphorylation par parkin. La liaison de parkin à l'endophiline A1 inhibe modiquement la phosphorylation de parkin par PINK1 et atténue l'activité de parkine. Des études supplémentaires devront être effectuées afin d'identifier le rôle potentiel de endophiline A1 dans la régulation de la mitophagie dans les neurones. Bref, ces études démontrent l'autoinhibition de parkine, son mécanisme d'activation, ainsi que comment son activité est atténuée par l'endophiline A1.

Table of Contents

List of Figures

List of Tables

List of Abbreviations

ALS - Advanced light source

ARJP - Autosomal recessive juvenile Parkinsonism

ATP - Adenosine triphosphate

BAR - Bin/amphiphysin/Rvs

CCCP - carbonyl cyanide m-chlorophenyl hydrazone

CV - Column volume

CHESS - Cornell High Energy Synchrotron Source

DTT - Dithiothreitol

DBS - Deep-brain stimulation

DRP1 - dynamin-related protein 1

DUB - deubiquitinating enzyme

Dyn2 - dynamin 2

EDTA - Ethylenediaminetetraacetic acid

EPS15 - Epidermal growth factor receptor substrate 15

FPLC - Fast protein liquid chromatography

FBS - Fetal Bovine Serum

GST - Glutathione S-transferase

GFP - Green Fluorescent Protein

GWAS - genome-wide association studies

HECT - Homologous to the E6-AP carboxyl terminus

HEPES - 4-(2-hydroxyethyl)-1-piperazineethanesulfonic acid

HOIL-1 - haem-oxidized IRP2 ubiquitin ligase 1

HOIP - HOIL-1-interacting protein

HSQC - Heteronuclear single quantum coherence

IBR - In-Between-Ring

IPTG - Isopropyl β-D-1-thiogalactopyranoside

ITC - Isothermal titration calorimetry

LC3 - Microtubule-associated protein 1A/1B-light chain 3

LB - Luria broth

PCR: Polymerase chain reaction

LRRK2 - Leucine-Rich Repeats Kinase 2

LUBAC - linear ubiquitin chain assembly complex

MDV - Mitochondria-derived vesicles

Mfn - Mitofusin

MPP - Mitochondrial Processing Peptidase

NMR - Nuclear Magnetic Resonance

OPA1 - optic atrophy protein 1

PINK1 - PTEN-induced putative kinase 1

PBS - Phosphate-buffer saline

PBS-T - Phosphate-buffer saline with Tween 20

PCR - Polymerase chain reaction

PDB - Protein Data Bank

PEG - polyethylene glygol

pParkin - phospho-parkin

pUb - phospho-ubiquitin

pUbl - phospho-Ubl

R0-RBR - RING0-RING1-IBR-RING2

RBR - RING-between-RING

REP - Repressor Element of Parkin

Rg - radius of gyration

ROS - reactive oxygen species

SAD - Single anomalous dispersion

SAXS - Small angle X-ray scattering

SDS-PAGE - Sodium dodecyl sulfate polyacrylamide gel electrophoresis

SV - synaptic vesicles

TBS - Tris-buffered saline

TCEP - tris(2-carboxyethyl)phosphine

Tris - tris(hydroxymethyl)aminomethane

TOM - Translocase of Outer Membrane

TOMM - Translocase of Outer Membrane Mammalian

Ubl - Ubiquitin-Like

UIM - ubiquitin interacting motif

UPS - Ubiquitin-proteasome system

VDAC - Voltage-Dependent Anion Selective Channel

$\Delta\psi m$ - Mitochondrial membrane potential

ZnF - Zinc finger

Preface

This is a hybrid manuscript-based thesis consisting of four published articles:

Chapter 1 and some parts in chapter 3, 4, and 6

Seirafi M, Kozlov G, Gehring K. Parkin structure and function. *FEBS J*. 2015 Jun;282(11):2076-88 (mini-review paper).

Chapter 3

Trempe JF*, Sauvé V*, Grenier K, **Seirafi M**, Tang MY, Menade M, Al-Abdul-Wahid S, Krett J, Wong K, Kozlov G, Nagar B, Fon EA, Gehring K. Structure of parkin reveals mechanisms for ubiquitin ligase activation. *Science*. 2013 Jun 21;340:1451–1455.

Chapter 4

Sauvé V*, Lilov A*, **Seirafi M***, Vranas M, Rasool S, Kozlov G, Sprules T, Wang J, Trempe J, Gehring K. A Ubl/ubiquitin switch in the activation of Parkin. *EMBO J*. 2015 Oct 14;34(20):2492–2505.

Chapter 5

Seirafi M, Kozlov G, Trempe JF, Gehring K. Endophilin A attenuates parkin activation by PINK1 (under review).

* Contributed equally to the manuscript

Author contributions

Dr. Kalle Gehring supervised the projects, and participated in manuscript preparations.

[1] **Seirafi M**, Kozlov G, Gehring K. Parkin structure and function. *FEBS J*. 2015 Jun;282(11):2076-88):

- **Marjan Seirafi** wrote the manuscript.
- Guennadi Kozlov and Kalle Gehring provided guidance and edited the manuscript.

[2] Trempe JF*, Sauvé V*, Grenier K, **Seirafi M**, Tang MY, Menade M, Al-Abdul-Wahid S, Krett J, Wong K, Kozlov G, Nagar B, Fon EA, Gehring K. Structure of parkin reveals mechanisms for ubiquitin ligase activation. *Science*. 2013 Jun 21;340:1451–1455:

- Jean-François Trempe performed molecular cloning, ubiquitination assays, SAXS data processing, assisted R0-RBR structure determination and wrote the manuscript.
- Véronique Sauvé performed protein purification, SAXS data acquisition and R0-RBR crystal structure determination.
- Karl Grenier performed the PINK1-dependent GFP-parkin recruitment assay and data analysis.
- **Marjan Seirafi** purified parkin, and crystallized full-length parkin and performed NMR titrations and ITC assay.
- Mathew Tang performed the GFP-parkin recruitment assay with time-lapse fluorescent microscopy and data analysis.
- Marie Ménade performed protein purification, crystallization trials and SAXS data acquisition.
- Sameer Al-Abdul-Wahid performed NMR titrations and data processing.
- Jonathan Krett cloned the GFP-parkin mutants.
- Kathy Wang produced proteins and acquired SAXS data.
- Guennadi Kozlov collected crystallographic data at CHESS, and assisted structure determination of full-length parkin
- Bhushan Nagar assisted structure determination of full-length parkin

- Edward A. Fon supervised Karl Grenier, Mathew Y Tang and Jonathan Krett, and edited the manuscript.

[3] Sauvé V*, Lilov A*, **Seirafi M***, Vranas M, Rasool S, Kozlov G, Sprules T, Wang J, Trempe J, Gehring K. A Ubl/ubiquitin switch in the activation of Parkin. *EMBO J.* 2015 Oct 14;34(20):2492–2505:

- Véronique Sauvé designed constructs of parkin deletion mutants, performed protein purification, pull-down assays, ITC assays and ITC data analysis.
- Asparouh Lilov performed protein purifications, Δ86–130 parkin crystallization and data collection, SAXS data acquisition, and ITC assays.
- **Marjan Seirafi** performed site-targeted mutagenesis, protein purification, protein phosphorylation, and preparation of SAXS samples, ITC assays and NMR experiments.
- Jean-François Trempe did crystal structure refinement, and SAXS data analysis.
- Jimin Wang did X-ray data processing and phasing.
- Martha Vranas performed the ubiquitination assay.
- Shafqat Rasool performed the kinase assays.
- Tara Sprules helped with NMR titrations and analysis.
- Guennadi Kozlov purified ^{15}N-labled Ubl domain of parkin and helped with NMR titrations.

[4] **Seirafi M**, Kozlov G, Trempe JF, Gehring K. Endophilin A attenuates parkin activation by PINK1 (under review).

- **Marjan Seirafi** designed experiments and performed the work in the manuscript.
- Guennadi Kozlov edited the manuscript.
- Jean-François Trempe edited the manuscript and designed experiments

Acknowledgements

First, I would like to express my deepest gratitude to my supervisor Dr. Kalle Gehring for accepting me in his laboratory, for the opportunity to work on such an outstanding project, and for support and advice during my research.

I am thankful to Dr. Guennadi Kozlov for always being available for questions and advice and for making this work possible. He patiently read all my papers and my thesis and provided helpful comments. Everything I learned from him throughout the course of my PhD is something I can never forget. He is not only the best mentor but also an amazing friend with whom I laughed a lot.

I am grateful to Dr. Marie Ménade and Dr. Véronique Sauvé for the guidance they provided me with laboratory training and help with various laboratory techniques.

I would like to take this opportunity to thank Dr. Jean-François Trempe, who contributed greatly to this project by performing experiments, X-ray data deposition in the Protein Data, and valuable advice.

I am thankful to my research advisory committee members, Dr. Bhushan Nagar and Dr. Edward A. Fon, for the valuable advice they offered during my PhD. Dr. Nagar also helped me with phasing of the parkin crytal structure and Dr. Edward A. Fon accepted me in his lab for 3 months (part of my Bionanomachines scholarship program).

I am deeply grateful to all my colleagues at the lab, Dr. Jingwei Xie, Dr. Juliana Munoz, Sara Bastos, Kathy Wong, Irina Gulerez, and Seby (Yu) Chen. They create such a very friendly and supportive environment. You all made these years the most joyful years ever.

I would like to take this opportunity to acknowledge my dearest friend Yogita Patel. Thank you for laughing with me, encouraging me, and always being there for me.

I am truly thankful to all my collaborators Karl Grenier, Mathieu Y. Tang, Sameer Al-Abdul-Wahid, Jonhathan Krett, Marta Macedo Vranas, Shafqat Rasool, Tara Sprules, for their contributions to the publications.

I am grateful to Dr. Kalle Gehring, CIHR grant, FRSQ, the CREATE Training Program in Bionanomachines, GRASP, the Department of Biochemistry, and McGill University for funding during my PhD studies.

Lastly, I would like to thank my family, for allowing me to realize my own potential. All the support they have provided me over the years was the greatest gift anyone has ever given me. I am thankful for the love, support, and constant encouragement I have gotten over the years. Without you none of this would have been possible and I would never have gotten to where I am today.

Chapter 1: General Introduction

1.1 Opening statement

My goal as a structural biology student was to study the structure of parkin protein at the molecular level. Parkin is a protein encoded by *Parkin (PARK2)* gene, the most frequently mutated gene in the genetic early-onset form of Parkinson's disease (PD). Parkin has neuroprotective roles via different pathways including the clearance of damaged mitochondria by autophagy, a process termed mitophagy. Impaired mitophagy seems to be a critical issue in the pathogenesis of neuronal dysfunction and the aggregation of misfolded proteins, which in turn impairs mitochondrial homeostasis in patients with mutations in the *Parkin* gene. Stimulating mitophagy to maintain mitochondrial health by activating parkin, therefore, is thought to be a helpful approach to delay the neurodegenerative processes in PD.

Further understanding of parkin structure and function will undoubtedly provide new insights into the pathogenic mechanisms of PD and may lead to prevention and better treatment of the disorder. Thus, we decided to do structural studies on the parkin protein.

In this chapter, PD is first described to illustrate the importance of parkin as a possible therapeutic target enzyme to cure PD patients. Then, the current knowledge of parkin is summarized and the information on parkin activation in mitophagy is provided. Endophilin A1 protein is then introduced. The gene encoding this protein has recently reported as a PD risk factor and the encoded protein has been reported to interact with parkin. We believe this interaction can affect mitophagy pathway in presynaptic terminals. Finally, this chapter ends with an overview of the following chapters.

1.2 Parkinson's disease (PD)

Parkinson's disease (PD) is a movement disorder that mainly affects the motor system. It is progressive, meaning that symptoms continue and worsen over time. There is no cure for PD and the average life expectancy after diagnosis is between 7 and 14 years [1].

PD affects about 1-2% of people over 65 years, and 5% of people over 80 in all countries and races [2, 3]. PD patients suffer from a variety of motor and non-motor symptoms that vary from one patient to another. The most typical motor symptoms include resting tremor, rigidity,

bradykinesia and postural instability while non-motor symptoms can include mood disorders such as depression, anxiety and irritability [4].

Most of PD cases are idiopathic (also named sporadic) with unknown causes. The idiopathic form is thought to be caused by a combination of environmental and genetic factors. However, in 5-10% of patients, PD can be can be inherited in a pure Mendelian fashion [2, 3].

PD pathology is thought to be caused by degeneration of the dopamine producing neurons in the substantia nigra pars compacta (SNpc) of the midbrain (Fig 1.1A) that leads to low levels of dopamine, a neurotransmitter, in the brain. The other hallmark of PD is the presence of proteinaceous aggregates in the surviving neurons called Lewy bodies (Fig 1.1B) [5]. Lewy bodies are largely made up of aggregated α-synuclein and ubiquitin. These inclusion bodies seem to be a common marker of neurodegeneration as they are found in other neurodegenerative diseases [6]. The Lewy bodies are initially formed in cholinergic and monoaminergic brainstem neurons and in neurons in the olfactory system, but are advancing to the neocortex regions with disease progression [7].

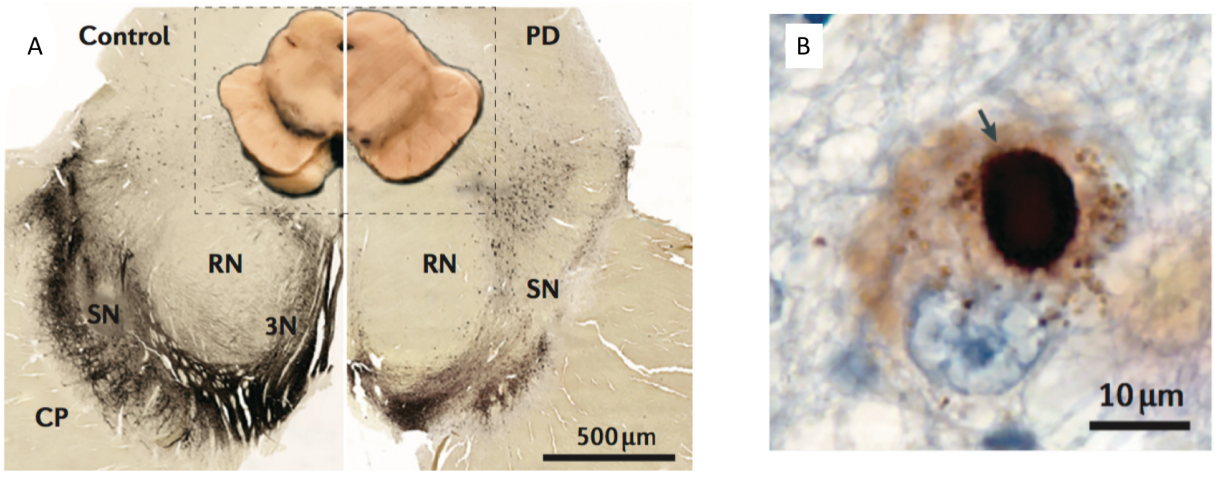

Figure 1.1 Neuropathological hallmarks of PD. (A) The loss of dopaminergic neurons in the substantia nigra pars compacta in PD patients compared to control (a healthy individual). Dopaminergic neurons appear black (left panel) due to the presence of neuromelanin pigments. This pigmentation is lost in PD patient upon dopaminergic neuronal demise (right panel). Macroscopical and transverse sections of the midbrain upon immunohistochemical staining for tyrosine hydroxylase, the rate limiting enzyme for the synthesis of dopamine, are shown. (B) Immuno-histochemical staining of α-synuclein in a dopaminergic neuron presenting the round, intra-cytoplasmic Lewy bodies [8]. Images were modified from Poewe *et al.*, 2017 [9].

1.3 History of PD

PD has existed since ancient times. This condition was first named as "shaking palsy" in Western medical literature by the physician, Galen, in AD 175. However, it was not until 1817 that detailed PD causes and symptoms were first medically described by British apothecary James Parkinson in a 66-page document entitled “An essay on the shaking palsy” [10]. His studies helped to make the disease a recognizable medical condition. However, it was not widely acknowledged at the time. He wrote about PD: " Involuntary tremolous motion, with lessened muscular power, in parts not in action and even when supported; with a propensity to bend the trunk forwards, and to pass from a walking to a running pace: the senses and intellect being uninjured." [10]

The term "Parkinson's disease" was attached to the disease in 1865 by William Sanders and later popularized by French neurologist, Jean Martin Charcot [11]. Charcot differentiated PD from other neurological diseases and detailed the symptoms. He was also the first who noticed the bradykinesia symptom of the disease. In 1895, French neurologist Brissaud suggested that the substantia nigra was the most affected brain region in PD [12]. In 1912, Fredrick Lewy described the presence of large cytoplasmic proteinacious inclusions in brains of patients who had died with the disease [13]. These inclusions were later named after him "Lewy bodies" [14]. Preferential locations of these inclusion bodies were regions most affected in Parkinson's including within surviving dopaminergic neurons of the substantia nigra, while their morphology was distinct from other inclusions found in other neurological disease. In the 1990’s it was discovered that Lewy bodies consist mainly of alpha-synuclein, a presynaptic protein that was later found to be mutated in familial PD, and ubiquitin, a critical modifier that tags proteins for degradation. Whether Lewy bodies are harmful to dopaminergic neurons or are a protective response remains controversial [15]. However, the finding of ubiquitin in Lewy bodies provided evidence for altered ubiquitin signaling and disrupted protein quality control in PD.

In 1957, Arvid Carlson demonstrated the presence of high level of dopamine in the striatum. He positioned dopamine as a neurotransmitter in the brain responsible for smooth, purposeful movement and established a link between dopamine and motor disorders [16]. For his successful discoveries, Carlson was awarded the Nobel prize in 2000. Dopamine levels have been found to be markedly diminished in PD patients by Oleh Hornykiewicz in 1960. He also

showed that the symptoms of Parkinsonism relate to the degree of loss of striatal dopamine [17-19]. Later, in the same year, L-dopa (levodopa) was administered to treat PD symptoms by Barbeau, Cotzias and Sourkes [20, 21]. L-dopa is a dopamine precursor capable of crossing the blood-brain barrier. L-dopa gets converted into dopamine in the substantia nigra later by dopa decarboxylase [22]. Most PD medications, still to this date, are revolved around increasing dopamine level in the brain to reverse the loss of dopamine, which occurs in early stages of the disease. Although dopamine-therapy alleviates PD symptoms for some time in the early stages of the disease, it has serious side effects including nausea, dyskinesias and joint stiffness, and is not effective in the later stages [23]. Dopamine antagonists and monoamine-oxydase B inhibitors are alternative options in the later stages or can be used in the early stages to delay the use of L-dopa [24]. Monoamine-oxydase B is an enzyme in human that degrades extracellular dopamine in basal ganglia and its inhibition increases the level of dopamine in synaptic clefts [25].

Deep-brain stimulation (DBS) surgery is another option in the later stages [26]. In this technique, a battery-powered medical device is implanted inside the brain that can electrically stimulate brain areas while sending electrical impulses through implanted electrodes [27]. While DBS has proven to diminish dyskinesia, and improve the lives of PD patients, its underlying mechanism is still a mystery.

Despite all the research in the field, all treatments up to now can only help manage some of the symptoms of the patients and improve quality of life, whereas there is yet absolutely no cure that can slow down the progression of the disease. Therefore, more studies need to be done to uncover the underlying mechanism that leads to PD.

1.4 Symptoms of PD

PD patients typically manifest a spectrum of both motor and non-motor symptoms (Table 1.1) that vary from one individual to another. Primary motor symptoms include resting tremor (trembling in hands, arms, legs, jaw, and face), bradykinesia (slowness in executing movements), rigidity (continuous contraction of muscles leading to joint pain, stiffness and difficulty of movement), and postural instability (leads to imbalance, and falls) [4]. Non-motor symptoms may vary from neuropsychiatric impairments, such as mood disorders, depression or cognitive impairments, sleep abnormalities, loss of sensory functions, such as olfactory dysfunction, and autonomic dysfunctions such as gastrointestinal disorders, postural

hypotension or urinary disorders, and fatigue pain.

Motor symptoms	Non-motor symptoms
➢ Cardinal: Tremor, bradykinesia, rigidity, postural instability ➢ Face: Hypomimia, dysarthria, dysphagia, sialorrhoea ➢ Body movements: Decreased arm swing, shuffling gait, festination difficulty arising from chair, turning in bed, micrographia, cutting food, feeding, hygiene, slow activities of daily living ➢ Contraction: Glabellar reflex, blepharospasm, dystonia, striatal deformity, scoliosis, camptocormia	➢ Dysautonomia: Orthostatic hypotension, constipation, urinary and sexual dysfunction, abnormal sweating, seborrhoea), weight loss ➢ Sensory symptoms: anosmia, ageusia, pain (shoulder, back), paresthesias ➢ Psychiatric problems: Depression, apathy, anhedonia, fatigue Cognitive impairment, bradyphrenia, tip-of-the-tongue (word finding) phenomenon ➢ Sleep disorders: REM behaviour disorder, vivid dreams, daytime drowsiness, sleep fragmentation, restless legs syndrome

Table 1.1 Motor and non-motor PD symptoms. Table modified from Jankovic *et al*., 2008 [4].

1.5 Why do the dopaminergic neurons die in PD?

PD symptoms are primarily caused by abnormally low and falling levels of dopamine. As mentioned earlier, the hallmarks of PD are the degeneration of the dopamine producing neurons in the substantia nigra pars compacta of the midbrain and the presence of proteinaceous aggregates in remaining neurons called Lewy bodies. It is not known why these neurons die. Despite intensive study in the field, the cause of PD is still not clear. Many scientists believe that PD is caused by a combination of genetic and environmental factors. In the genetic cases, genetic factors are the primary cause, however exposure to environmental toxins or other events including aging may contribute to death of dopaminergic neurons and PD pathogenesis. It is believed that understanding the sequence of events that leads to the loss of dopamine neurons may help scientists develop treatments to stop or reverse the progress of PD.

1.6 Genetic and environmental factors contribute to PD pathogenesis

While most PD cases occur sporadically, research on inherited forms of PD in the past two decades have shed new light on the disease and pathogenic mechanisms leading to neuronal demise [28]. Analysis of physiological functions of PD-linked genes now allows us to concentrate on cellular pathways involved in PD pathogenesis.

Advances in genetics led to discovery of nearly 20 genes mutated in rare familial forms of the disease (Table 1.2). The proteins encoded by these genes have been implicated in diverse cellular pathways, including mitochondrial quality control (PINK1, parkin, and DJ-1); protein misfolding, and aggregation (α-synuclein); membrane trafficking and autophagy (α-synuclein, LRRK2, PINK1, and parkin); and synaptic function and vesicle release (α-synuclein, synaptojanin, and TMEM230) [29]. Interestingly, several of these genes encode direct components of ubiquitin signaling including parkin and F-box only protein 7 (FBX07), or substrate proteins of ubiquitin signalling (α-synuclein).

PD-linked genes are classified as causative and genetic risk factors. Causative genes are inherited in a Mendelian manner and lead to autosomal PD, whereas genetic risk factors may predispose an individual to disease. According to their pattern of inheritance, causative genes are further classified as either autosomal recessive or autosomal dominant. Remarkably, mutations in autosomal-recessive genes mostly lead to an early onset PD whereas mutations in autosomal dominant genes mostly lead to late-onset PD which is indistinguishable from idiopathic PD. This may suggest that two distinct molecular pathways might interact in PD pathology [30]. Key molecular processes implicated in parkinsonism by genetic findings are shown in Fig 1.2.

Mutations in *SNCA*, *LRRK2, and VPS35* are the most common causes of late-onset Autosomal-dominant PD.

1.6.1 Autosomal-dominant PD-associated genes

SNCA - In 1997, a mutation in *SNCA* gene was found in a large Italian kindred and in several Greek familial cases as the first genetic defect identified to be associated genetically and neuropathologically with PD [31]. *SNCA* encodes a small 14 kDa presynaptic neuronal protein named α-synuclein [32]. This ground-breaking discovery, led to a flood of studies researching other PD causative genes.

The function of α-synuclein is not completely clear. Nevertheless, it has been suggested that it plays a role in maintaining a supply of synaptic vesicles in presynaptic terminals by clustering synaptic vesicles and promoting exocytosis [33, 34]. It may also assist in the regulation of dopamine release in neurons [35]. In addition to single amino acids mutation, duplication and triplication of the gene were also found to cause PD [36, 37].

Symbol	Gene locus	Inheritance	Gene	Name of protein	Protein function	Comments
PARK1	4q21-22	AD	*SNCA*	α-synuclein	Synaptic protein	Protein is major component of LB
PARK2	6q25.2–q27	AR	*Parkin*	parkin	Ubiquitin-protein ligase	Most common cause of AR-JP
PARK4	4q21–q23	AD	*SNCA*	α-synuclein	Excess of α-synuclein protein	Multiplication of *SNCA* gene
PARK5	4p13	AD	*UCHL1*	UCHL1	Hydrolyze small C-terminal adducts of ubiquitin	Role uncertain
PARK6	1p35–p36	AR	*PINK1*	PINK1	Mitochondrial kinase	Second most common cause of AR-JP
PARK7	1p36	AR	*DJ-1*	DJ-1	Oxidative stress protection	Rare
PARK8	12q12	AD	*LRRK2*	LRRK2	Multiple functions by several domains	Most common cause of dominant PD
PARK9	1p36	AR	*ATP13A2*	ATPase type 13A2	Lysosomal protein	Complex phenotype (Parkinsonism, spasticity, and dementia)
PARK14	22q13.1	AR	*PLA2G6*	A2 phospho-lipase	Phospholipid remodeling	Allelic to neuroaxonal dystrophy: adult - onset dystonia-parkinsonism in two patients
PARK15	22q12–q13	AR	*FBX07*	F-box protein 7	Phosphorylation-dependent ubiquitination	Early-onset, severe phenotype with spasticity and dementia
PARK17	16q11.2	AD	*VPS35*	VPS35	Retrograde transport from the endosomes to the trans-Golgi network formation of MVDs	

Table 1.2 Several known PARK genes with confirmed roles involved in causative PD. Table modified from Kumar *et al.*, 2011 [30].

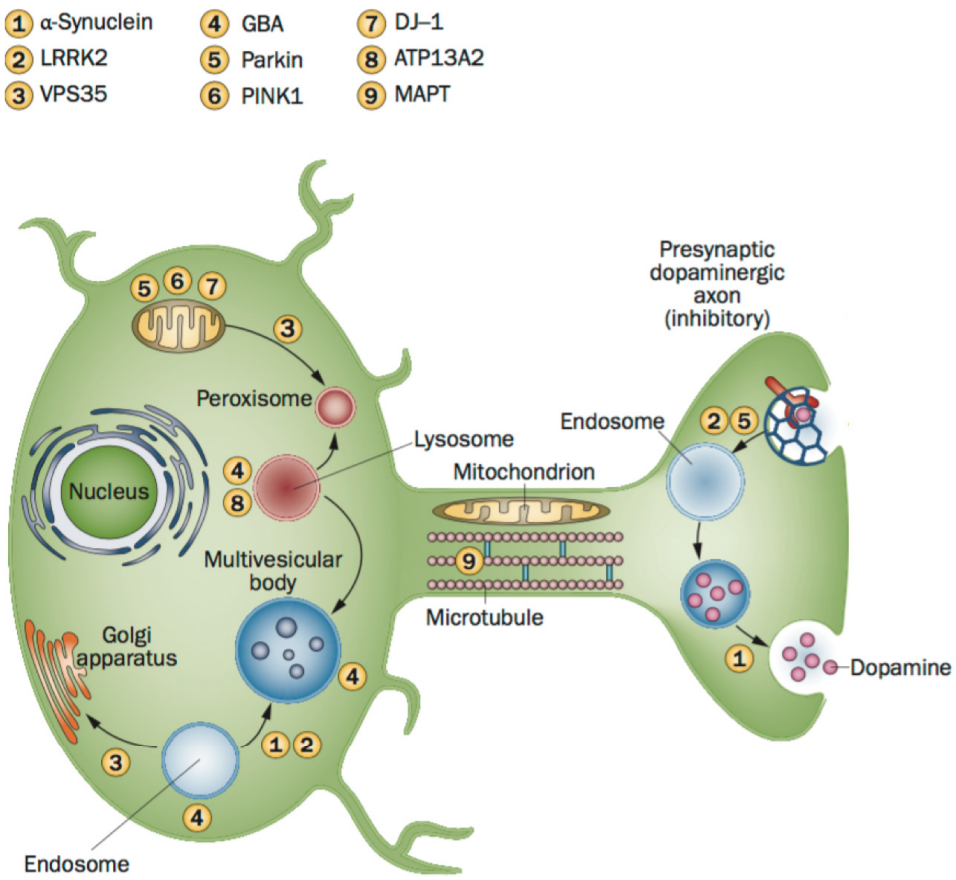

Figure 1.2 Key molecular processes involved in PD by genetic findings. A dopaminergic substantia nigra neuron is depicted in green. In presynaptic terminals, α-synuclein promotes exocytosis and is also involved in endocytosis. In postsynapses, LRRK2 phosphorylates endophilin A (a PD risk factor) and regulates the release of clathrin-coated endocytic vesicles and macroautophagy, neuronal polarity and morphology. VPS35 is a key component of the membrane protein–recycling retromer complex, responsible of the retrograde transport from the endosomes to the trans-golgi network. VPS35 mediates the formation of mitochondria-derived vesicles (MDVs), which shuttle cargo from mitochondria to peroxisomes. glucocerebrosidase (GBA; another PD-linked gene) and other lysosomal acid hydrolases also require this retromer for receptor recycling. Loss-of-function of parkin, PINK1 and DJ-1 affect mitochondrial biogenesis and maintenance. ATP13A2 has a role in lysosome-mediated autophagy. The microtubule-associated protein tau (MAPT; a PD risk factor) helps to regulate cargo trafficking and delivery, primarily in axons. Figure modified from Trinh *et al.*, 2013 [30].

α-synuclein is normally unstructured and soluble in a tetramer form. However, it is unstructured and insoluble in its monomeric state [38-40]. α-synuclein is a major component of Lewy bodies and Lewy neurites, a neuropathological feature of PD [41, 42]. However, the

presence of protein aggregates is not correlated with cellular toxicity [43]. Interestingly, when α-synuclein aggregates, it converts from a random coil conformation to a beta-sheet stable conformation [44].

***LRRK2* (*PARK8*)** - Discovered in 2004, leucine-rich repeat serine/threonine-protein kinase 2 (*LRRK2*) also known as *PARK8* gene is the greatest known genetic contributor to PD [45]. Most *LRRK2* mutations result in autosomal dominant PD symptoms indistinguishable from idiopathic PD [45]. LRRK2 encodes a large 286-kDa protein cytosolic protein that associates with the mitochondrial membrane.

LRRK2 belongs to the Roco superfamily of proteins containing leucine rich-repeats (LRR), a Ras-like GTPase domain (Roc), a C-terminal of Roc domain (COR), and a kinase domain [46]. Most pathogenic mutations have been shown to increase the kinase activity of LRRK2 [47, 48]. PD mutations in the ROC-COR domain result in abolished GTPase function, suggesting that GTPase activity can inhibit kinase activity [49-52].

LRRK2 has been linked to a multitude of cellular functions and pathways including neurotransmission [53], synaptic vesicle endocytosis and recycling [54], synaptic morphology [55, 56], neuronal survival [57, 58], regulation of neurite outgrowth [59], Wnt signaling, mitochondrial disease [60], translation [61], immunity [62], actin remodeling [63] and autophagy by regulating phosphorylation of endophilin A [64-66]. However, it is not clear which of these functions and pathways are crucial in PD pathogenesis.

***VPS35* (*PARK17*)** - Vacuolar protein sorting associated protein 35 (VPS35) gene was discovered in 2011 by linkage analysis [67, 68]. VPS35 encodes a key component of the membrane protein–recycling retromer complex, which is responsible of the retrograde transport from the endosomes to the trans-golgi network [69, 70]. VPS35 is the third autosomal-dominant gene associated with PD. Retromer dysfunctions caused by VPS35 PD mutants leads to protein trafficking defects in PD [71]. VPS35 also has a distinct role in the formation of mitochondria-derived vesicles (MDVs), which shuttle cargo from mitochondria to peroxisomes or lysosomes [72]. Interestingly, lysosome-targeted MDVs have recently been shown to require parkin and PINK1, two autosomal-recessive PD-associated genes [73].

1.6.2 Autosomal-recessive PD-associated genes

Mutations in *Parkin*, *PINK1*, and *DJ1* are the most common causes of early-onset

autosomal-recessive PD.

Parkin (PARK2) - Discovered in 1998 from linkage analysis in patients with autosomal-recessive juvenile Parkinsonism (AR-JP), *Parkin* was the second identified PD gene and the first gene causing PD in an autosomal recessive manner [74-77].

Clinically, patients with mutations in the *Parkin* gene represent earlier onset, accounting for 90% of PD cases before age 21 and half of the cases before age 45 [78]. Their phenotype is mild but distinct with strong association with dystonia, slow progress, and L-Dopa responsive [23]. Strikingly, most patients with parkin mutations have no Lewy bodies in postmortem brain, whereas the pathology was relatively restricted to the striato-nigral system [79]. Interestingly, all patients bearing compound heterozygous parkin mutations were reported to have Lewy bodies [80].

Parkin encodes a 465-residue E3 ubiquitin ligase enzyme involved in the ubiquitination pathway [81]. Ubiquitination is a post-translational modification that typically marks proteins for degradation through the covalent attachment of ubiquitin and ubiquitin chains to lysine residues or the N-terminal amino group of a substrate protein [82]. In addition to degradation via the proteasome, ubiquitination can act as a signal for autophagy [83] – degradation via lysosomes – as well as alter substrate protein activity or location [84].

Ubiquitination is carried out through the sequential action of three enzymes: E1 ubiquitin-activating enzymes, E2 ubiquitin-conjugating enzymes, and E3 ubiquitin ligases (Fig 1.3). In the pathway, E1 first uses ATP to activate ubiquitin for conjugation by forming a thioester between its catalytic cysteine and the C-terminal carboxyl group of ubiquitin. The ubiquitin is then passed to a second cysteine of an E2 ubiquitin conjugating enzyme. In the final step, the ubiquitin-charged E2 enzyme interacts with a specific E3 ubiquitin ligase and transfers the ubiquitin to the amino group of a substrate protein. Ubiquitin contains seven lysine residues as well as an N-terminal amino group that can be used to build chains of polyubiquitin. The most common chain-types are K48- and K63-chains in which multiple ubiquitin molecules are linked in a linear arrangement with the C-terminus of one molecule attached to lysine 48 (or 63) of the next.

In the ubiquitination pathway, the E3 ubiquitin ligases typically provide the majority of specificity and regulation in recognition of substrates and control of activity [85]. Mammalian genomes encode approximately 1-2 E1 enzymes, 30–40 E2 enzymes, and hundreds of E3

enzymes. The diversity of these enzymes suggests a wide variety of protein substrates or functions with different regulatory mechanisms for each one.

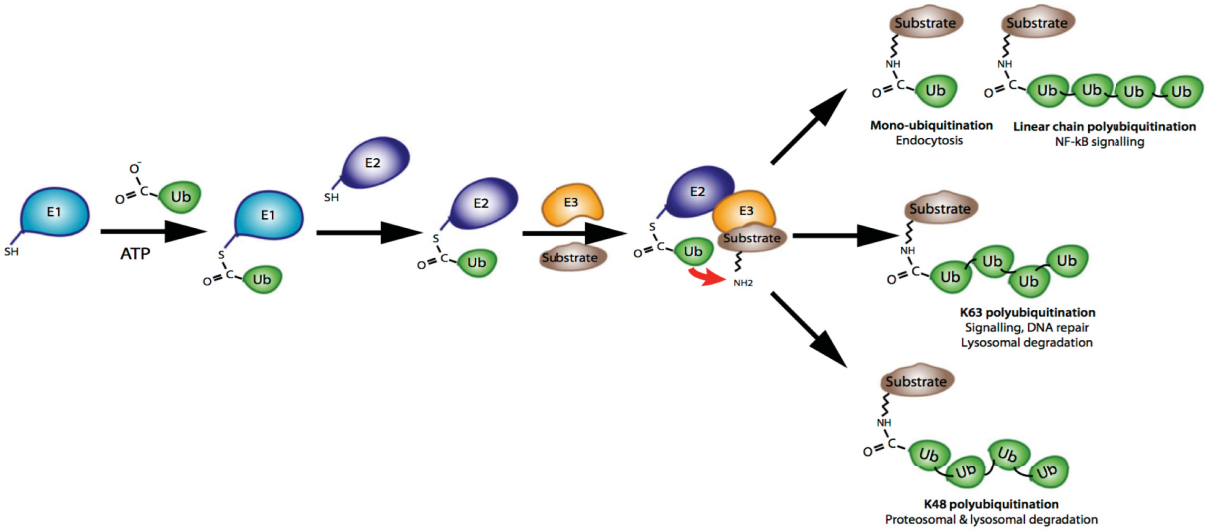

Figure 1.3 Ubiquitination pathway. Cascade of enzymes are involved in this pathway. The ubiquitin-activating enzyme E1 uses ATP to conjugate the C-terminal carboxylic acid group of ubiquitin to an active site cysteine. This is then transferred to a cysteine on one of a number of E2 enzymes that work in concert with E3 enzymes to ubiquitinate substrate proteins on amino groups of lysine residues or protein N-termini. The formation of monoubiquitin or polyubiquitin chains on substrates are signals for different downstream pathways. Figure modified from Seirafi *et al.*, 2015 [86].

Parkin consists of a ubiquitin-like domain (Ubl) at the N-terminus and four zinc-coordinating Really-Interesting New Gene (RING) and RING-like domains: RING0, RING1, IBR and RING2 (Fig 1.4). More than 120 pathogenic PD mutations are spread throughout these parkin domains, attesting to critical functions for each of the individual domains [87].

Parkin interacts with multiple proteins including endophilins A [88], BAG5 [89], CASK [90], EPS15 [91], PAEL-R [92], and p38 [93, 94]. Parkin has been hypothesized to play a role in the formation and/or the clearance of protein aggregates, since ubiquitin is a major component of Lewy bodies in patients. However, no Lewy body was observed in most patients with parkin loss-of-function mutations [79].

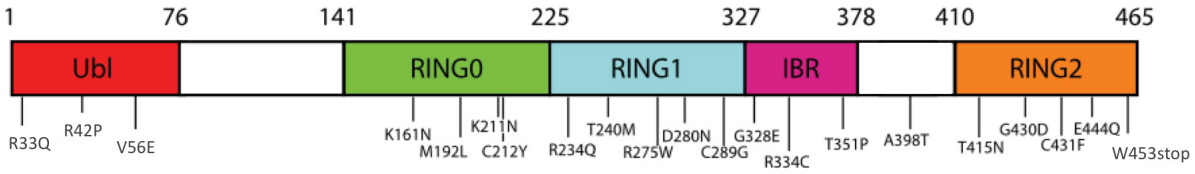

Figure 1.4 Domain architecture of parkin. Selected PD mutations are shown in five domains indicating the importance of all domains in parkin function. Figure from Seirafi *et al*., 2015 [86].

Parkin exhibits low basal activity whereas its activation requires PINK1 (another PD-linked protein) kinase activity [95-98]. Remarkably, patients with parkin or PINK1 mutations exhibit clinical similarity which suggests they might function in a common pathway maintaining mitochondrial fidelity [99, 100]. Supporting this notion, *Drosophila melanogaster* lacking *Parkin* or *PINK1* show pronounced mitochondrial abnormalities and similar (and relatively unique) phenotypes including the triad of muscle degeneration, disrupted spermatogenesis, and loss of dopaminergic neurons within a specific cluster [99-103]. Additionally, *Parkin* overexpression in the dPINK1 null *Drosophila* and not the converse partially compensates for this phenotype, indicating that dPINK1 is upstream of dParkin in the same pathway [99-101]. Moreover, loss of PARKIN or PINK1 in mice leads to one phenotype similar to that in human (albeit milder), consistent with the notion of a common PINK1 pathway regulating mitochondrial homeostasis [104-106].

More recently, parkin and PINK1 were shown to be involved in a common pathway and induce mitochondrial autophagy, a process termed mitophagy. In this pathway, PINK1 activates and recruits cytosolic autoinhibited parkin to damaged mitochondria. Activated parkin ubiquitinates mitochondrial proteins for degradation and induces the clearance of the damaged organelle [134].

While parkin and PINK1 have independent functions in various cellular pathways, it is suggested that they might work together in common pathways relevant to PD pathogenesis.

***PTEN-induced kinase 1* (*PINK1* also named *PARK17*)** - Discovered in 2004, *PINK1* was first identified as a PD-associated gene by linkage analysis in patients with AR-JP [107]. Mutations in *PINK1* are rare and responsible for <8% of AR-JP cases [108]. *PINK1* is quite conserved, as homologues are found in most known animal species, including flies, worms, and mice, but not in bacteria or plants [109]. PINK1 encodes a 581-residue serine-threonine kinase that consists

of an N-terminal mitochondrial targeting sequence (MTS), a transmembrane domain (TM), a kinase domain and a C-terminal domain of unknown function [110]. More than 50 mutations in PINK1 have been discovered most of which in the kinase domain, that mainly lead to PINK1 loss of function or proper localization to mitochondria [111]. Several lines of evidence suggest that similar to parkin, PINK1 is in an autoinhibited state and requires activation [112, 113]. Upon activation, PINK1 phosphorylates many substrates, including itself [114], parkin [112, 115, 116], TRAP1 [117], HTRA2 [118], NDUFA10 [119], and ubiquitin [120-122].

PINK1 is involved in several pathways regulating mitochondrial morphology [123-126], mitochondrial calcium buffering [127-129], mitochondrial membrane potential ($\Delta\psi_m$) [105, 130, 131], electron transport chain activity [105, 119, 126, 127, 131-133], mitochondrial transport [134-136], and importantly, mitophagy [95-97]. Several lines of evidence suggest that PINK1 may be involved in multiple pathways dependent on mitochondrial homeostasis [110]. When mitochondria are healthy, PINK1 is imported to the mitochondria and is processed by multiple mitochondrial proteases [98, 137-139] and gets degraded by the proteasome [140]. However, when $\Delta\psi_m$ is lost, PINK1 import to mitochondria is blocked. In this condition, PINK1 accumulates onto the outer mitochondrial membrane, recruits parkin from the cytosol and activates parkin to trigger mitophagy [95-97]. Mitophagy is discussed in more detail in section 1.6.

DJ-1 (*PARK7*) - *Deglycase DJ-1* gene product DJ-1 was found to be associated with PD in 2004, half a decade after it was classified as an oncogene [141, 142]. DJ-1 PD mutations are very rare (less than 1% of all reported PD-associated mutations) [79] and lead to similar clinical futures as parkin and PINK1 [79]. *DJ-1* encodes a small 189-residue protein containing one single globular domain [143-145]. DJ-1 is proposed to function either as a protease [146] or a glyoxalase [147]. DJ-1 is an evolutionarily ancient protein, with homologs in all aerobic species; DJ-1 is homologous to bacterial enzymes Pfp1, Thij, and YajL, which respectively are involved in proteolytic cleavage, thiamine biosynthesis, and redox sensing [148, 149].

Although the precise function of DJ-1 is not clear, it has been proposed that DJ-1 may regulate mitochondrial dynamics [150-152] and have neuroprotective function against reactive oxygen species (ROS) [153-158]. *DJ-1* null *Drosophila* present increased sensitivity to oxidative stress but do not show abnormal mitochondrial morphology like *Parkin* and *PINK1* null flies [154-156, 159, 160], and DJ-1 does not interact genetically with *Parkin* or *PINK1* in

flies, suggesting that it might have important neuroprotective roles in PD independent of parkin or PINK1 [101].

1.6.3 PD Genetic risk factors

More than 40 genetic risk factors have been identified using genome-wide association studies (GWAS) and meta-analyses to contribute to the development of PD [161]. GWAS compare the frequencies of common variants associated with a trait among patients and controls; meta analysis is a statistical analysis that combines the results of multiple GWAS studies [30].

All GWAS indicate a strong association to several polymorphisms within the *SNCA* gene [11]. Most studies also confirm an association with the *microtubule-associated protein tau* (*MAPT)* gene that is enriched in neuronal axons and encodes a microtubule-binding protein involved in cargo transport [4]. Many inherited defects may result in greater vulnerability to neurotoxins and to a higher susceptibility of PD [162].

Among these risk factors, SH3 domain-containing GRB2-like 2 (SH3GL2) (a gene that encodes endophilin A1 protein) was identified in a recent meta-analysis of GWAS [161]. Endophilin A1 is a presynaptic protein involved in endocytosis [163]. Interestingly, endophilin A1 is a parkin interactor and gets ubiquitinated by parkin [88]. Additionally, phosphorylation of endophilin A1 by LRRK2 (another PD-linked protein), regulates bulk autophagy in neurons [164].

Other important PD genetic risk factors are GBA (mutated in Gaucher Disease-a lysosomal storage disorder- and in Ashkenazi Jewish PD patients GBA catalyzes the conversion of glycolipid glucocerebroside to glucose and ceramide [165, 166] and is involved in autophagy and α-synuclein processing [167, 168]. SCN3A (associated with epilepsy in both animals and human), Elovl7 (associated with neurodegeneration) and several transcription factors including SATB1 (associated with T cell function), ZNF184, and TOX3 (implicated in neuronal survival) are among the newly identified PD risk factors [161].

DNAJ6, which encodes Auxilin, a protein involved in clathrin-mediated endocytosis, RAB7L1, which encodes a small GTPase also involved in endosomal trafficking and GAK-DGKQ (Cyclin G associated kinase-diacylglycerol kinase), which encodes a kinase homologous to auxilin and is also involved in clathrin-mediated endocytosis. Among these risk factors, RAB7L1 has been shown to interact with VPS35 and LRRK2 in endosomal-lysosomal

trafficking pathways [169]. Taken together, these genetic risk factors suggest that endocytosis, cargo trafficking and autophagy are central pathways in the pathology of Parkinson's disease [161].

1.7 PD environmental and life-style risk factors

While age is the biggest risk factor contributing to PD development, many chemicals and factors have been identified to affect the individual's risk of developing PD. Strikingly, gender plays a role whereas male PD cases are about 1.5 times more than the female cases [170]. Other risk factors such as exposure to MPTP (1-methyl-4-phenyl-1,2,3,6-tetrahydropyridine), a by-product generated accidentally during the synthesis of a meperidine analog, pesticides including paraquat, permethrin and rotenone, and traumatic head injury especially combined with genetic risk factors have been shown to increase the risk of developing PD [171]. On the other side, coffee intake, exercise and the use of nonsteroidal anti-inflammatory drugs NSAIDs (especially ibuprofen) seems to reduce the risk of developing PD [170].

1.8 What we learn from PD genetic and environmental factors

Over the past two decades, the identification of PD genes has profoundly changed our understanding of pathogenic mechanisms leading to neuronal demise in PD that allows us to focus directly on key cellular pathways involved in PD pathology. Among these pathways, dysregulation of mitochondrial quality control is one of the most important pathways that can lead to many neurodegenerative diseases including PD.

1.9 Mitochondria, the powerhouses of cell

Mitochondria are double membrane-bound organelles found in almost all eukaryotic organisms. Mitochondria further play significant roles in different pathways including apoptosis, fatty acid metabolism, calcium buffering, iron-sulfur clusters and heme biosynthesis [172]. Mitochondria are highly dynamic organelles and continuously undergo fission (divide) and fusion (fuse) (Fig 1.5). Mitochondria are also linked to other organelles and move through the cytoskeleton to delicately regulate energy production and most other mitochondrial process in cells.

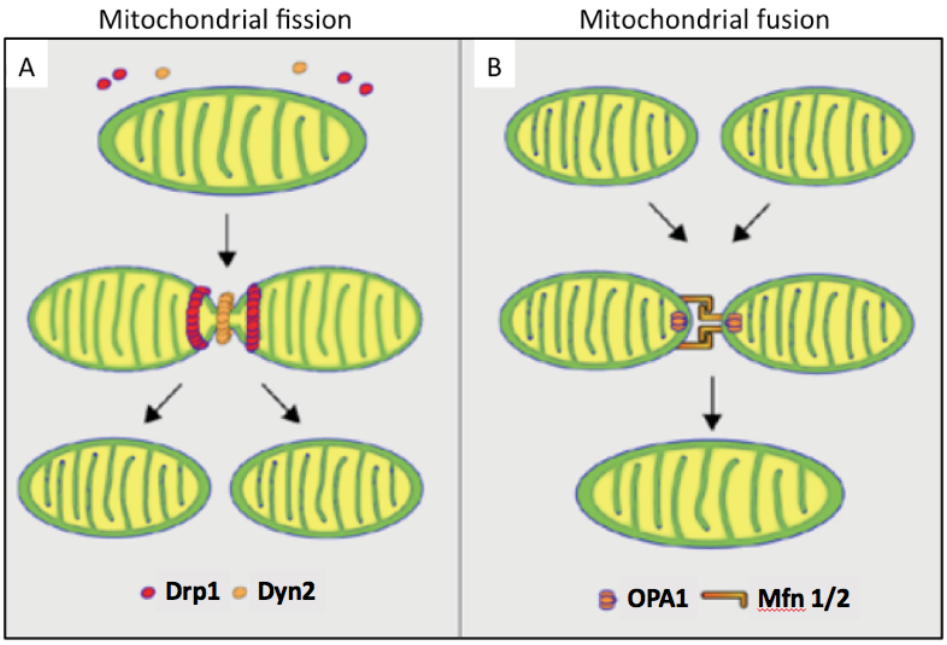

Figure 1.5 Mitochondrial fission and fusion. The morphology of the mitochondrial network is regulated by a balance between fusion and fission events. These two opposing processes are mainly regulated by several large dynamin-related GTPase proteins, including dynamin-related protein 1 (Drp1) and dynamin 2 (Dyn2), Mitofusin 1 (Mfn1), Mitofusin 2 (Mfn2) and optic atrophy protein 1 (OPA1). Drp1 and Dyn2 regulate mitochondrial fission while Mfn 1/2 and OPA1 are involved in mitochondrial outer and inner membrane fusion. Figure modified from Gao *et al*., 2017 [173].

Mitochondria generate energy by taking in nutrients, breaking them down and creating energy-rich molecules, a process termed oxidative phosphorylation. During oxidative phosphorylation, mitochondria shuttle electrons along four protein complexes (complex I-IV) in the inner mitochondrial membrane. These four protein complexes form the electron transport chain (ETC). ETC generates a proton gradient across the inner membrane, thus producing a voltage difference across the inner membrane. This voltage difference provides the energy to drive ATP synthase and generate ATP. This process produces toxic by-products including reactive intermediates and oxidizing agents, which in turn damage mitochondrial DNA, proteins and lipids and lead to apoptosis [172]. Therefore, mitochondria quality must be precisely controlled to maintain mitochondria homeostasis and to avoid cell death.

1.10 Current mechanisms of mitochondrial quality control

Mitochondria have distinct quality control mechanisms to stay healthy. Damaged outer mitochondrial membrane proteins can be degraded by the proteasome [174, 175]. Mitochondria also have their own proteolytic system to degrade misfolded proteins [176]. Moreover, continuous mitochondria fission and fusion help the repair of damaged components by allowing the isolation of damaged mitochondria via fission and the exchange of material between healthy mitochondria via fusion [177, 178]. Under mild oxidative stress conditions, a more elaborate mitochondria quality control mechanism occurs through the budding of a portion of mitochondria containing oxidized mitochondrial proteins to form mitochondria-derived vesicles (MDV). These MDVs later fuse with lysosomes and get degraded [179]. Under extreme oxidative stress conditions where mitochondrial inner membrane potential is lost, damaged mitochondria are getting enveloped by autophagosomes and degraded in a lysosomal-autophagy pathway, a process termed mitophagy [180, 181].

The effectiveness of mitochondrial quality control mechanisms is of great importance in neurons, as neurons are high energy-demand cells with requirement of high calcium-buffering capacity due to the action potential-driven calcium influxes [182]. Thus, neurons are tremendously prone to mitochondrial damage, and efficient mitochondrial quality control pathways are essential for neuronal survival. Highlighting this notion, mitochondrial damage has been implicated in various neurodegenerative diseases.

1.11 Central involvement of mitochondria in PD

PD pathology has a long-standing proven relationship with mitochondrial damage. Discovery of PD symptoms caused by mitochondrial neurotoxins including MPTP, rotenone and paraquat first highlighted the role of mitochondria in PD. These toxins have been shown to inhibit complex I, a major component of mitochondrial electron transport chain [183, 184], as the postmortem brains from these PD patients were shown to have complex I deficiency [185], and significantly higher number of mtDNA alterations in the dopaminergic neurons of the substantia nigra compared to healthy individuals [186]. Reports of respiratory chain defects in the brain from sporadic PD patients complemented this theory. Another piece of evidence comes from reports of the accumulation of mitochondrial DNA (mtDNA) deletions in human dopaminergic neurons of the substantia nigra, the most affected cells in PD patients, during

aging compared to other brain neurons [186, 187]. This elevation seems to be compensated by an increase in the number of wild-type mitochondrial DNA copies in healthy individuals but not in PD patients [188]. However, the most persuasive evidence for a central involvement of mitochondria in PD was provided in the past decade by the discovery of PARKIN and PINK1, both associated with recessively inherited PD, and the role of the proteins encoded by them in mitochondrial control pathways [110].

1.12 Parkin is an RBR E3 ubiquitin ligase

Based on considerations of structure and chemistry, three classes of E3 ligases are distinguished: RING-type (including U-box ligases), HECT-type and RING-HECT hybrids [189] (Fig 1.6). RING-type E3s are characterized by the presence of a canonical C3HC4-type RING domain that binds the E2 enzyme but does not participate directly in catalysis. This class of E3s functions as inert scaffolding ligases that facilitate the direct transfer of ubiquitin from the E2 onto the substrate. HECT-type E3s contain a HECT (homologous to the E6-AP carboxyl terminus) domain with an active site cysteine, which accepts ubiquitin from an E2 enzyme in the form of a thioester intermediate and then transfers it to substrates. The third class consists of the RBR (RING-between-RING) family of E3 ubiquitin ligases that combine the chemistry of HECT-type ligases with structural similarity to RING-type ligases (Fig 1.6) [190].

RBR E3 ubiquitin ligases comprise a group of 12 complex multidomain enzymes [191]. RBRs contain a canonical C3HC4-type RING (named RING1), followed by two conserved Cys/His-rich Zn-binding domains, In-Between-RING (IBR) and RING2 domains, that contain an active site cysteine residue. This cysteine accepts ubiquitin from the E2 enzyme and transfers it onto substrates; hence, ligases in this class are sometimes referred to as RING-HECT hybrids [190].

Historically, initial sequence alignment methods suggested that two of the domains in the RBR modules (RING1 and RING2) contained multiple cysteine residues coordinating zinc ions that roughly conformed to the RING E3 ligase consensus sequence [192, 193]. A third domain heavily populated by cysteine residues that lay between the proposed RING domains was later identified by multiple sequence alignment methods and properly named an IBR (In-Between-RING) domain [194]. In this way, the RBR nomenclature was born.

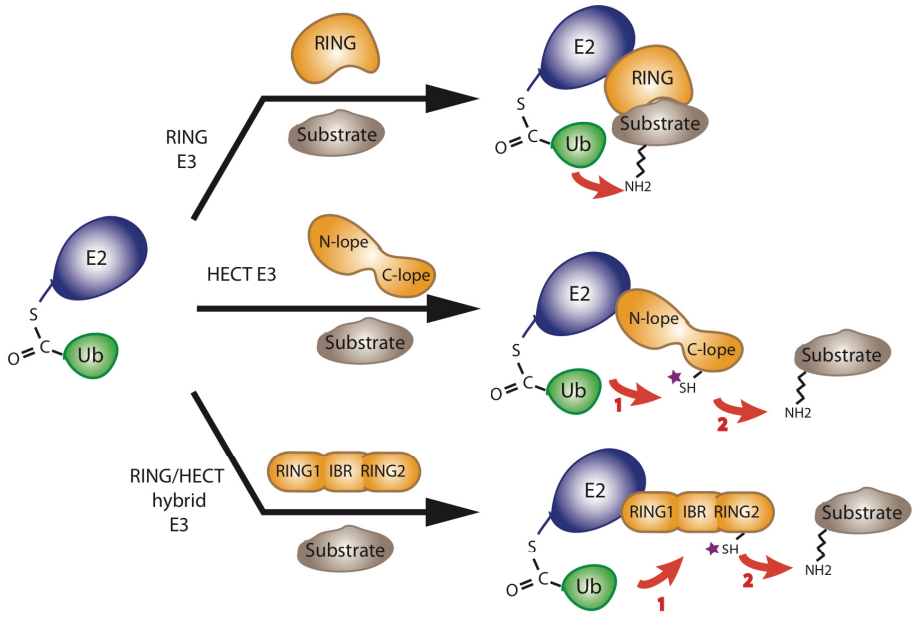

Figure 1.6 Three different classes of E3 ubiquitin ligases. E3 ligases can be distinguished based on the presence of a RING domain, a catalytic cysteine, or the presence of both. RING and U-box domain ligases act as scaffolds to bring the substrate and ubiquitin-conjugated E2 together. HECT ligases have a catalytic cysteine in their C-lobe that is transiently conjugated to ubiquitin as an intermediate in a two-step process of substrate ubiquitination. Parkin is a RING/HECT hybrid ligase that contains a RING domain that binds the E2 enzyme and a catalytic cysteine that transfers ubiquitin to the substrate. Figure from Seirafi *et al*., 2015 [86].

The overall domain architectures of the 12 RBR E3 ligases found in humans are illustrated in Fig 1.7 [191]. Interestingly, no protein has been identified to date that contain an isolated IBR or RING2 suggesting that this triad of RING1, IBR and RING2 domains are always found together in nature. Furthermore, the RBR domains are invariably found in a particular order with the RING1 being sequentially followed by IBR then RING2 [192, 193], indicating that all three domains are required for RBR-mediated ubiquitination. However, the mechanism underlying ubiquitination is still unclear.

In general, the RBR module of all human proteins is found near the C-termini of the E3 ligases, except for ANKIB1 (ankyrin repeat- and IBR domain-containing 1) and Dorfin where the RBR is located near the center and N-terminus respectively [191]. Intriguingly, most RBR ligases contain a variety of protein-protein interacting motifs near their N-termini [191]. For example, both HOIL-1 (haem-oxidized IRP2 ubiquitin ligase 1) and parkin contain N-terminal ubiquitin-like domains. The Ubl of parkin interacts with the RBR domain and acts as an

intramolecular auto-inhibitory domain attenuating ubiquitination [195]. Similarly, the Ubl of HOIL-1 acts as a recruitment factor for HOIP (HOIL-1-interacting protein) through its UBA (ubiquitin-associated) domain at the N-terminus [32] to form the linear ubiquitin chain assembly complex (LUBAC). Likewise, HOIP has two zinc finger motifs (NZF); NZF1 and NZF2) domains, where NZF1 binds to ubiquitin and NZF2 is required for SHARPIN (SHANK-associated RH domain interactor) Ubl recruitment [196].

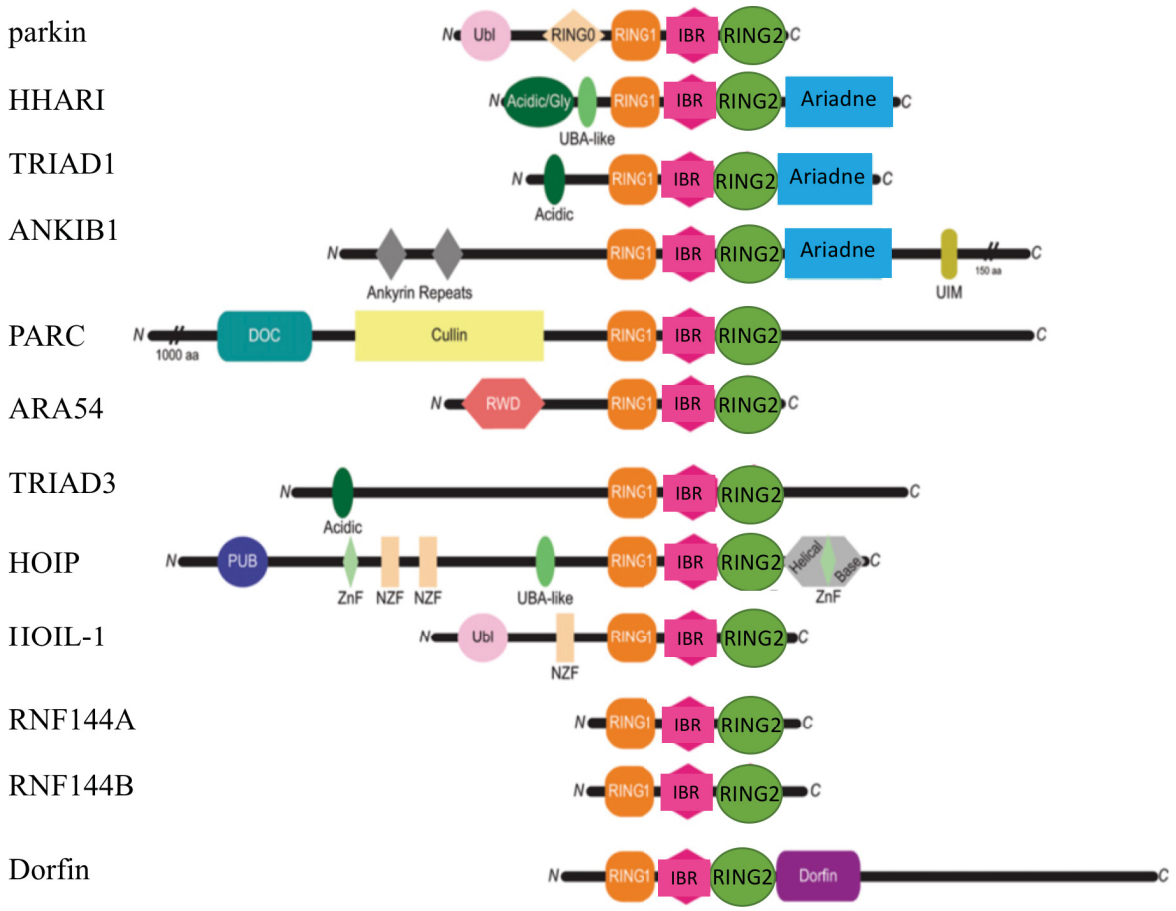

Figure 1.7 Domain architecture of the RBR E3 ubiquitin ligases. Domains found in each RBR E3 ligase are RING1, IBR, and RING2. Other domains listed include the Ubl, RING0 and Npl4 NZF, acidic/Gly N-terminal extension (Acidic/Gly or Acidic), UBA-like, Ariadne domain, UIM (ubiquitin interacting motif), ankyrin repeats, docking domain (DOC), Cullin, RWD (The RWD domain has been named after the better characterized RING finger and WD repeat containing proteins and DEAD-like helicases), PUB (PNGase/UBA- or UBX-containing domain), ZnF (Zinc finger), helical base and Dorfin domain. Figure modified from Spratt *et al.*, 2014 [191].

Parkin is the best studied RBR E3 ubiquitin ligase that ubiquitinates a wide variety of cytosolic and outer mitochondrial membrane proteins upon mitochondrial depolarization [197, 198]. It forms multiple types of ubiquitin chains, most frequently K63, K48, K11 and K6 linkages [199]. Parkin also shows relatively lax substrate specificity [197, 198]. Accumulation of polyubiquitin chains on mitochondria signals recruitment of the autophagosome and proteasome machinery to initiate mitophagy [95, 97, 114, 197]. Parkin itself becomes ubiquitinated by the attachment of K6 ubiquitin chains, which may play a role in its own degradation [200]. The activity of parkin is tightly regulated and normally repressed [195, 201-203].

In cells, parkin activity can be activated under a variety of conditions such as depolarization of mitochondria or epidermal growth factor signaling [91]. A large number of treatments that disrupt its structure are also known to de-repress its ligase activity *in vitro*. These include heat-treatment, N-terminal deletions, and some point mutations [191, 201-203].

1.13 Parkin/PINK1 mediated mitophagy

In parkin/PINK1 mediated mitophagy, cytosolic E3 ubiquitin ligase parkin and the only known mitochondrial protein kinase PINK1 act in a common pathway regulating mitochondrial quality control and promoting the selective autophagy of depolarized mitochondria (mitophagy) (Fig 1.8) [204].

Under basal conditions, parkin E3 ligase activity is repressed in the cytoplasm and PINK1 is imported into mitochondria via TOM40 and TOM20 core containing complexes [205] and cleaved sequentially by mitochondrial proteases such as MPP and PARL [98, 102, 138, 206]. Cleaved PINK1 then degrades rapidly in the cytosol via the N-end rule pathway so that levels of PINK1 are low in healthy cells [140]. However, when the organelle loses its inner membrane electrochemical gradient, import of PINK1 to the mitochondria is inhibited and the protein is stabilized on the mitochondrial outer membrane with its kinase domain at the cytosolic face [207, 208]. The accumulation of PINK1 on the mitochondria triggers parkin recruitment and activation. Activated parkin produces ubiquitin chains on various outer mitochondrial membrane (OMM) proteins leading to autophagic elimination of the damaged organelle (Fig 1.8) [95-98]. Pathogenic mutations in either of these genes lead to loss of this

quality control pathway and accumulation of impaired mitochondria, which are thought to be a source of toxic reactive oxygen species (ROS) and contribute to neuronal cell death and PD.

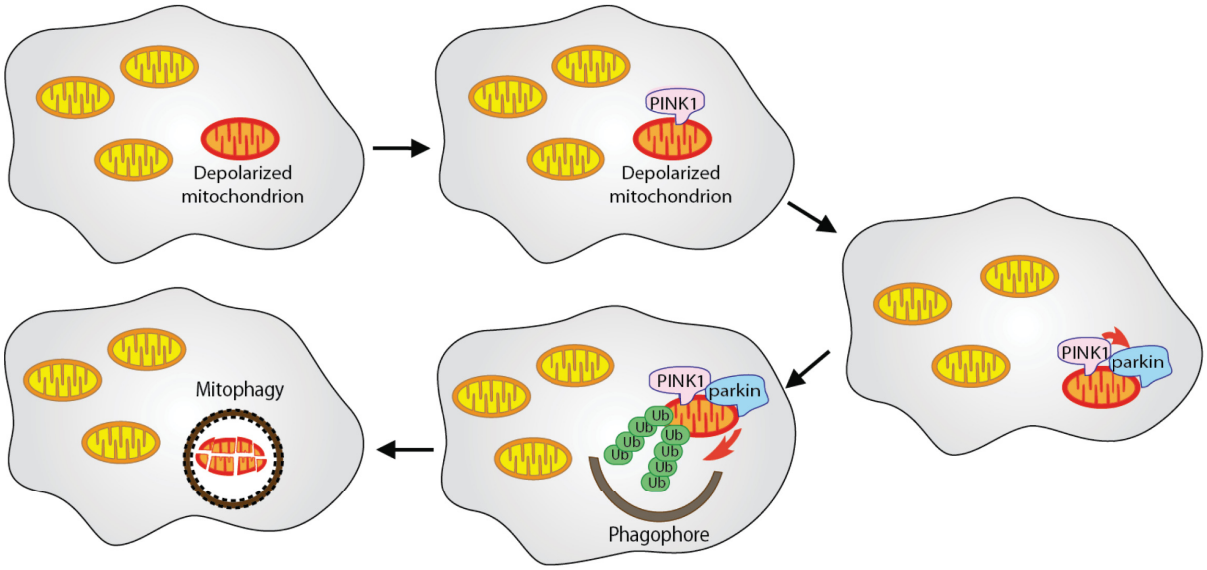

Figure 1.8 PINK1/Parkin mediated mitophagy. PINK1/Parkin mediated mitophagy identifies dysfunctional mitochondria, isolates them from the mitochondrial network, and promotes their degradation by autophagy. PINK1 is continuously imported to the mitochondria where it is rapidly degraded. Upon mitochondrial damage PINK1 degradation is inhibited, and PINK1 accumulates at the mitochondrial outer membrane (MOM). There, PINK1 promotes the recruitment of cytoplasmic parkin and activation of its ubiquitin ligase activity. Active parkin causes extensive polyubiquitination of MOM proteins and triggers clearance of damaged organelle by recruitment of autophagic adaptor proteins. Figure from Seirafi *et al*., 2015 [86].

1.14 Parkin activation by PINK1

A clue to the parkin activation mechanism first came from the discovery of parkin phosphorylation by PINK1 in 2012 [112]. They have shown that PINK1 phosphorylates parkin Ubl domain at a conserved residue serine 65 and mutating this residue to Ala prevented parkin (or an N-terminal Parkin fragment containing the isolated Ubl domain; residues 1–108) phosphorylation by PINK1 thereby confirming that this residue represents the major site of PINK1 phosphorylation. Subsequently, the same group demonstrated that this phosphorylation activates parkin E3 ubiquitin ligase activity by showing that only WT parkin and WT PINK1 are able to ubiquitinate Miro1, a mitochondrial parkin substrate *in vitro* [209]. However, using a kinase-inactive PINK1 mutant or the nonphosphorylatable parkin mutant S65A does not allow for Miro1 ubiquitination.

In cultured cells, PINK1/parkin pathways can be activated by depolarizing mitochondria with uncouplers, such as carbonyl cyanide m-chlorophenyl hydrazone (CCCP). Following CCCP treatment, parkin shows a very robust and complete recruitment to mitochondria within several hours, which is then followed by the clearance of mitochondria. Parkin recruitment to mitochondria requires PINK1 kinase activity; however, there is no fixed stoichiometry between PINK1 levels and parkin recruitment [115]. This suggests that a molecule other than PINK1 is recognized by parkin.

In the same year, Shiba-Fukushima has shown that parkin phosphorylation at Ser65 accelerates the mitochondrial translocation of parkin upon mitochondria depolarization (CCCP treatment) and is needed for its activity [115]. However, non-phosphorylatable S65A parkin mutant as well as parkin lacking the Ubl domain have shown delay in recruitment and subsequent mitophagy, but were not completely dead mutants. Moreover, S65E (phospho-mimetic parkin mutant) was not able to bypass PINK1 requirement [115]. Thus, they concluded that parkin activation and translocation to mitochondria upon depolarization is a multi-step mechanism in which parkin phosphorylation at Ser65 is combined with unknown factor(s).

Surprisingly, another group displayed that PINK1 artificially targeted to peroxisomes is sufficient to recruit and activate parkin on peroxisomes [205], indicating that parkin recruitment is not dependent on mitochondrial proteins and that this activation and recruitment requires a membrane protein or a protein that is ubiquitous in cells.

1.15 PINK1 phosphorylates ubiquitin

In 2014, three different groups concurrently reported that ubiquitin is the unknown PINK1 substrate *in vitro* and *in vivo* by proteomic studies [120-122]. The structure of parkin Ubl domain resembles that of ubiquitin, and Ser 65 is conserved in both proteins (Fig 1.9). They also performed phosphate-affinity (Phos-tag) PAGE in which the phosphorylated ubiquitin can be easily distinguished from the non-phosphorylated form as a slower migrating band. In Phos-tag gels, a phosphate group binds to the divalent manganese ions in Phos-tag and decreases the migration speed of phosphorylated proteins compared to non-phosphorylated proteins.

They also displayed that phosphorylation of both parkin and ubiquitin is required for full parkin activation [120-122] in a feed-forward mechanism (Fig 1.10). Kazlauskaite and coworkers showed that this activation can occur through direct binding of pUb to parkin [120].

The non-phosphorylatable S65A ubiquitin and/or S65A parkin and/or kinase inactive (KI) PINK1 does not lead to appearance of poly-ubiquitin chains.

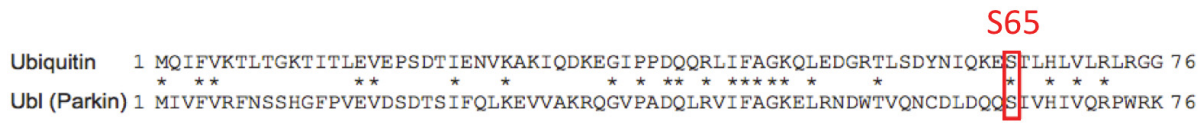

Figure 1.9 Serine 65 is conserved in parkin Ubl domain and ubiquitin. Figure from Koyano *et al*., 2014 [122].

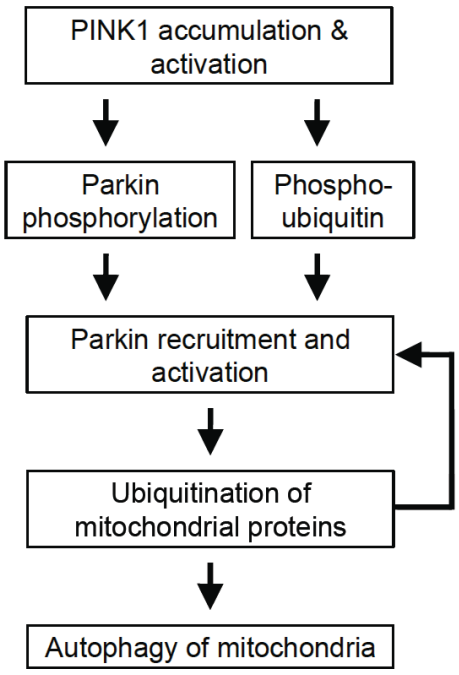

Figure 1.10 Suggested feed forward-type mechanism to explain parkin activation by PINK1. Flowchart of feed-forward activation of parkin showing that PINK1 accumulates on depolarized or damaged mitochondria and phosphorylates ubiquitin and parkin present on the surface. Activated parkin produces additional ubiquitin chains on the mitochondria, which in turn are phosphorylated by PINK1 to promote the recruitment of more parkin. The autophagosome forms around the heavily ubiquitinated mitochondria, which are then eliminated by autophagy. Figure from Seirafi *et al*., 2015 [86].

1.16 Other functions of parkin

Parkin plays a number of roles outside of the induction of mitophagy. Parkin ubiquitination of OMM proteins such as mitofusins, OPA1, and Miro alters the balance of fission to fusion and mitochondrial motility, facilitating the isolation of dysfunctional mitochondria from mitochondrial network for mitophagy [210].

Parkin and PINK1 also work together to repair mildly damaged mitochondria in response to mild oxidative stress through the formation of mitochondria derived vesicles

(MDVs) enriched in oxidized proteins [73]. These MDVs carry damaged cargo to lysosomes for degradation [211]. Complementary to mitophagy, parkin and PINK1 balance the turnover of mitochondria by promoting synthesis of new mitochondria [212]. Overexpressing parkin in proliferating cells and SH-SY5 cells increases mitochondrial transcription through interaction with TFAM [213, 214].

Parkin has been reported to promote cell survival through various mechanisms, although how parkin becomes activated in these pathways is not always clear. Parkin has been ascribed as preventing cell death through proteosomal degradation of several proteins such as parkin interacting substrate (PARIS), aminoacyl-tRNA synthetase complex-interacting multifunctional protein-2 (AIMP2), and Fbw7b, a substrate-binding adaptor protein subunit of SCF E3 ubiquitin ligase complex [215-217]. Parkin may activate prosurvival pathways by increasing nuclear factor kappa B (NF-kB) signaling [218] or decreasing activation of c-jun N-terminal kinase [219-221]. A number of recent papers describe interactions between parkin and Bcl proteins in the mitochondrial apoptotic pathway [217, 222-225]. Parkin transcription is under the control of p53, and reportedly mediates the Warburg effect of p53 on glucose metabolism [226]. Parkin has also been implicated in cell surface signaling by controlling EGF-receptor internalization and Akt signaling by ubiquitination of the endocytic scaffold protein Eps15 [91]. Parkin is a tumor suppressor and its inactivation has been reported in various human cancers. Parkin is deleted in 30% of human tumors and parkin-deficient mice are more susceptible to tumorigenesis [226-230].

Parkin also has a key role in pathogen defense through xenophagy, a pathway related to mitophagy. In xenophagy, bacteria are marked with ubiquitin chains that recruit ubiquitin-binding autophagy adaptors, leading to autophagosome formation and eventually fusion with the lysosome. The ubiquitinated substrates and ligases involved in this pathway are poorly understood. Genomic studies identified parkin as a susceptibility factor for the intracellular bacterial pathogen *Mycobacterium leprae* [231]. In a recent paper, parkin has been shown to be required for resistance to intracellular pathogens such as *Mycobacterium tuberculosis* and *Salmonella enterica* through an autophagy-dependent mechanism [232]. The shared ancestry between mitochondria and bacteria points to a common mechanism of parkin-mediated autophagy, but whether PINK1 or a related kinase is required for xenophagy is unknown.

1.17 Endophilin proteins

Endophilin A1 is a parkin substrate and has been shown to have physical interactions with parkin. This interaction leads to ubiquitination of endophilin A1 and PRD-associated synaptic endophilin A1 binding partners including synaptojanin 1, dynamin, and ataxin-2 [233-235].

Endophilins are essential elements of cellular trafficking and have prominent functions in synaptic vesicle endocytosis (SVE), receptor trafficking and apoptosis, and in other processes that require remodeling of the membrane structure [163]. Dys-regulation of endophilins have been linked to both cancer and neurodegenerative diseases [163]. Endophilins can be divided into two subfamilies of endophilins A and endophilins B.

The endophilins A were discovered in 1997 by screening an embryonic mouse cDNA expression library with a proline-rich peptide ligand for SH3 domains [236]. The positive clones were named SH3p4, SH3p8, and SH3p13, corresponding to the three endophilin A genes endophilin A1, A2, and A3, respectively. These genes were later renamed to endophilin A, as SH3p4 showed affinity to endocytic proteins [237]. Another independent PCR-based screen of cDNA from normal human brain and brain tumor tissue in the same year also identified the three endophilin A isoforms, named in that study SH3GL for SH3-containing Grb2-like protein [238]. A second endophilin subfamily, endophilins B, was later discovered in 2000 [239]. Using proapoptotic protein Bax as bait, endophilin B1 was pulled out in yeast two-hybrid screens by two different groups and named SH3GLB1 or Bif-1 (Bax-interacting factor-1) [240, 241]. A second endophilin B protein, SH3GLB2 (endophilin B2), was identified later by using SH3GLB1 itself as bait [241].

1.18 Synaptic vesicle cycling

Endophilins are key regulators of the synaptic vesicle cycling [88]. Presynaptic terminals in neurons are responsible for the conversion of electrical signals into secreted chemicals [242]. Fig 1.11 shows the schematic of the synaptic vesicle (SV) cycle.

In the SV cycle, neurotransmitters are packaged into small vesicles and cluster near the active zone. Upon arrival of an action potential stimulus, these vesicles fuse with the plasma membrane and release their content through a process termed exocytosis. Upon exocytosis, the transmembrane proteins of SVs transiently incorporate into the plasma membrane. As nerve

terminals are located distal to the cell body and the number of SVs is limited, the synaptic transmission is accompanied by local recycling of SVs to retrieve synaptic vesicle proteins, a process termed endocytosis. Multiple steps in synaptic vesicle recycling are assisted by a variety of proteins, including synaptobrevin/VAMP, synaptotagmin, and the vacuolar ATPase, syntaxin, clathrin triskelia, adaptins, dynamin, and endophilin [243, 244].

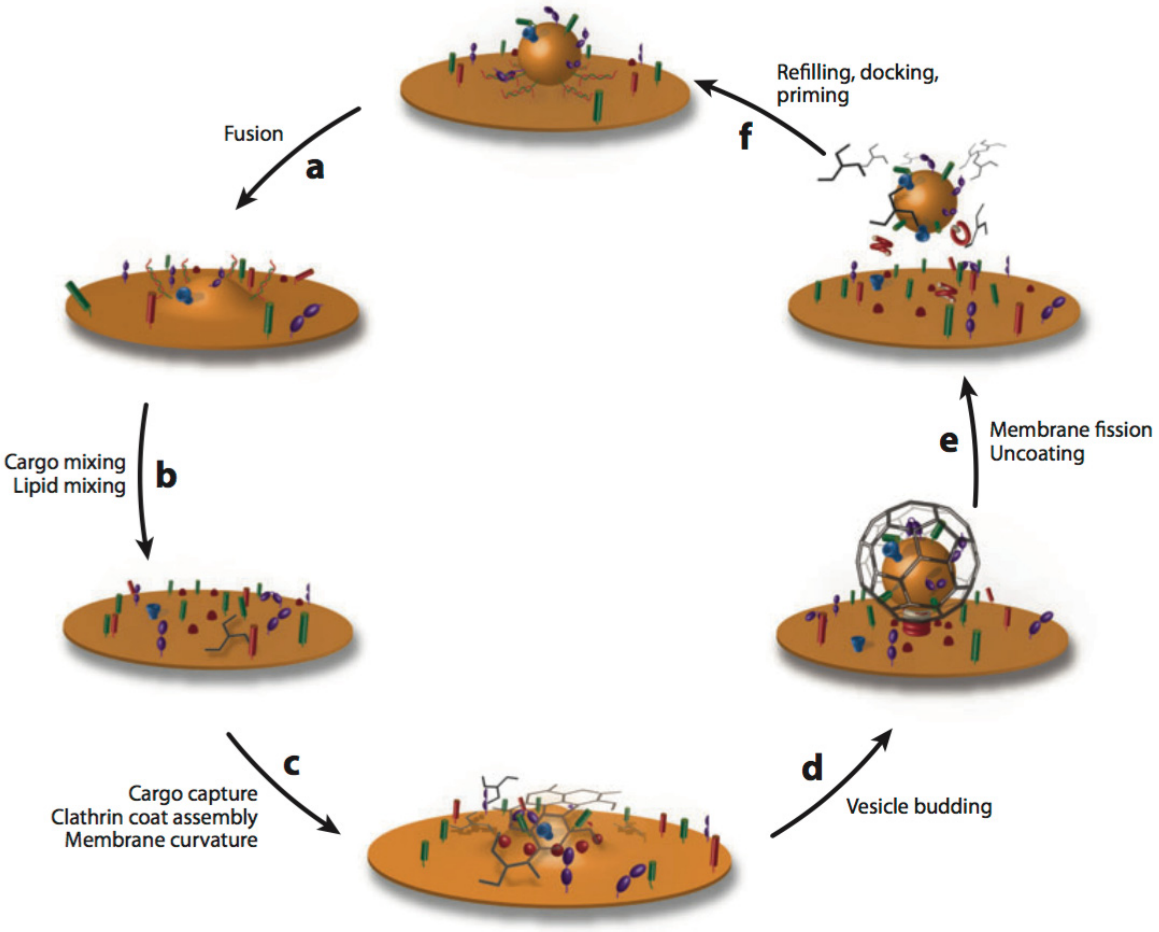

Figure 1.11 The synaptic vesicle (SV) cycle. Synaptic vesicles fuse with the plasma membrane (a) and is consequently rebuilt through the assembly of a clathrin-coated pit (b and c) followed by budding (d), and fission and uncoating of the endocytic coat proteins (e). The vesicle is refilled with neurotransmitter and returned to the vesicle pool for further rounds of exocytosis (f). Several SV proteins are depicted here including synaptobrevin/VAMP (green), synaptotagmin (purple), and the vacuolar ATPase (blue). Syntaxin is shown as red rods, and the assembled SNARE complex is represented by red-green coils. Other depicted proteins are clathrin triskelia (gray), adaptins (red ellipses), dynamin, and endophilin (red helices). Figure from Dittman *et al.*, 2009 [242].

Endophilins have been suggested to play roles in coordinating clathrin-coated pit neck constriction, via their BAR domain, and recruiting dynamin and synaptojanin via their SH3 domain. Endophilins are recruited to the clathrin-coated pit shortly before fission [245] and independently of dynamin recruitment [246]. Endophilins localize to synaptic vesicle membranes and the cytosol, and recruits to the presynaptic membrane in response to synaptic stimulation.

All endophilins (A and B isoforms) consist of a N-terminal dimeric BAR (Bin/amphiphysin/Rvs) domain that binds curved membranes upon dimerization and function as curvature sensors and/or inducers [247] and a SH3 domain at the C-terminus that binds to proline-rich motifs [163].

Three human endophilin A isoforms, but not endophilin B isoforms interact with the Ubl domain of parkin (A1 and A3 with higher affinity than A2) [88]. While endophilin A1 is brain specific, endophilin A3 is mainly found in the brain and testis, and endophilin A2 is expressed in multiple tissues [163]. Endophilin A1 is highly enriched in presynapses, where mitochondria quality is of great importance. Interestingly, endophilin A1 is among recently-published PD risk factors [161]. Moreover, endophilin A1 binding to parkin has been reported to be phosphorylation dependent in nerve terminals [88]. Therefore, we decided to focus on endophilin A1 as part of my project and figure out how this interaction is affected by parkin activation.

Endophilin A1 architecture of domains is depicted in Fig 1.12. Endophilin A1 SH3 domain at the C-terminus binds to proline-rich motifs present in dynamin and synaptojanin 1 as well as to the Ubl domain of parkin [247, 248]. Structural studies show that the SH3 domain of endophilin A1 interacts with the hydrophobic patch surrounding Ile44 in the Ubl domain of parkin (Fig 1.13).

1.19 Overview of thesis

There is clear evidence that a strong association between mitochondrial quality control and Parkinson's disease exists. However, how mitochondrial quality control pathway operates in neurons is still unclear. The main theme of this thesis is to elucidate the structure of parkin at the molecular level.

Figure 1.12 Domain architecture of endophilin A1. The SH3 domain at the C-terminus binds Ubl domain of parkin.

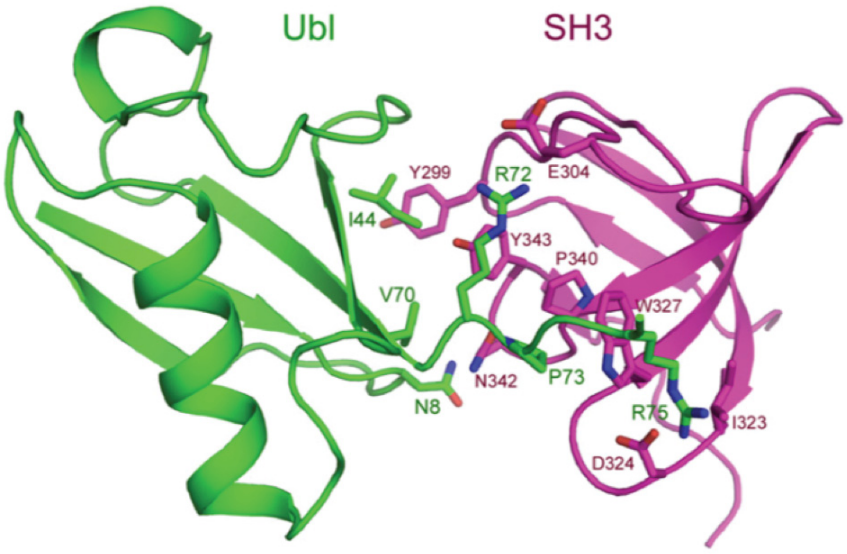

Figure 1.13 Schematic representation of the complex of parkin Ubl with endophilin A1 SH3. Endophilin A1 SH3 domain interacts with the hydrophobic patch surrounding Ile44 in parkin Ubl domain and residues 70-75. Figure from Trempe *et al.*, 2009 [88].

Parkin is a well-characterized protein with central roles in mitochondria quality control mechanism as well as in other various pathways. When I started the project in 2011, the reason why parkin is not active as an E3 ubiquitin ligase in the cytosol was not clear. The biggest mystery at the time was how PINK1 activates and recruits parkin to depolarized mitochondria simultaneously as parkin PD loss of function mutants were unable to translocate to damaged organelle by PINK1. Moreover, little was known about the structure of RBR E3 ubiquitin ligases proteins, except that their sequence is composed of a real RING domain (RING1 domain) and two additional RING-like domains (IBR and RING2). A study suggested a central mechanism of ubiquitin transfer for this class of E3 ubiquitin ligases in that these enzymes bind to ubiquitin-charged E2 enzymes through their RING1 domain, transfer ubiquitin to their active cysteine on RING2 domain, and then to lysine on substrate molecules.

In the first part of my results, I describe the structure of rat parkin that revealed the mechanism of parkin autoinhibition through multiple distinct hydrophobic inter-domain interactions. This structure revealed a novel autoinhibition mechanism unique to parkin, uncovered the structural basis for E2 binding, demonstrated the reason behind pathogenesis of most PD mutants, and suggested a potential binding pocket for therapeutic drugs to activate parkin and upregulate mitophagy.

In the second part of my results, I studied parkin activation upon binding to phospho-ubiquitin and phospho-parkin (pre-phosphorylated by PINK1) by NMR and ITC studies combined with small-angle X-ray scattering, and uncovered the mechanism of parkin activation at the molecular level.

Finally, in the third part of my results, I have used binding studies and activity assays on the activated form of parkin in the presence and absence of endophilin A1. This work helps to expand our understanding of how the parkin Ubl domain recognizes its binding partners and how it can govern the ligase activity of parkin, which is important for mitophagy in nerve terminals. Ultimately, the objective is to further define the biology of parkin and to identify novel therapeutic targets to treat PD.

Chapter 2: Experimental Procedures

2.1 Methodologies

Structural biologists are interested in getting a complete and coherent picture of biological phenomena at the molecular level. For this purpose, a combination of X-ray crystallography, SAXS, NMR spectroscopy, and ITC is usually powerful to address questions regarding the structure of the macromolecule and the mechanisms of interactions and complex assembly.

2.1.1 X-ray crystallography

Proteins can crystallize in the presence of solubility-manipulating agents called precipitants in periodical arrangement of atoms called protein crystals. Protein crystals grow in 3 dimensions as the result of inter-molecular interactions in homogeneous solutions with concentrations close to saturation point. Electrons in protein crystals interact with monochromatic X-rays beam when subjected to X-ray radiation, resulting in scattering. These scatterings give rise to constructive and destructive interference from many points from a crystal lattice resulting in a distinct diffraction pattern that can be further recorded on a 2D detector. This unique diffraction pattern is provides information of intensities and geometrical arrangement of the reflections by calculating the intensities and the positions of the diffraction spots and basic geometric parameters of experimental setup. This information can later be used for indexing, which determines the identical units that form the crystal (unit cell), and their internal symmetry (space group). Diffraction intensities contain partial information about the structure of the molecules and their arrangement that is not described by crystallographic symmetry (asymmetric unit). However, the detector is not capable of measuring the phases of X-ray beams, a challenging requirement for structure determination, known as the “phase problem”.

To solve the phase problem, one of the common approaches is molecular replacement [245]. In MR, we make a guess of the conformation of a protein and use prior structural information. This approach is used when we have a closely related protein structure for a reasonably large fraction of the protein in hand. We can test our guesses by calculating

diffraction patterns and comparing them to the observed one. If a guess places the atoms in about the right places, then the calculated phases will be approximately correct and a useful electron density map can be computed by combining the observed amplitudes with the calculated phases. If the model is somewhat accurate, this map will show features missing from the model and later we can improve the model.

The other approaches that are commonly being used to solve the phase problem are experimental phasing methods, such as isomorphous replacement (IR) and anomalous dispersion (AD). These techniques are more difficult and time-consuming approaches than molecular replacement. In isomorphous replacement, a change by adding a heavy atom to the crystal structure is made that will perturb the structure factors. Based on how they are perturbed, we can predict possible phase values. All of the electrons in a heavy atom scatter essentially in phase with one another. Therefore, they change the scattered intensities significantly by contributing disproportionately to the overall intensity. On the other hand, the contributions from the lighter atoms in this condition tend to cancel out, as they scatter with different phase angles. This technique enables us to explain the change to the crystal with only a few parameters. Anomalous dispersion includes single and multiple anomalous dispersions (SAD and MAD, respectively), and is based on the anomalous x-ray scattering by one or multiple heavy atom(s) incorporated into the protein crystals. This technique allows us to indirectly measure the phases by comparison of differences in intensities of the scattered beams in the presence and absence of anomalous scattering.

Crystallography is the most powerful technique that can provide high-resolution structural information with atomic resolution from the crystallized, rigid state of the molecule. However, it does not provide insights into the dynamics of the macromolecules in solution. Moreover, the intermolecular interactions that form the crystals can potentially alter its conformation. Besides, not all proteins crystallize and proteins with long flexible/unfolded regions do not typically form highly ordered crystals.

2.1.2 Small-angle X-ray scattering (SAXS)

To confirm the validity of the crystal structures in solution and to reveal aggregation states of a protein, a technique called small-angle X-ray scattering (SAXS) is often used. SAXS is fundamentally similar to X-ray crystallography, in which an intense beam of X-ray is used to obtain structural information about the sample. The advantage of SAXS over crystallography

is that a crystalline sample is not required. Moreover, SAXS analysis can be applied to flexible proteins that do not easily crystallize. However, due to the random orientation of molecules in solution or partially ordered molecules, the spatial averaging leads to loss of information compared to crystallography and the scattering intensity is radially symmetric.

In SAXS, the elastic scattering intensities of X-rays I(q) are recorded at very small angles q (Ang^{-1}) when travelling through the protein sample in solution. This angular range provides information about the shape and size of macromolecules. The intensity of diffractions increases exponentially with the particle size, and the scattering intensity decays with increasing angle between the incident and scattered beams, generating the scattering profile on a 2D detector. As scattering intensity exponentially increases with the particle size in SAXS, mono-dispersed aggregation-free sample with no impurities is required to obtain reliable information, whereas even a tiny amount of aggregated protein in solution may result in a multi-dispersed solution.

A useful piece of SAXS information addressing monodispersity of protein sample is the radius of gyration (R_g). R_g is an indicator of how the mass of a particle is distributed around the center of mass and is defined as the root mean square of the distances between points in the particle and the center of gravity. Rg can be measured using a Guinier or a Kratky plot.

The scattering profile is in reciprocal space and can be processed by the program GNOM to generate the pair distance distribution function P(r) plot [249]. The P(r) function represents the histogram of distances between pairs of points within the particle, thus the plot shows the dimensions of the particle in real space, and instantly provides the maximum dimension of the molecule (D_{max}) as P(r) gradually falls to zero at D_{max}.

The information extracted from SAXS studies can also be combined with crystal structures and provide information about the dynamics of the protein and its conformation in solution [250].

2.1.3 Nuclear magnetic resonance (NMR)

NMR is a very powerful technique that can map the interacting site of proteins upon binding to their ligands. While most biophysical techniques have limitations characterizing ligand binding to a protein of interest, NMR titrations are not only able to detect the binding, but also could display where it binds. This technique is based on analyzing $^{1}H,^{15}N$ heteronuclear single quantum correlation (HSQC) spectra of the ^{15}N-labeled protein. In order to label a protein

with ^{15}N isotopes, we have to express the protein in minimal medium that contains $^{15}NH_4Cl$ as the only source of nitrogen. Many peaks in a HSQC spectrum correspond to backbone amides in the protein; thus, we see roughly as many peaks as the number of residues in the protein. An HSQC spectrum is like a "fingerprint" of the protein and correlates the chemical shift of protons with the chemical shift of the directly bonded nitrogens. Chemical shifts are sensitive to the chemical environment of the two nuclei that make NMR a sensitive technique to map the interacting site of a protein with its binding partner.

In a set of NMR titrations, the spectrum of the ^{15}N-labelled protein is first recorded. The spectra are then recorded upon addition of increasing amounts of its unlabeled partner. If there is an interaction between the two, some peaks show changes in the chemical shifts or peak broadenings. These shifts can be due to perturbation of chemical shifts of the residues at the interface by the proximity of the partner, or by inducing structural changes in the protein itself upon the addition of the partner. The dissociation constant of the binding can be measured by measuring the chemical shift. The mapping of the chemical shifts on the protein structure can give us information on the binding interface. When the produced complex is large, the tumbling rate of molecules in solution becomes slower which leads to peak broadening and disappearance.

2.1.4 Isothermal titration calorimetry (ITC)

Isothermal titration calorimetry (ITC) is a quantitative methodology that can determine the thermodynamic parameters of interactions in solution including the binding affinity between two macromolecules or a macromolecule and a small ligand. The isothermal titration calorimeter is composed of two cells that are enclosed in an adiabatic jacket. One macromolecule of interest is placed in the sample cell, while the possible ligand (a macromolecule or a small molecule) is injected in precisely known aliquots into the sample cell with a syringe. The buffer in which the samples are both dissolved in is also placed in a reference cell, to be used as a control. Sensitive circuits are then used to detect temperature differences between the reference cell and the sample cell and a heater is used to maintain equal temperatures between the sample and reference cells. Addition of ligand into the sample cell causes heat to be either taken up or released (depending on the nature of the reaction). The measurements of heat as a function of molar ratio are then analyzed to give the thermodynamic parameters of the interaction.

2.2 Materials and methods

2.2.1 Constructs

Full-length *Rattus norvegicus* (85% identity to human parkin) parkin DNA was codon-optimized for *E. coli* expression (DNAexpress Inc., Montreal, Canada). The genes were then synthesized using the gene assembly method and then cloned into the *Bam*HI and *Xho*I restriction sites of the pGEX-6P-1 plasmid (GE Healthcare). Construct for parkin R0-RBR (141-465) was sub-cloned from the full-length construct using the following primers: 5'-CCGGCGGGATCCCCGACCTACCACTCTTTCTTC-3'(forward) and 5'-CTAGCTCGAGCT AAACGTCGAAC-3' (reverse). The fragment was amplified by PCR, digested with *Bam*HI and *Xho*I, and ligated into the pGEX-6p1 plasmid. Parkin deletion constructs (77-465, 95-465, 141-465, 220-465) were generated by PCR amplification from *Rattus norvegicus* full-length parkin. All other parkin mutants (L266K, N273K, L266K R0-RBR and N273K R0-RBR) were prepared using the QuikChange Lightning Multi Site-Directed Mutagenesis Kit (Agilent), following the protocol provided with the kit. Minipreps were performed using the QIAprep Spin Miniprep Kit from QIAGEN. Mutagenesis was confirmed by Sanger sequencing, done by the Genomics Platform at the Institut de Recherche en Immunologie et Cancérologie at the University of Montreal. The pET28a-LIC-UbcH7 vector was a gift from C. Arrowsmith (Structural Genomics Consortium, Toronto, Canada).

2.2.2 Protein expression and purification

Protein expressions were done in BL21 (DE3) E. coli cells. All proteins were grown in Luria broth (LB) until the optical density (OD) at 600 nm reached 0.6-0.8. Then the temperature was lowered, and isopropyl β-D-1-thiogalactopyranoside (IPTG) was added to induce expression. Parkin constructs were induced overnight at 16ºC using 25 μM IPTG and 250 μM zinc chloride, while UbcH7, SH3 and Ubl constructs were induced for 3 hours at 28 ºC using 500 μM IPTG, and PINK1 was induced overnight at 16ºC using 100 μM IPTG. ^{15}N-labeled proteins were produced in M9 minimal medium supplemented with ^{15}NH4Cl.

Parkin proteins were purified by GST-Sepharose 4B (GE healthcare) and eluted with 20 mM reduced glutathione in 20 mM Tris, 120 mM NaCl, 2 mM DTT, pH 7.4. Eluted proteins were used without buffer-exchange for ubiquitination assays with GST-parkin. To produce untagged parkin constructs for crystallization, the GST-purified protein was further cleaved with PreScission

protease overnight at 4ºC and applied onto Superdex 75 16/60 size exclusion column (GE healthcare) in 20 mM Tris pH 7.4, 150 mM NaCl, 2 mM DTT. The peak containing cleaved parkin was reapplied onto fresh GST-Sepharose 4B to remove traces of GST and concentrated. To produce untagged parkin constructs for ubiquitnation assays, the GST-purified proteins were cleaved with PreScission protease overnight at 4ºC and buffer-exchanged into 10 mM HEPES pH 7.0, 50 mM NaCl, 0.5 mM TCEP using Zeba desalting spin column (Thermo). GST-*Tc*PINK1 (143-570) was purified in a similar manner to parkin, as previously described [122]. His6-tag UbcH7 was purified by Ni-NTA (Qiagen) followed by gel-filtration on Superdex 75 16/60 (GE healthcare).

Phosphorylated ubiquitin was produced and purified as previously described [251] using GST-*Tc*PINK1. Phosphorylated Ubl and parkin were produced and purified according to a published procedure [199]. Protein concentrations were determined using UV.

GST-SH3 was purified by glutathione-Sepharose affinity and eluted with 20 mM glutathione, followed by 3C cleavage for untagged SH3, and size-exclusion chromatography on Superdex 75 16/60 (GE Healthcare) in 20 mM Tris pH 7.4, 120 mM NaCl, 1 mM DTT.

2.2.3 Protein crystallization

Crystals of parkin R0-RBR were grown at 4°C using hanging drop vapor diffusion method by mixing 1 µl of protein at 12 mg/ml in 15 mM Tris pH 8.0, 0.2 M NaCl, 10 mM DTT and 1 µl of mother liquor containing 0.9 M sodium malonate pH 7.0, 0.1 M HEPES pH 7.0, 5% (v/v) glycerol, 56 mM β-mercaptoethanol. Crystals appeared after a week and reached their maximal size of 50 µm x 50 µm x 200 µm after three weeks. Crystals were cryoprotected in a solution of 2 M sodium malonate pH 7.0, 0.1 M HEPES pH 7.0, 5% (v/v) glycerol before being flash-frozen in liquid nitrogen. Crystals of full-length parkin were grown at 4°C using hanging drop vapor diffusion method by mixing 1 µl of protein at 7 mg/ml in 20 mM Tris pH 7.4, 2 mM DTT and 1 µl of mother liquor containing 22.5% PEG3350, 0.2 M $(NH_4)_2SO_4$, 0.1 M HEPES pH 7.0, 10% (v/v) glycerol, 3% sorbitol and 25 mM β-mercaptoethanol.

2.2.4 Data collection and structure determination

Diffraction data for parkin R0-RBR were collected at the CMCF beamline 08ID-1 at the Canadian Light Source (Table 3.2). A total of 250 images with an oscillation angle of 1° were measured at the Zn K-edge. Reflections were integrated using Mosflm [252] and scaled with

SCALA as implemented in the CCP4 package [253]. The structure was solved by SAD using AutoSol as implemented in the PHENIX package [254]. Twenty-four zinc sites were found corresponding to 3 molecules in the asymmetric unit. The model was built using the program COOT [255], and was refined using the program PHENIX. No explicit non-crystallographic symmetry restraints and no Translation-Libration-Screw-rotation (TLS) were used during refinement.

Low-resolution data for full-length parkin were collected at the F1 beamline at the Cornell High Energy Synchrotron Source (Table 3.2). Reflections were integrated and scaled using HKL2000 (HKL Research Inc.). The structure was determined by molecular replacement using Phaser [256]. A first molecular replacement search was performed using trimer from the R0-RBR crystal structure as a search model. The solution (Z-score > 20) consisted of four trimers in each asymmetric unit (12 molecules in total). In a second molecular replacement round, the crystal structure of murine parkin Ubl (PDB 2zeq [257]) was used as a search model, using the solution of the first search. One copy of the Ubl was found (Z-score > 9) and applied to all twelve chains using non-crystallographic symmetry operators. Rigid-body refinement was performed with PHENIX, treating the Ubl, IBR and RING0-RING1-REP-RING2 as distinct rigid bodies.

Coordinates and structure factors of the R0-RBR and full-length parkin crystal structures were deposited in the Protein Data Bank under accession codes 4K7D and 4K95.

2.2.5 SAXS experiments

Small-angle X-ray scattering data of R0-RBR and full-length parkin (in chapter 3) were collected on in-house Anton Paar SAXSess camera equipped with a PANalytical PW3830 X-ray generator and a Roper/Princeton CCD detector. The beam length was set to 18 mm, and the beam profile was recorded using an image plate for subsequent desmearing. Scattering data were collected at 20°C using different protein concentrations 2.9, 5.5, and 11.0 mg/ml for 3, 6 and 3 hours respectively for R0-RBR; 3.0 and 6.0 mg/ml, both for 6 hours for W403A R0-RBR; and 2.5, 5.0 and 10.0 mg/ml all for 1 hour for full-length parkin. Background scattering from the buffer (20 mM Tris pH 7.5, 150 mM NaCl, 8 mM DTT) was measured for 6 hours. Data were recorded by CCD camera for all constructs, except for W403A construct that image plate was used. Dark current correction, scaling, buffer subtraction, binning, desmearing and merging were performed using SAXSquant 3.0 (Anton Paar). Small-angle X-ray scattering data in chapter 4 were collected on SIBYLS beamline (12.3.1) at the Advanced Light Source at Lawrence Berkeley National

Laboratory. Scattering data were collected at 20°C at protein concentrations of 2, 4 and 8 mg/ml for 0.5-1 sec for Δ86-130 parkin, L266K parkin and at 1.5, 3, and 6 mg/ml for 0.5-1sec for R0-RBR; R0-RBR-pUb complex, full-length parkin; pParkin, pParkin-pUb complex and W403A parkin. Background scattering from the buffer (50 mM Tris pH 8.0, 150 mM NaCl, 2% glycerol, 10 mM DTT) was measured for 0.5-1 sec. Scaling, buffer subtraction, and merging were performed using ATSAS [258]. The merged scattering curve was fitted to individual chains in the crystal structure using *CRYSOL* [259]. The pair-distance distribution were calculated using *GNOM* [249]. Molecular mass were estimated using the Porod volume method [258] or the Q_R method [260].

Ab initio shape calculations were performed using the program *GASBOR* against intensity in reciprocal space [258]. Forty models were generated with $\chi^2 < 2$ and averaged using *DAMAVER* [258]. The R0-RBR structure (PDB 4K7D, chain A) was superposed to the averaged *GASBOR* model using *SUPCOMB* [258]. Rigid-body modeling of the R0-RBR-pUb complex was performed with *CORAL* [258], using the crystal structure of R0-RBR (PDB 4K7D, chain A) and the major conformation of pUb (PDB 4WZP, chain A) as input models. Calculations were performed with two different distance restraints based on the conserved sulfate-binding sites: Ser65 was set to be within 10 Å (Cα-Cα) of either H302/R305, or K161/K211. Because the SAXS data could not be fitted by simple rigid-body fits, the IBR domain was allowed to move. Flexible linker residues were defined as G328-G329 (between RING1 and IBR), and M380-Y391 (between IBR and REP). Forty models were generated, and the 10 models with the lowest χ^2 (< 2) and penalty (< 1) were selected.

2.2.6 Autoubiquitination assays

Ubiquitination assays in chapter 3 were performed at 37°C in the presence of 50 mM Tris pH 7.5, 50 mM NaCl, 0.5 mM DTT, 2 mM ATP, 10 mM MgCl2, 40 nM E1, 2-4 μM UbcH7 and 1 μM untagged parkin or GST-parkin. Reactions were stopped with 3X sample buffer containing 100 mM DTT and analyzed by SDS-PAGE. Proteins were then transferred to nitrocellulose and stained with Ponceau. Membranes were blocked with 5% milk in PBS-T (0.1% Tween 20) and incubated with mouse anti-ubiquitin (Covance) or rabbit anti-parkin (Abcam ab15954) diluted in PBS-T with 3% bovine serum albumin (BSA). The membrane was washed with PBS-T and incubated with HRP-coupled goat anti-mouse or anti-rabbit (Jackson Immunoresearch). Detection was performed with Western Lightning ECL (Perkin Elmer).

Ubiquitination assays in chapter 4 were performed for 45 min at 37°C in the presence of 50 mM Tris pH 7.5, 120 mM NaCl, 1 mM DTT, 4 mM ATP, 50 μM ubiquitin, 10 mM $MgCl_2$, 50 nM E1, 2 μM UbcH7 and 2.5 μM parkin with or without 5 μM of pre-phosphorylated ubiquitin. Reactions were stopped with the addition of SDS-PAGE sample buffer containing 100 mM DTT and analyzed by gel electrophoresis and Coomassie staining.

Parkin Ubiquitination assays in chapter 5 were performed for 45 min at 37 °C in the presence of 50 mM Tris pH 7.5, 120 mM NaCl, 1 mM DTT, 4 mM ATP, 50 μM ubiquitin, 10 mM $MgCl_2$, 50 nM E1, 2 μM UbcH7, and 2.5 μM parkin with or without 200μM of SH3. Reactions were stopped with the addition of SDS–PAGE sample buffer containing 100 mM DTT and analyzed by gel electrophoresis and Coomassie staining. Quantification of parkin autoubiquitination was performed using ImageJ (v1.51, NIH).

2.2.7 NMR spectroscopy

^{15}N-labeled UbcH7, Ubl, pUbl, and pUb and unlabeled parkin constructs (full-length, R0-RBR, W403A parkin, L266K R0-RBR, W403A R0-RBR, pParkin, and A240R/W403A parkin) were buffer-exchanged into NMR buffer (20 mM Tris, 100 mM NaCl, 2 mM DTT, pH 7.4). All samples were processed in a similar manner and the pH was the same for all samples used in comparisons. pUb was added to pParkin and parkin in excess (1:2 molar ratio) to form the complex. The pUb/R0-RBR complex was purified by size-exclusion chromatography in NMR buffer. Titrations were performed by adding unlabeled parkin proteins to 0.03-0.2 mM ^{15}N-labeled proteins to obtain the molar ratios indicated. ^{1}H-^{15}N correlation spectra were acquired at 293 K at field strengths of 600 MHz Bruker spectrometer (Fig 3.19C, 4.11B and 4.11E) and 800 MHz Varian spectrometer (Fig 3.11, 3.19B, 4.2B, 4.2C, 4.5, 4.11A, 4.11C and 4.11D) both equipped with a triple-resonance (^{1}H, ^{13}C, ^{15}N) cryoprobe. Spectra were processed using NMRpipe [261] and analyzed with NMRView J (One Moon Scientific) and adjusted to account for differences in concentration and acquisition time. ^{15}N-^{1}H backbone assignments for UbcH7 were obtained from the BMRB entry 15498 [262]. ^{15}N-^{1}H backbone assignment for Ubl and pUbl were obtained using ^{15}N-NOESY/TOCSY experiments for ^{15}N-labeled proteins and HNCACB and CBCA(CO)NH for ^{13}C,^{15}N-pUbl. Weighted chemical shift perturbations were calculated according to the equation $(\Delta HN^2 + (0.2*\Delta N)^2)^{1/2}$.

^{15}N-labeled SH3 (chapter 5) and unlabeled constructs (Ubl, pUbl, pUb, full-length parkin) were buffer-exchanged into NMR buffer (20 mM Tris, 120 mM NaCl, 2 mM DTT, pH 7.4). All

samples were processed in a similar manner, and the pH was the same for all samples used in comparisons. pUb was added in 10 % excess to pParkin and parkin to form the pUb complexes. The titrations in Fig 5.3B were performed by adding 20, 30, 60, 120 µl of ^{15}N-labeled SH3 to 300 µl of 400 µM unlabeled Ubl, pUbl, and 110 µM parkin to obtain the molar ratios indicated. The titrations in Fig 5.3D were performed by adding 5 mM ATP and 10 mM $MgSO_4$, 220 µM pUb, 200 µM parkin, and 10 µM PINK1 to 200 µM ^{15}N-labeled SH3 protein. ^{1}H-^{15}N correlation spectra were acquired at 20 °C at a proton frequency of 600 MHz. Spectra were processed using NMRpipe [261] and analyzed with NMRView J (One Moon Scientific) and adjusted to account for differences in concentration and acquisition time. Dissociation constants were estimated by least-square minimization of the mean-squared chemical shifts difference calculated according to the equation:

$$C = C_{max}\frac{K_d + P_{tot} + L_{tot} - \sqrt{(K_d + P_{tot} + L_{tot})^2 - 4P_{tot}L_{tot}}}{2P_{tot}}$$

where C is the chemical shift perturbation, $C_{\max}$ is the chemical shift perturbation at saturation, K_d is the dissociation constant, P_{tot} is the total concentration of the labeled protein, and L_{tot} is the total ligand concentration.

2.2.8 Cell culture and plasmid DNA

HeLa cells were maintained in Dulbecco's modified Eagle's medium (DMEM) supplemented with 10% FBS, 4 mM L-glutamine, and 0.1% Pen/Strep and maintained in a 37°C incubator with 5% CO2. *Homo sapiens* full-length parkin was cloned in pEGFP-C2 (Clontech) and mutated by PCR mutagenesis. Construct expression was verified by immunoblotting using rabbit anti-GFP (Invitrogen) and mouse anti-VDAC1 (Abcam, ab14734) as a loading control [203].

2.2.9 Mitochondrial GFP-parkin recruitment time-lapse microscopy

HeLa cells (1.5x105) were seeded onto a 35mm Glass Bottom Microwell Dish (MatTek Corporation, Ashland, MA) 24 hours prior to transfection with 2 µg of eGFP-parkin wild-type, W403A or C431S plasmid DNA using GeneJuice® (EMD Millipore) according to the manufacturer's protocol. After 24 h, cells were transferred onto a heated stage maintained at 37°C and at 5% CO2 using a Zeiss temperature controller and cell perfusion system (Carl Zeiss, Thornwood, NY). To visualize mitochondria, cells were transduced with CellLight®

mitochondria-RFP (Invitrogen) as per the manufacture protocol. Cells were treated with carbonyl cyanide m-chlorophenyl hydrazone (CCCP) (Sigma), at a final concentration of 20 μM. Microscopy was performed 24 hours post-transfection on a Zeiss AxioObserver. Z1 inverted fluorescent microscope for a total of 2 hours. Images were acquired with a 20x objective (Plan-Apochromat) with a side-mounted AxiocamMRm camera, using the Zeiss XBO75 Xenon illumination system and detected using the appropriate filters. Images were taken at 1 minute intervals for 2 h [203].

2.2.10 PINK1-dependent GFP-parkin recruitment confocal microscopy

HeLa cells were transfected with 10 nM non-targeting or PINK1 SMARTpool® ON-TARGETplus siRNA (Dharmacon, Thermo Scientific) using Lipofectamine RNAiMAX (Invitrogen) according to the manufacturer's protocol for reverse transfections. Knockdown efficiency after CCCP treatment was tested separately by immunolotting using rabbit anti-PINK1 (Novus, C8830) and mouse anti-actin (EMD Millipore) as a loading control. After 24 h, cells were transfected with GFP-parkin WT or W403A using jetPRIME® (Polyplus Transfection). After another 24 h, cells were treated for 3 h with 20 μM CCCP and fixed with 4% formaldehyde in PBS. After washing and blocking with 3% BSA, cells were incubated with rabbit anti-Tom20 (Santa Cruz) followed by Alexa Fluor® 555 donkey anti-rabbit (Invitrogen). Images were acquired with a 63x Plan Apo oil objective using a Zeiss LSM710 confocal microscope.

2.2.11 Isothermal titration calorimetric assays

ITC measurements were carried out at a constant temperature of 20°C using VP-ITC (Malvern) for the experiment in chapter 3 and ITC200 (Malvern) for experiments in chapter 4. Samples were in 50 mM Tris pH 7.4, 150 mM NaCl, 1 mM TCEP. Data were analyzed using Origin v7 software. Protein concentrations in the cell and syringe are indicated in the figures. The stoichiometry was determined experimentally for Ubl and pUb titrations (Fig 4.2A and table 4.2), and generally refined to values between 0.8 and 1.0.

2.2.12 Pull-down assays

In vitro pUb pull-down assays with R0-RBR variants (Fig 4.7A and 4.7B) were performed using 1 nmol of His-ubiquitin previously phosphorylated by PINK1 and 25 μl of Ni-NTA resin (Qiagen). The His-bound resin was incubated for 15 min with 1 nmol of R0-RBR wild-type,

K161N, K211N, R271A, R275A, H302A, R305A, R314A, R334A, K369A and GST, in TBS with 2 mM BME with 0.02% [v/v] Igepal 630. The resin was washed with 3 x 1 ml of buffer for 30 s and eluted with 25 µl of SDS-PAGE loading buffer containing 0.3 M imidazole pH 8.0. The products were resolved using 12% Tris-Tricine SDS-PAGE and stained with Coomassie Brilliant Blue.

In vitro parkin (wild-type and mutants), Ubl and Ub (modified and unmodified) pull-down assays (Fig 5.2B, 5.3A, 5.3B and 5.3D) were performed using 200 µg of GST-SH3 and 25 µl of glutathione–Sepharose resin (Pierce). The GST-bound resin was incubated for 15 min with 50 µg of Ubl, pUbl, Ub, pUb, parkin, pParkin, parkin/pUb (1:1) molar ratio, pParkin/pUb complex (the complex was purified by gel filtration), L266K parkin, N273K parkin in 20mM Tris, 120mM NaCl, 5mM DTT, pH 8 and 0.02% [v/v] Igepal 630. The resin was washed twice with 0.2 ml of buffer for 30 s and eluted with 25 µl of SDS–PAGE loading buffer. The products were resolved using 12.5% Tris-tricine SDS–PAGE and stained with Coomassie Brilliant Blue.

2.2.13 Kinase assay

Parkin phosphorylation assays in chapter 4 were performed with 0.1 µM GST-TcPINK1 (143-570), 50 mM Tris, 100 mM NaCl, 1 mM DTT, 2 mM $MgSO_4$ and 1 mM ATP in a reaction volume of 25 µl at 30°C. The assays in Fig 4.6A included 3 µM parkin wild-type, L266K or H302A as substrates in the presence or absence of 3 µM pUb. The assays in Fig EV3B included 30 µM parkin wild-type in the presence or absence of 30 µM pUb or 30 µM UbS65A. Reactions were quenched by the addition of SDS-PAGE loading buffer. Aliquots of 20 µl (Fig 4.6A) or 2 µl (Fig 4.6B) of the reactions were loaded on 10% Tris-Glycine gels containing 20 µM Phos-tag and 40 µM $MnCl_2$ and visualized with Coomassie stain.

Parkin phosphorylation assays in chapter 5 were performed with 0.02 µM GST-*Tc*PINK1 (143–570), 50 mM Tris, 100 mM NaCl, 1 mM DTT, 2 mM $MgSO_4$, and 1 mM ATP in a reaction volume of 25 µl at 30 °C. The assays included 3 µM parkin wild type, as substrate in the presence or absence of 3 µM pUb and 200 µM SH3. Reactions were quenched by the addition of SDS–PAGE loading buffer. Aliquots of 20 µl of the reactions were loaded on 10% Tris-glycine gels containing 20 µM Phos-tag (Wako Chemicals, Japan) and 40 µM $MnCl_2$ and visualized with Coomassie stain. Quantification of parkin phosphorylation was performed using ImageJ (v1.51, NIH).

2.2.14 Mitochondria isolation and *in organello* ubiquitination assay

HeLa cells treated with 10 μM CCCP or dimethylsulphoxide (DMSO) for 3 h and were suspended in mitochondrial isolation buffer (20 mM HEPES/KOH (pH 7.4), 220 mM mannitol, 10 mM KAc and 70 mM sucrose) on ice. Cells were disrupted by nitrogen cavitation, and mitochondria were isolated using conditions previously described [263]. Mitochondria pellets were suspended in mitochondria isolation buffer to a concentration of 2 mg ml−1 and stored at −80 °C until further use. Forty micrograms of CCCP- or DMSO-treated mitochondria were supplemented with ubiquitination reaction mix (20 nM Ub-activating enzyme 1 (E1), 100 nM of Ub-conjugating enzyme 2 (E2), 5 μM Ub, 1 mM ATP, 5 mM MgCl2 and 50 μM TCEP in mitochondria isolation buffer) and 100 nM of recombinant parkin with or without 200 μM SH3 domain of endophilin A1. After a 30-min incubation at 37 °C, reactions were stopped with 3 × sample buffer with 100 mM DTT and analysed by western blotting. Reactions were loaded on 8% Tris-glycine gels. Proteins were transferred to nitrocellulose and stained with Ponceau. Membranes were blocked with 5% milk in PBS-T (0.1% Tween 20) and incubated with rabbit anti-mitofusin2 (1:2,000, mAb D2D10, Cell Signaling) and rabbit anti-PDH (1:2,000, mAb C54G1, Cell Signaling) diluted in PBS-T with 3% BSA. Membranes were washed with PBS-T and incubated with anti-rabbit IgG antibodies (1:10,000, Cell Signaling). Detection was performed with Clarity Lightning ECL (Bio-Rad) and images acquired with a FluorChem HD2 AIC (Cell Biosciences). Quantification of mitofusin 2 ubiquitination was performed using ImageJ (v1.51, NIH).

Chapter 3: Parkin Autoinhibition

3.1 Abstract

Mutations in the *Parkin* or *PINK1* genes are the leading cause of autosomal recessive form of Parkinson's disease (PD). The gene products, the E3 ubiquitin ligase parkin and the serine/threonine kinase PINK1, are neuroprotective proteins, which act together in a mitochondrial quality control pathway. Parkin is a cytosolic RBR E3 ubiquitin ligase with low basal activity. Upon mitochondrial damage, parkin is activated and recruited simultaneously to the impaired organelle by PINK1. Here, we determined the structure of full-length parkin that shed light on the mechanism of parkin auto-inhibition and parkin's function as a ubiquitin ligase. In this structure, the RING0 domain occludes parkin catalytic cysteine (the ubiquitin acceptor site) Cys431 in the RING2 domain. Moreover, the Ubl domain and a repressor element of parkin REP bind the RING1 domain of parkin and block proposed E2-binding site, whereas disruption of Ubl/RING1 interface increases E2 binding supporting our crystal structure. Mitochondria accumulate damage with age in neurons and the quality of mitochondria is of great importance in aging and neurodegenerative disease. Our crystal structure of parkin provides a structural framework for increasing parkin ligase activity and upregulating mitochondrial quality control mechanism.

3.2 Rationales and hypothesis

Mutations in *Parkin* gene are responsible for early-onset form of PD. Parkin is a 465-residue cytosolic E3 ubiquitin ligase with low basal activity. Upon mitochondrial damage, another PD linked protein kinase PINK1 accumulates on mitochondria and recruits parkin to the damaged organelle and activates it. Activated parkin tags wide range of mitochondrial outer membrane proteins with ubiquitin that leads to the clearance of the impaired organelle by autophagy in a process known as mitophagy. Parkin consists of a ubiquitin-like (Ubl) domain at the N-terminus, followed by RING0 domain, a zinc-finger domain unique to parkin, and RING-Between-RING (RBR) catalytic module. RBR catalytic module contains three additional zinc-finger domains RING1, In-Between-RING (IBR) and RING2. The RBR catalytic module is present in 12 other E3 ubiquitin ligases including Ariadne/HHARI, HOIL, and HOIL-1L interacting protein (HOIP). This class of E3 ubiquitin ligases use a RING/HECT hybrid mechanism in which they form a

thioester intermediate with ubiquitin through a cysteine side-chain in RING2 before transferring ubiquitin to a lysine on substrate proteins forming an isopeptide bond. Over 120 PD mutations were found in every domain of parkin protein and lead to parkin loss of function and impaired mitochondrial translocation. When I started my project, the reasons of why PD parkin mutations were leading to parkin loss of function and impaired recruitment to damaged mitochondria were not clear. In addition, most studied RBR E3 ubiquitin ligases were showing low basal activity with no clear explanation. The only known structural information on parkin at the time was limited to crystal structure of Ubl domain of murine parkin [257] and NMR structure of *Drosophila* IBR domain in solution (Fig 3.1)

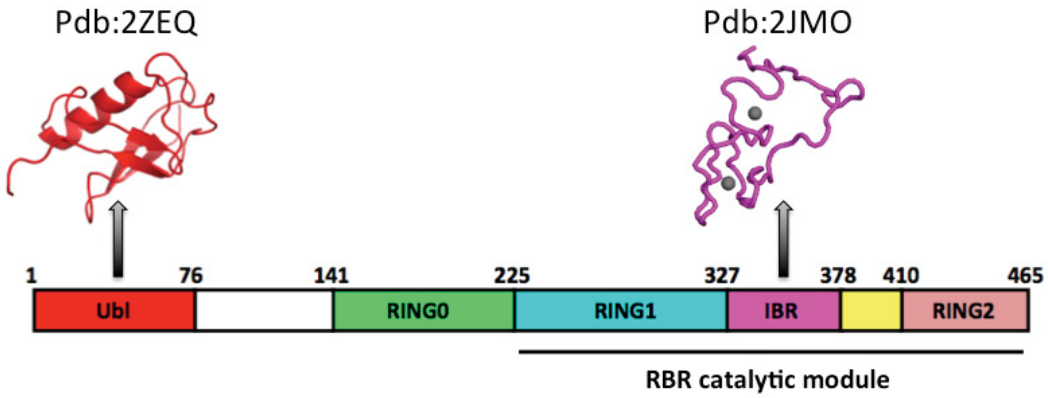

Figure 3.1 Crystal structure of Ubl domain and NMR structure of IBR domain of parkin. Parkin consists of a ubiquitin-like (Ubl) domain at the N-terminus and four zinc finger domains including RING0, RING1, In-Between-RING (IBR) and RING2 domains. The last three domains form the RBR catalytic module. The structure of the Ubl and IBR domains were solved by X-ray crystallography and NMR, respectively. IBR domain binds 2 zinc ions that are shown as grey spheres.

Given the importance of parkin in mitochondrial turnover, it is crucial to gain insight into how parkin autoinhibition is regulated. We hypothesized that parkin autoinhibition is stemmed from interdomain interactions that occlude required sites for the ubiquitin transfer. To gain insight into parkin autoinhibited conformation, our objectives were to:

1. Purify recombinant parkin, crystallize parkin and determine crystal structure of parkin by X-ray crystallography.
2. Perform biophysical analysis to confirm the structure in solution.

3. Assess the role of different parkin domains, interdomain interactions and determine the mechanism of parkin autoinhibition.

Parkin is a difficult protein to work with unless certain precautions are taken [264]. The ligase activity is normally repressed and surprisingly some mutations or heat treatment increase activity [195, 201-203]. The bound zinc ions are required for structural stability and properly regulated enzymatic activity[265]. While supplemental zinc is not required during purification, metal-chelating agents such as ethylenediaminetetraacetic acid (EDTA) need to be avoided since they denature the protein. With a total of 35 cysteine residues, parkin requires a high concentration of a reducing agent such as dithiothreitol to maintain the cysteine thiols reduced and available for coordinating zinc ions. [86]

3.3 Results

3.3.1 Crystallization of full-length parkin

Recombinant rat full-length parkin was expressed and purified as explained in Chapter 2. Upon purification, parkin was dialyzed against 20 mM Tris, 2 mM DTT, pH 7.4 at 4°C overnight and concentrated to 7 mg/ml. Multiple crystallization screens were set up using 7 mg/ml and 3.5 mg/ml (2 times dilution in the same buffer) protein at room temperature and 4 °C to crystallize parkin. 1 µL of β-mercaptoethanol (14.3 µM) was added to each crystallization condition (500 µL) to maintain the cysteine thiols reduced and available for coordinating zinc ions.

The initial hit was observed in the first screen in condition 68 of Classics II (QIAGEN) crystallization screen consisting of 0.2 M ammonium sulfate, 0.1 M HEPES pH 7.5, 12% (w/v) polyethylene glygol (PEG) 3350 (including 25 mM β-mercaptoethanol). However, the crystals were very small and we were unable to harvest and screen them for diffraction. To improve the crystals, we tried optimizing the concentration of protein, salt (NaCl), precipitant (PEG) and buffer of the mother liquor at room temperature, and also at 4 °C. We also tried using different additives to the crystallization drops and to reservoir solutions. I was able to optimize these crystals to larger-size diffracting crystals in a condition containing 0.1 M HEPES pH 7, 0.1 M ammonium sulfate, 3% sorbitol, 10% glycerol, 22.5% PEG 3350, 25 mM β-mercaptoethanol at 4 °C. In this condition, the crystals were growing within few hours and reached their maximum size in less than two days.

These crystals diffracted at 8-10 Å at home source X-ray machine and 6.5-7 Å at synchrotron (Fig 3.2). Different approaches to improve the crystals are listed in Table 3.1.

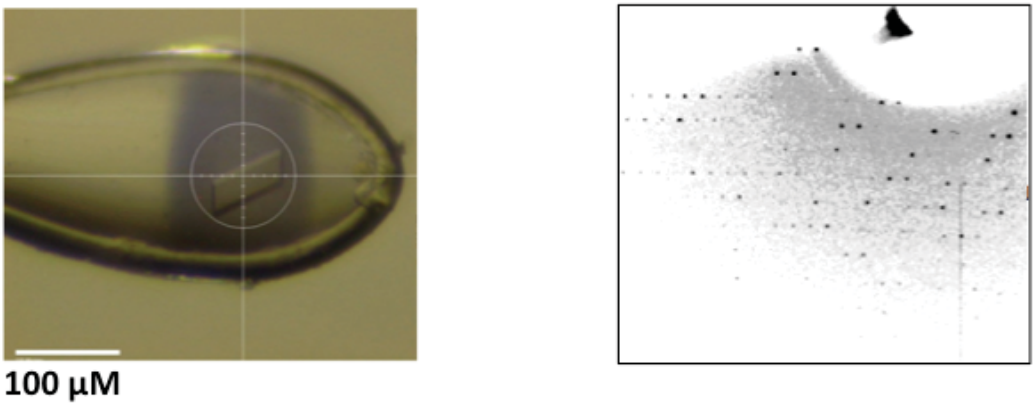

Figure 3.2 Full-length parkin crystal and the diffraction pattern collected. Full-length parkin crystal mounted in a loop and part of the diffraction pattern collected from this crystal at 6.5 Å resolution. The dimensions of the crystal are approximately 100 x 100 x 100 µm.

3.3.2 Truncation of parkin to shorter stable fragments

Protein stability is a fundamental prerequisite for protein crystallization. Finding and crystallizing shorter stable fragments of proteins can often be a key factor in successful structure solution. *In situ* limited proteolysis techniques including trypsinization and chymotrypsinization [8, 266], combined with mass-spectrometric analysis are helpful tactics to identify smaller fragments of protein that are more stable over the time frame of a crystallization experiment [267]. Moreover, solvent exposed, flexible linkers frequently have a negative influence on the quality of protein crystals [268]. Structures of smaller truncated form of proteins are also helpful in solving the structures of larger truncated forms or full-length proteins that diffract poorly using molecular replacement strategy.

Hence, we digested full-length parkin protein with two different proteases, trypsin and chymotrypsin. The digestion was stopped by the addition of formaldehyde and fragments were separated by gel electrophoresis. Gel bands were analyzed by mass-spectrometric analysis and a stable fragment was identified as a truncated form of parkin that lacks the Ubl domain and the following linker. We named this fragment R0-RBR (a.a. 141-465), as it consists of RING0 domain and the RBR catalytic module.

Crystallization condition	Crystallization set up	Protein optimization
Different buffers and pHs	Additive screen (trehalose, sorbitol and dioxane showed some improvement)	Different concentration of parkin, different crystallization drop sizes and ratios
Different concentration of ammonium sulfate and other salts	Different concentration of glycerol as additive in protein sample, precipitant, or both	Parkin with different tags and N-terminal extra residues (no improvement)
Different QIAGEN crystallization screens (No other hits)	Sitting drops and batch crystallization under oil	Chemical modification methylation of lysines in the loops (no improvement)
Different types of PEG	Seeding (no improvement)	Adding binding partners including different E2s (UbcH7 and Ubc7) and SH3 domain of endophilin A1 (no improvement)
Different concentration of PEGs	Set up screens at 4 °C	Different parkin constructs including C431A parkin (catalytically dead) and constructs with deletions at the C-terminal (no improvement)

Table 3.1 Different approaches used to improve parkin crystals.

3.3.3 Structure of parkin R0-RBR

R0-RBR was subcloned into pGEX-6P-1 vector, expressed and purified, as explained in chapter 2. Crystallization trials were set up and better-diffracting crystals were obtained. As expected, deletion of the long, flexible linker improved the diffraction to 2.8 Å resolution. The structure was solved by experimental phasing using zinc anomalous scattering, as there are 8 zinc atoms in a parkin molecule (Fig 3.3) [269].

Three R0-RBR molecules were found in the asymmetric unit (Fig 3.4). Superposition of these three molecules revealed some flexibility for the IBR domain as its position varies by up to 13 Å between different chains in the structure of the C-terminal fragment (Fig 3.5). Superposition of the three chains in the asymmetric unit displayed that R0-RBR molecules adopt the same conformation in all three chains (Fig 3.6). Only a fragment of the linker (residues 391–403) followed by this domain was visible in the structure (Fig 3.5). This fragment contains an α-helix bound to RING1. This helix has been termed the Repressor Element of Parkin (REP) due to its role in the regulation of parkin activity. While the REP in chains A and B is exposed to a solvent channel, it mediates weak crystal contacts in chain C.

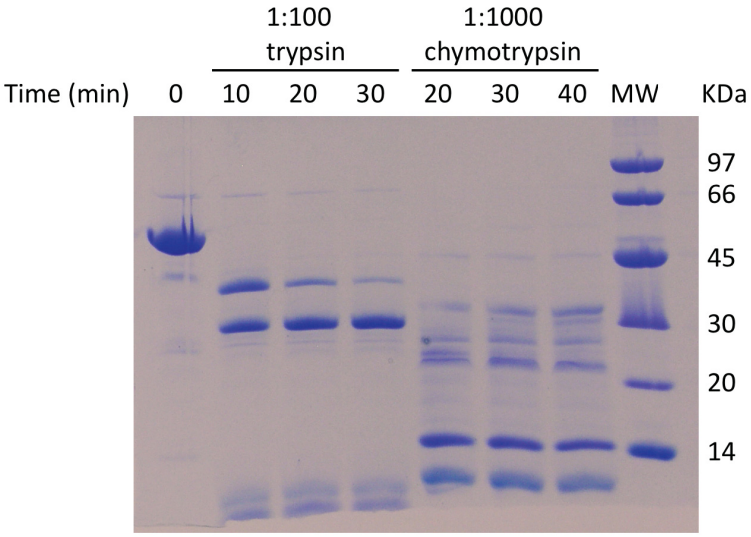

Figure 3.3 Limited proteolysis of parkin by trypsin and chymotrypsin. Parkin was incubated with trypsin and chymotrypsin at 37°C. The reactions were stopped by adding 5% formaldehyde and ran on a 12.5% tris-tricine gel upon addition of 4x lamelli buffer.

3.3.4 Structure of full-length parkin

Using the R0-RBR trimer and murine Ubl structure (PDB 2ZEQ) [257] as search models in molecular replacement, we were able to find the position of the Ubl domain in full-length parkin and solve the structure at 6.5 Å (Fig 3.7). The refinement statistics and the electron density maps are shown in Table 3.2 and Fig 3.8.

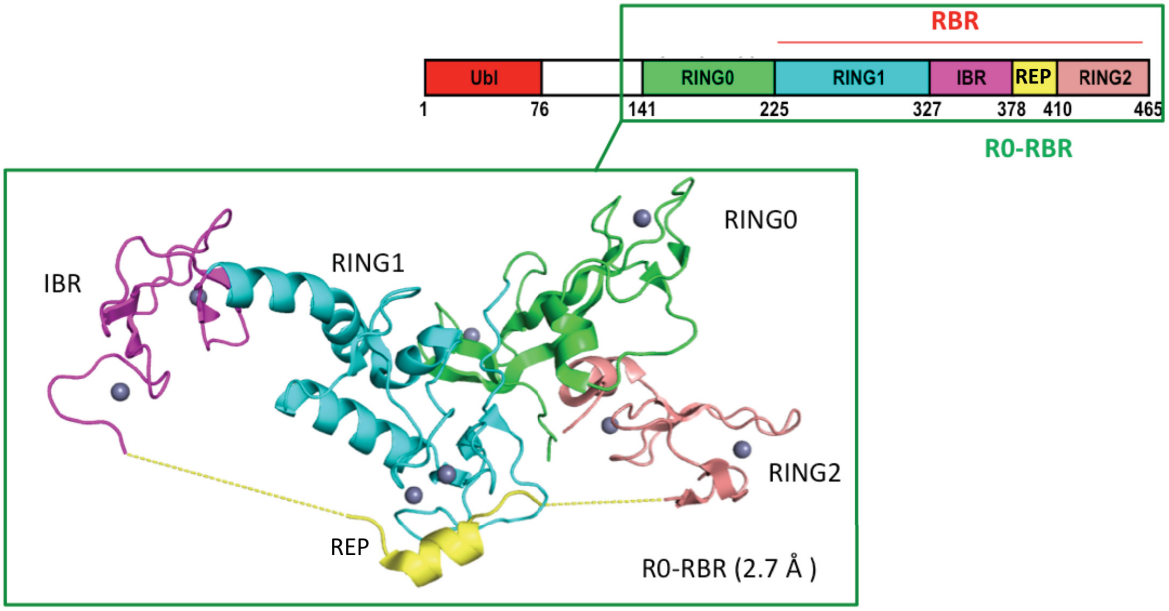

Figure 3.4 Structure of parkin R0-RBR. The ensemble of RING0 (green), RING1 (cyan), In-Between-RING (magenta) and RING2 (salmon) domains is referred to as the R0-RBR module. Structure of parkin R0-RBR was solved at 2.8 Å by SAD. Zinc atoms are shown as spheres.

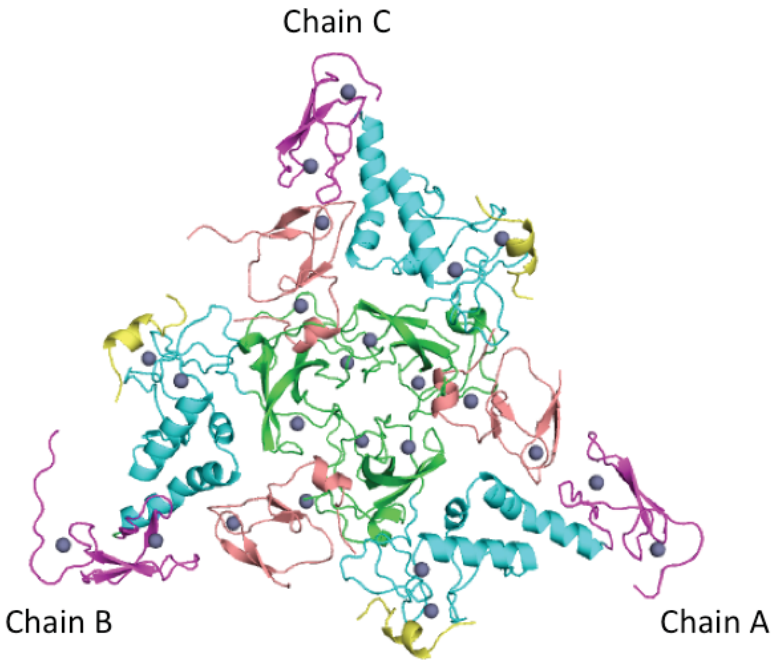

Figure 3.5 Asymmetric unit composition of parkin R0-RBR. Cartoon representation of three parkin chains found in in the asymmetric unit of R0-RBR, colored by domains (RING0, green; RING1, cyan; IBR, magenta; REP, yellow; RING2, salmon). Zinc atoms are shown as spheres.

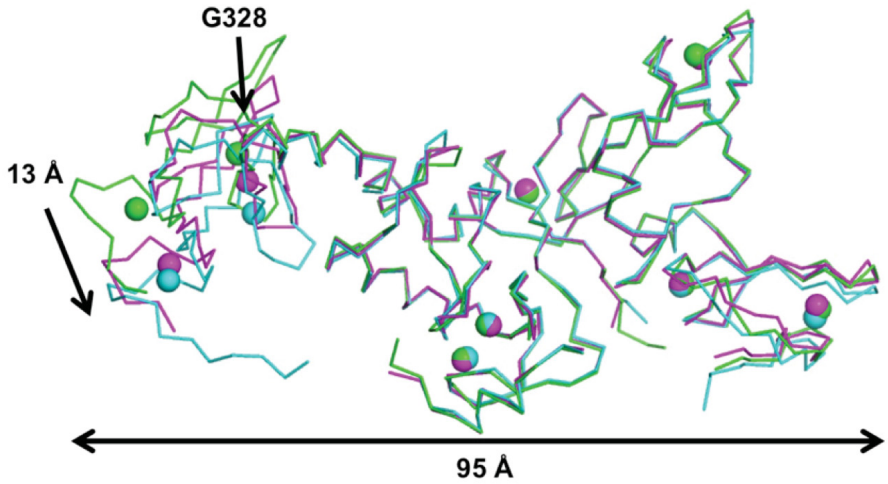

Figure 3.6 Superposition of the three chains in the asymmetric unit of R0-RBR crystal. The structures were superposed by PyMol. Chains A, B, C (green, cyan, magenta) are displayed as Cα trace. Zinc atoms are shown as spheres. The molecules are displayed in similar orientation to Fig 3.3. The REP adopts the same conformation in all three chains. The arrow on the left indicates the distance between the IBR domains in chains A and B. Figure from Trempe *et al.*, 2013 [203].

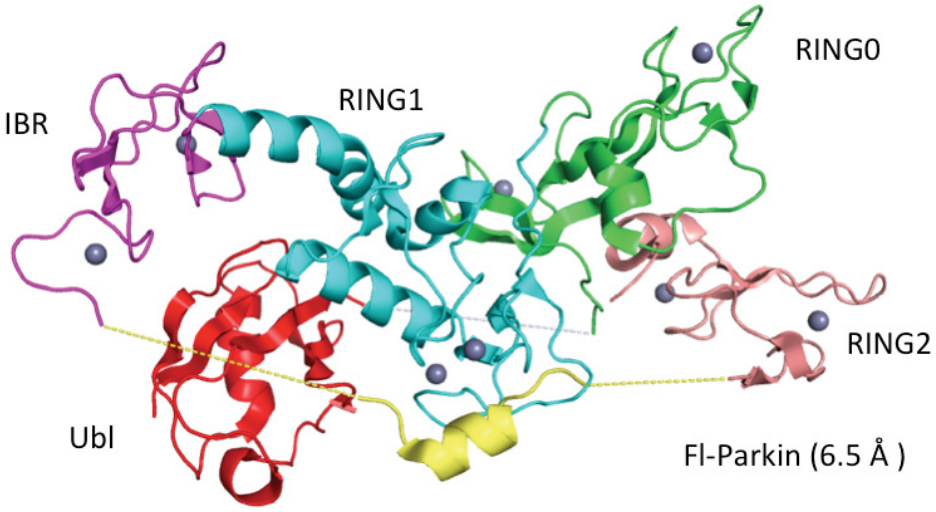

Figure 3.7 Structure of full-length rat parkin at 6.5 Å. Full-length parkin consists of Ubl (red), RING0 (green), RING1 (cyan), In-Between-RING (magenta) and RING2 (salmon) domains. The structure of R0-RBR fragment is similar to R0-RBR crystal structure, whereas this structure provided information about the position of the Ubl domain in the full-length protein.

In the full-length structure the N-terminal Ubl domain is bound to RING1 domain through the hydrophobic surface centered at Ile44 of the Ubl domain interacting with leucine 266, valine 269 and asparagine 273 of the RING1 domain (Fig 3.9). This interaction was consistent with the

reported interaction between the Ubl and the rest of protein (a.a 77-465) [195]. Using ITC, we quantified a K_d of 6.7 (±0.3 μM) between Ubl and R0-RBR (Fig 3.10). Ubl domain of parkin was also reported to bind to ubiquitin-interacting motifs (UIMs) [91, 270, 271] and SH3 domains [88] using the same surface. Moreover, this hydrophobic surface of the Ubl domain is similar to that in ubiquitin and other ubiquitin-like domains.

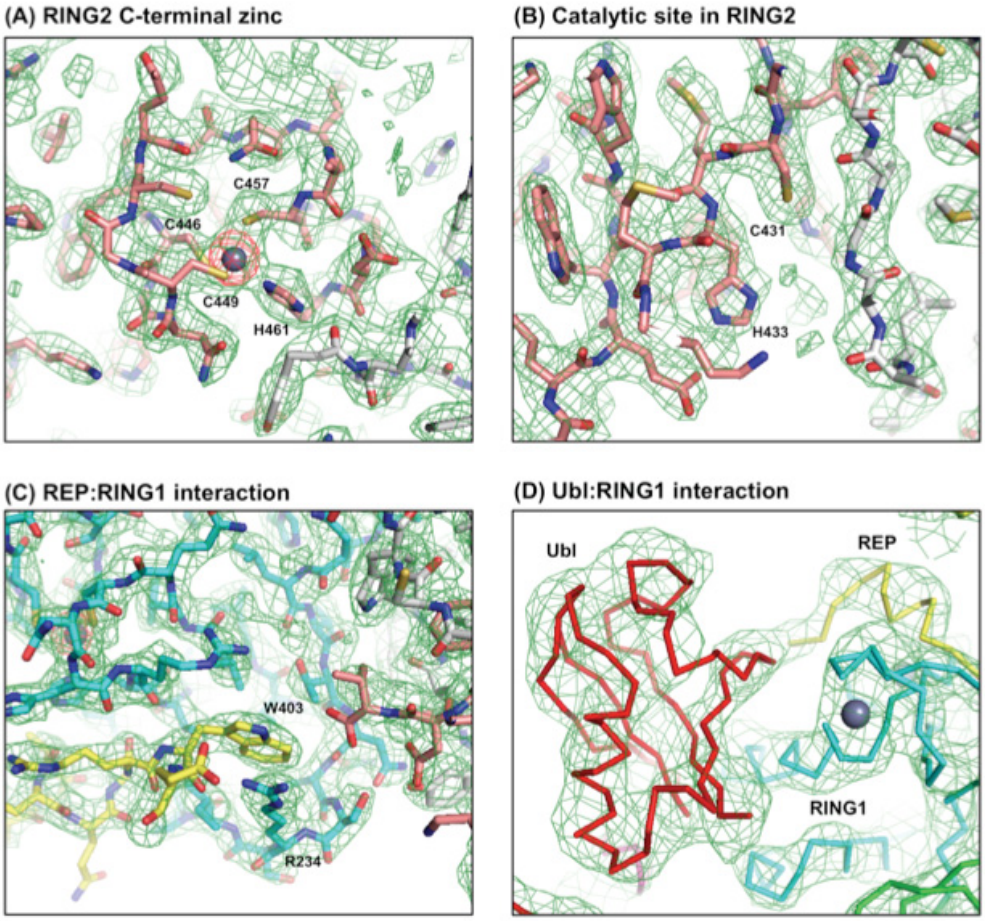

Figure 3.8 Electron density in the crystal structures of Fl-parkin and R0-RBR parkin. (A, B, C) Snapshots of three different regions in the crystal structure of R0-RBR parkin at 2.8 Å resolution. The original SAD-phased, density-modified map is contoured in green at 1.0σ. The anomalous difference map is contoured in red at 10.0σ. The refined structural model is shown as sticks (RING0, white; RING1, cyan; REP, yellow; RING2, pink). Zinc atoms are shown as spheres. (D) Snapshot of a region in the crystal structure of full-length parkin at 6.5 Å resolution. The rigid-body refined 2Fo-Fc density map is contoured in green at 1.0σ. Cα trace of different domains (Ubl, red; RING1, cyan; REP, yellow). Figure from Trempe *et al.*, 2013 [203].

Data collection	**R0-RBR parkin**	**parkin full-length**
X-ray source	CLS 08ID-1	CHESS F2
Wavelength (Å)	1.2824	0.9183
Space group	$P2_12_12_1$	$P2_12_12$
Cell dimensions		
a, b, c (Å)	84.7, 106.6, 154.2	208.6, 277.4, 125.9
α, ß, γ (°)	90, 90, 90	90, 90, 90
Resolution (Å)	53 – 2.80 (2.95 – 2.80)*	53 – 6.50 (6.73 – 6.50)
R_{merge}	0.079 (0.464)	0.172 (0.805)
I/σ(I)	7.3 (1.6)	15.1 (2.5)
Completeness (%)	99.9 (100.0)	99.9 (100.0)
Multiplicity	9.7 (9.7)	7.2 (7.3)
Anom. Completeness (%)	100.0 (100.0)	-
$\Delta F^{+/-}$ correlation half-sets	0.726 (0.061)	-
FOM (phasing)	0.447	-
FOM (density mod.)	0.776	-
Refinement		
Resolution	53 – 2.8	49.3 – 6.5
Used reflections	35,065	14,865
R_{work}	0.18	0.31
R_{free}	0.23	0.33
FOM	0.83	0.72
Number of atoms		
Protein	7,244	35,700
Zn^{2+}	24	96
Water	45	-
Malonate	21	-
Chloride	1	-
B-factors (Wilson)	56	227
Protein, Zn^{2+}	54	-
Water, Chloride	41	-
Malonate	68	-
R.m.s. deviations		
Bond lengths (Å)	0.010	0.011
Bond angles (°)	0.91	1.174
Ramanchandran statistics		
Favoured region (%)	95.4	97.2**
Allowed region (%)	4.6	2.8**
Disallowed region (%)	0	0**

*Data for the highest resolution shell are shown in parentheses.
**Statistics derived from molecular replacement search models.

Table 3.2 X-ray crystallography data collection and refinement statistics for R0-RBR and full-length parkin.

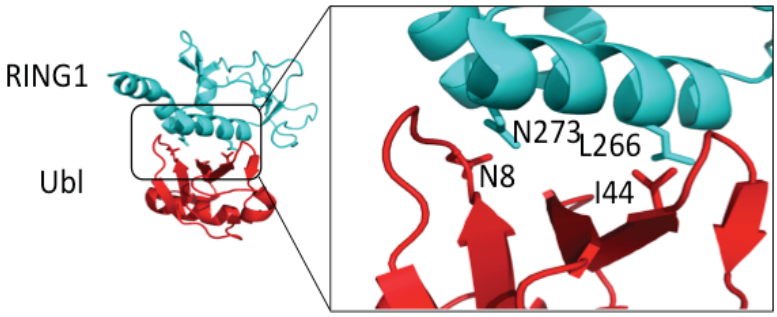

Figure 3.9 Interface between the Ubl domain and RING1 in parkin crystal structure. Zoomed-in view of interface between the Ubl domain and RING1 in the full-length structure. L266 and N273 are facing I44 patch in the Ubl domain of parkin.

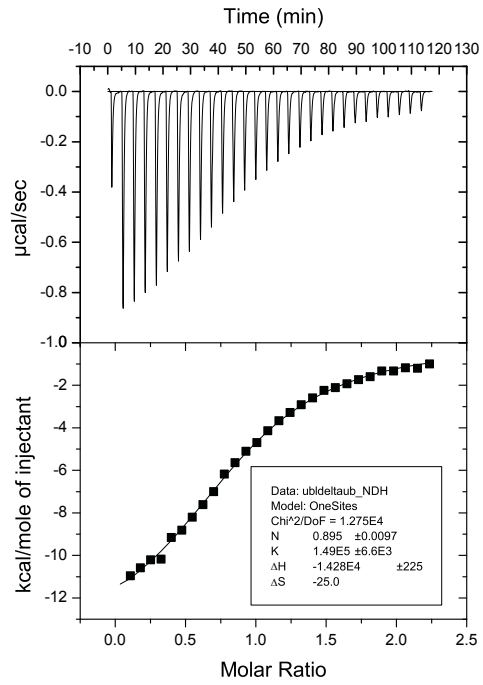

Figure 3.10 ITC measurement of the affinity of parkin Ubl to R0-RBR fragment. The binding affinity (K_d) of the Ubl domain for R0-RBR was measured 6.7 (± 3 µM) under our experimental conditions (50 µM R0-RBR). The value was obtained is in the same order of magnitude as the value reported in the literature for Ubl and delta-Ubl, 2.5 µM [195].

3.3.5 Mutagenesis confirms Ubl position in the low-resolution crystal structure

To confirm the Ubl domain position in the low-resolution crystal structure, three mutations (L266K, V269K and N273K) were designed that would prevent binding of the Ubl domain to RING1, and the interactions between the R0-RBR mutants and the Ubl domain were studied.

These lysines would increase side chain lengths and stericly hindering Ubl binding. Moreover, the positive charge of lysines would create an electrostatic repulsion with the mostly positively charged face of the Ubl domain.

We expressed and purified ^{15}N-Ubl domain and added unlabeled wild type and mutant parkin R0-RBR in a set of NMR titration experiments (Fig 3.11). Ubl signals (Fig 3.11A) disappeared upon addition of wild type R0-RBR (Fig 3.11B), but not the L266K and N273K mutants. (Fig 3.11C). This peak disappearance is due to the formation of a large molecular weight complex, suggesting that the mutations abrogated Ubl binding to R0-RBR.

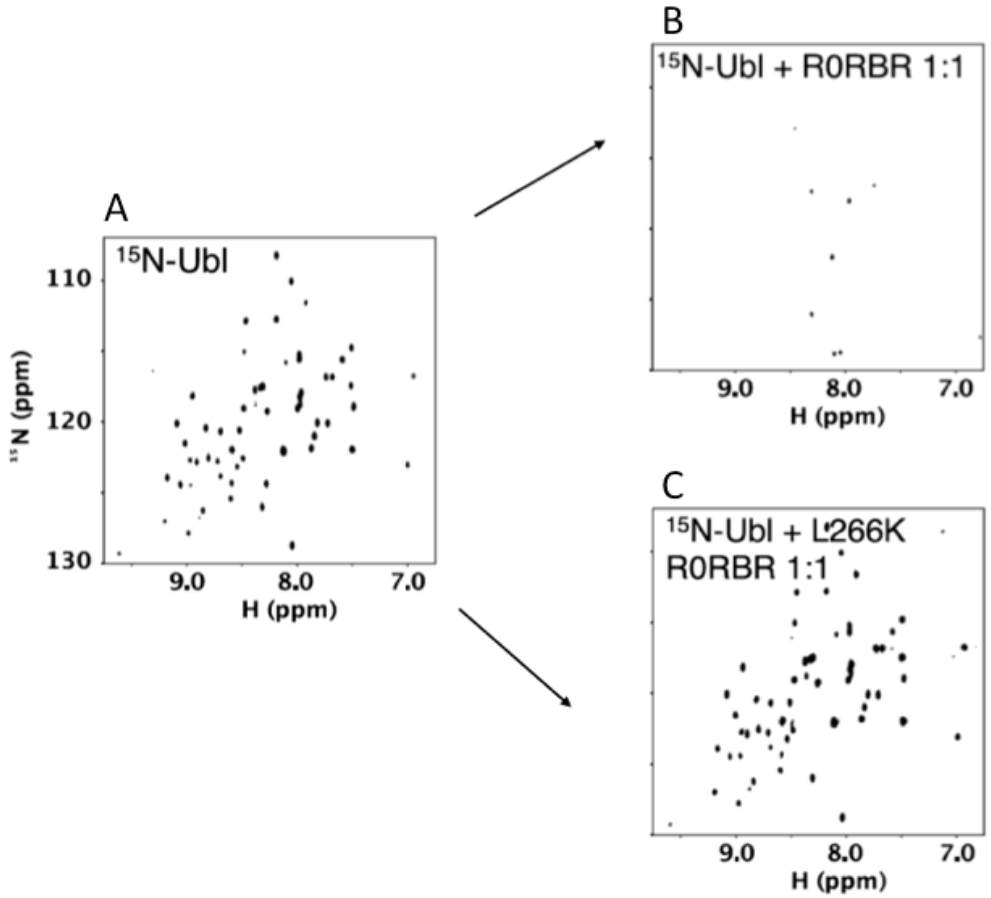

Figure 3.11 NMR titration of ^{15}N-Ubl domain with wild type and L266K R0-RBR parkin. (A) HSQC spectrum of ^{15}N-Ubl before addition of parkin (B and C) HSQC spectra of ^{15}N-Ubl upon addition of WT (B) and L266K R0-RBR (C). HSQC peaks disappeared upon addition of 1:1 molar ratio of wild type, but not the mutants implying that this mutation abrogates Ubl binding to R0-RBR parkin.

3.3.6 Full-length parkin and the R0-RBR adopt the same conformation in solution as in the crystals

To confirm that the crystal structures are valid in solution and to reveal aggregation state of parkin, SAXS experiments were performed (Fig 3.12). R_g parameters were estimated as 27.9 ± 0.2 Å and 31.1 ± 0.4 Å for R0-RBR (MW = 41 kDa) and full-length parkin (MW = 53 kDa), respectively (Fig 3.12). This corresponds to a monomeric state in solution for both constructs.

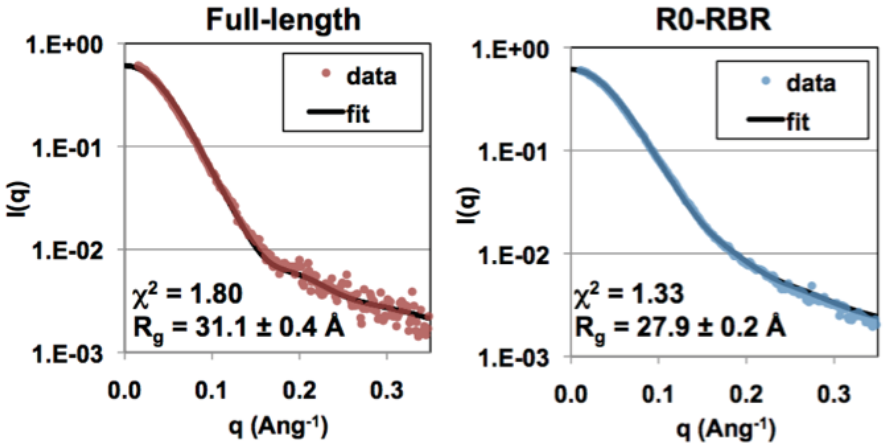

Figure 3.12 SAXS analysis of R0-RBR and full-length parkin. Obtained SAXS data for full-length and R0-RBR parkin in solution. The data were fitted to single chains in each crystal structure. Figure from Trempe *et al.*, 2013 [203].

The scattering profiles for different parkin constructs in reciprocal space were then processed by the program GNOM to generate the pair distance distribution function P(r) plot in real space [249] (Fig 3.13). A Gaussian curve that decays back to zero was obtained both for parkin and R0-RBR indicating that both constructs are globular, whereas the D_{max} for parkin R0-RBR mutant is larger than the full-length protein.

The information extracted from SAXS studies can also be combined with crystal structures and provide information about the dynamics of the protein and its conformation in solution [250]. The SAXS analysis of full-length parkin and the R0-RBR confirmed that they both adopt the same conformation in solution as in the crystals (Fig 3.12 and 3.13) as the scattering data were fitted very well to single chains in each crystal structure using CRYSOL (Fig 3.12)[259].

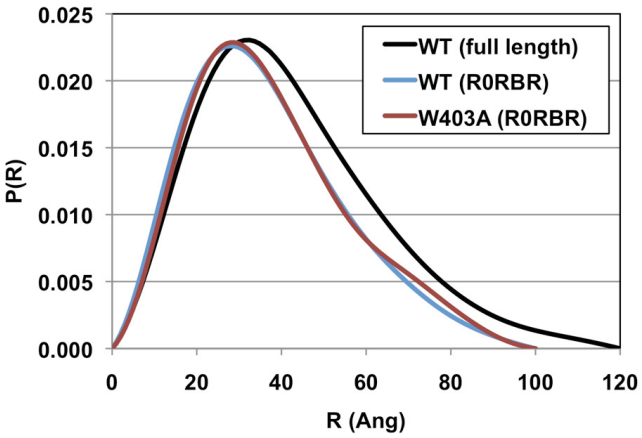

Figure 3.13 Pair-distance distribution functions for different parkin constructs. Pair-distance distribution functions were obtained from SAXS curves for different parkin constructs. The D_{max} for W403A parkin is similar to that of WT parkin, while the full-length parkin is larger. Figure from Trempe *et al.*, 2013 [203].

3.3.7 Topology of parkin zinc finger domains

Parkin zinc fingers fold with distinct topologies (Figure 3.14) each coordinating two zinc ions through histidine and cysteine residues, confirming the stoichiometry of eight zinc ions per parkin [272]. The RING0 domain binds zinc ions in a hairpin arrangement unique to parkin while the RING2 and IBR domains show a sequential arrangement of zinc-coordinating residues. RING0 and RING2 were originally identified RING domains based on the primary amino acid sequence, but their structural topology differs from a classical RING fold. The RING1 domain is the only RING domain with the cross-brace zinc coordination topology observed in other RING-type E3 ligases. The similarity of RING1 to other RING E3 ligases suggested that it is the E2 binding site on parkin. Modeling based on the structures of five E2-RING complexes reveal the E2 binding surface on RING1 (Figure 3.14). The RING2 domain is the catalytic module harboring the catalytic cysteine (Cys431). While RING0 is unique to parkin, the IBR domain is conserved among the RBR E3 family; the precise function of these domains is currently unknown.

3.3.8 Parkin structure provides rationales for many of the mutations associated with PD

The parkin structure provides rationales for many of the mutations associated with PD. Certain mutations compromise the structural integrity of the protein. Others interfere with binding of substrates or directly affect the enzyme catalysis. Among the best understood, mutations C212Y, C289G, and C441R affect zinc coordination, while R42P, K211N, T351P disrupt protein

folding or stability. C431F and G430D are in the catalytic site, and T240R prevents E2 binding. The effects of other mutations such as R33Q, D280N, G328E, or T415N are less clear. These may disrupt the interdomain interactions or affect binding of other proteins by parkin. The flexibility of the IBR is probably important for parkin's activity as the mutation G328E in the hinge between RING1 and IBR is a PD mutation. This could affect parkin function by preventing conformational flexibility, as in our structure, the Gly328 backbone torsion angles ($\phi \sim 90°$; $\psi \sim 20°$) are not compatible with glutamate.

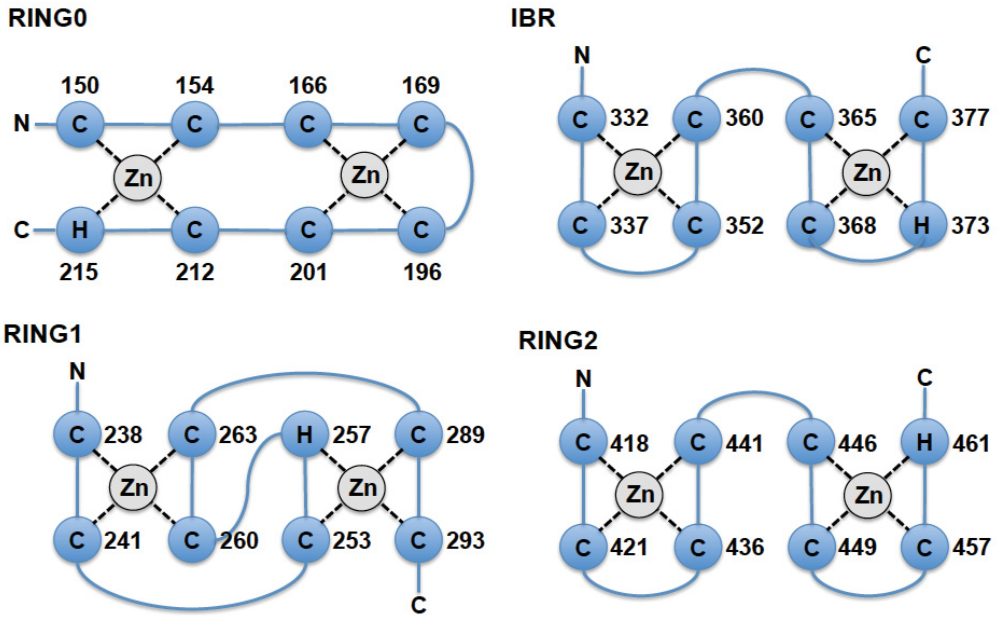

Figure 3.14 Topology of zinc finger domains in parkin. Cysteine or histidine zinc ligands are shown in blue circles connected by lines from the N- to the C-terminus. The RING0 domain displays a hairpin topology, the RING1 domain displays the cross-brace motif characteristic of RING domains, whereas IBR and RING2 display sequential topologies. Figure from Trempe *et al.*, 2013 [203].

3.3.9 Parkin is in an autoinhibited state

The activity of parkin is tightly controlled by parkin auto-inhibition. A number of structural features explain mechanisms of autoinhibition. The first is that access to the catalytic cysteine in RING2 domain is blocked by RING0 (Fig 3.15A and 3.15B), whereas the side-chain of Phe463 is inserted into a hydrophobic groove formed by Phe146 in RING0 domain. Moreover, Cys457 and H461 (not conserved in other RBR proteins, but well-conserved in parkin) (Fig 3.16), are part of

a helix that mediates multiple interactions with RING0 domain (Fig 3.15A).

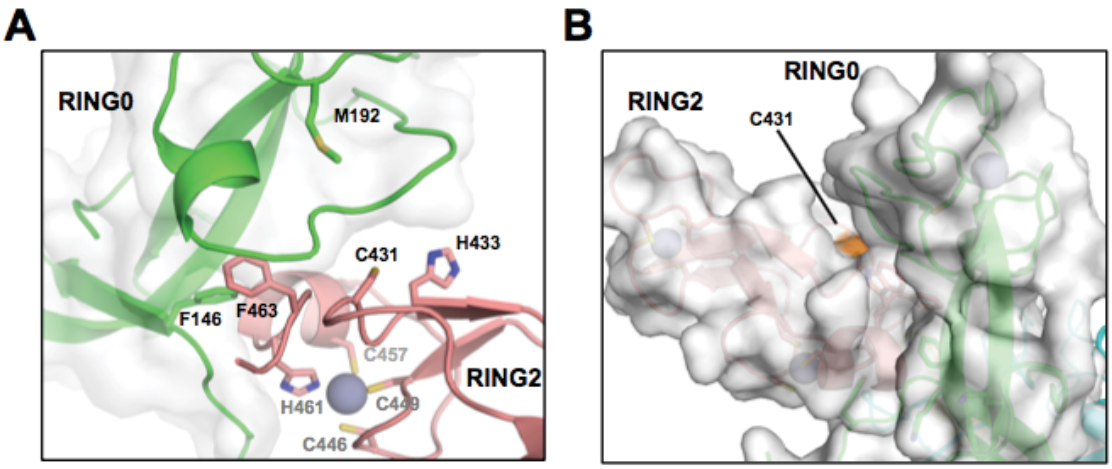

Figure 3.15 Auto-inhibitory role of RING0 domain. (A) Cartoon representation of the interface between RING0 and RING2 domains. The side-chain of Phe463 is inserted into a hydrophobic groove formed by Phe146 in RING0 domain. (B) Surface view of the interface between RING0 and RING2 showing that the active site Cys431 (orange) is blocked by RING0 domain. Figure from Trempe *et al.*, 2013 [203].

A second mechanism of autoinhibition is the control of binding of the upstream E2 enzyme to parkin. Modeling the E2 binding site on the RING1 domain (Fig 3.17A) suggests that this position is located beside the Ubl domain and REP linker and is occluded by these domains. (Fig 3.17A and 3.17B). The REP is a regulatory two-turn helix, well-conserved across parkin orthologs, and is held in place by insertion of the indole group of Trp403 into a pocket mainly formed by the side chain of Arg234, a residue mutated in PD (Fig 3.17B).

Finally, the large distance between the E2 binding site and catalytic site on RING2 prevents transfer of ubiquitin from the ubiquitin~E2 conjugate to the parkin catalytic cysteine (Fig 3.17A).

To test the role of the Ubl domain, and the REP/RING1 and RING0/RING2 interactions on parkin activity, we performed a series of autoubiquitination assays using parkin deletion and point mutants. Autoubiquitination assay is *in vitro* assay where ligase activity of E3 ligase enzymes is tested through assessment of their ability to undergo autoubiquitination [273]. This assay is performed using E1 ubiquitin-activating enzyme and E2 ubiquitin-conjugating enzyme, the enzymes involved in the ubiquitination cascade. This assay could be followed by Western blot analysis using antibodies to the protein of interest to monitor the appearance of higher molecular

weight poly-ubiquitinated E3 and the loss of unmodified protein.

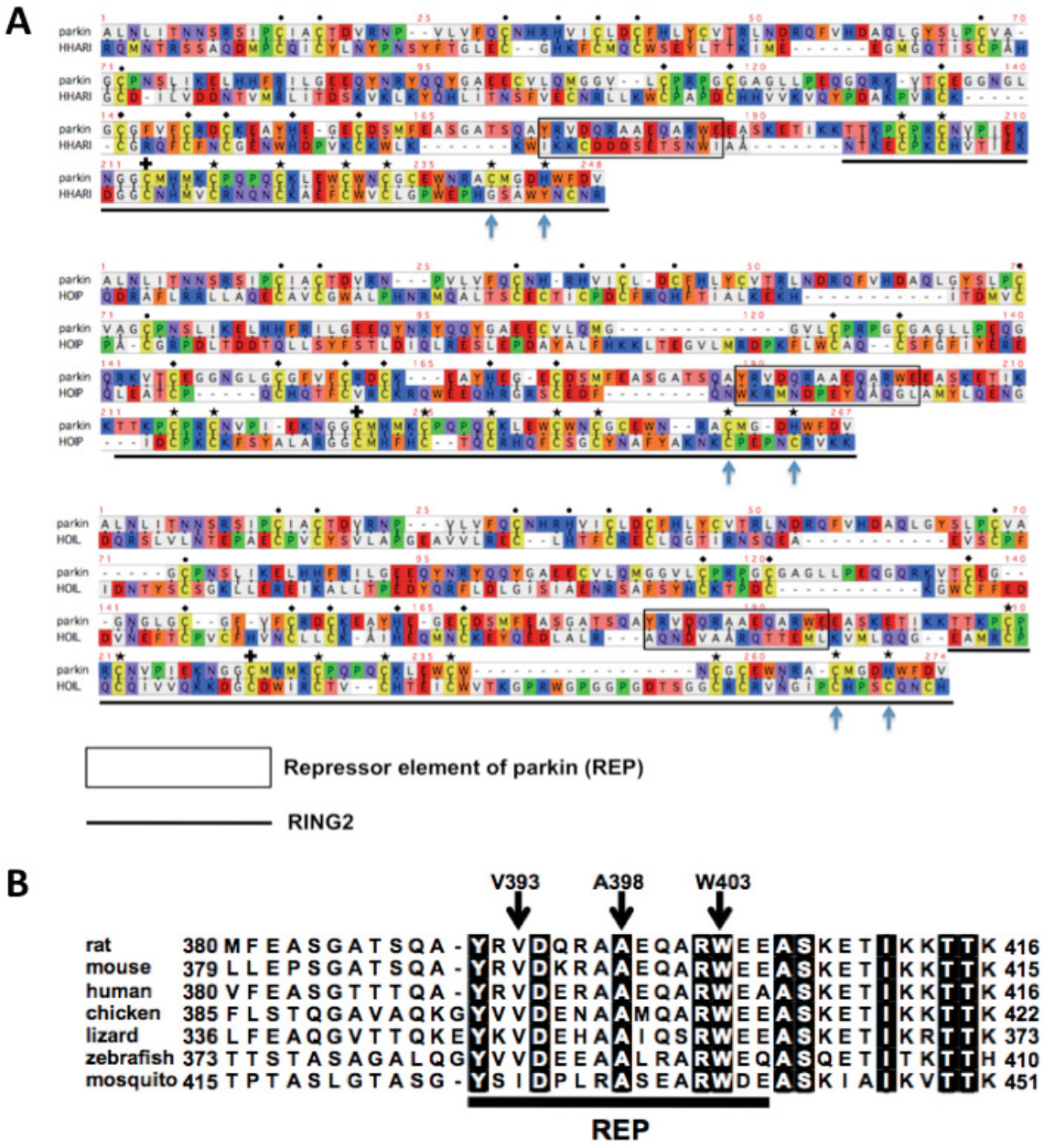

Figure 3.16 Alignment of REP in different RBR E3 ligases and parkin species. (A) Parkin was aligned with HHARI, HOIP and HOIL by matching zinc-coordinating Cys and His residues in RING1 (●), IBR (◆) and RING2 (★), as well as the active site Cys (✚). The REP region is boxed and shows little conservation with other RBR proteins. The positions of Cys457 and His461 in parkin are indicated by arrows [203]. (B) Sequence alignment of the REP sequence in parkin from different species. Invariant residues are shown as white letter on black background. Figure from Trempe *et al.*, 2013 [203].

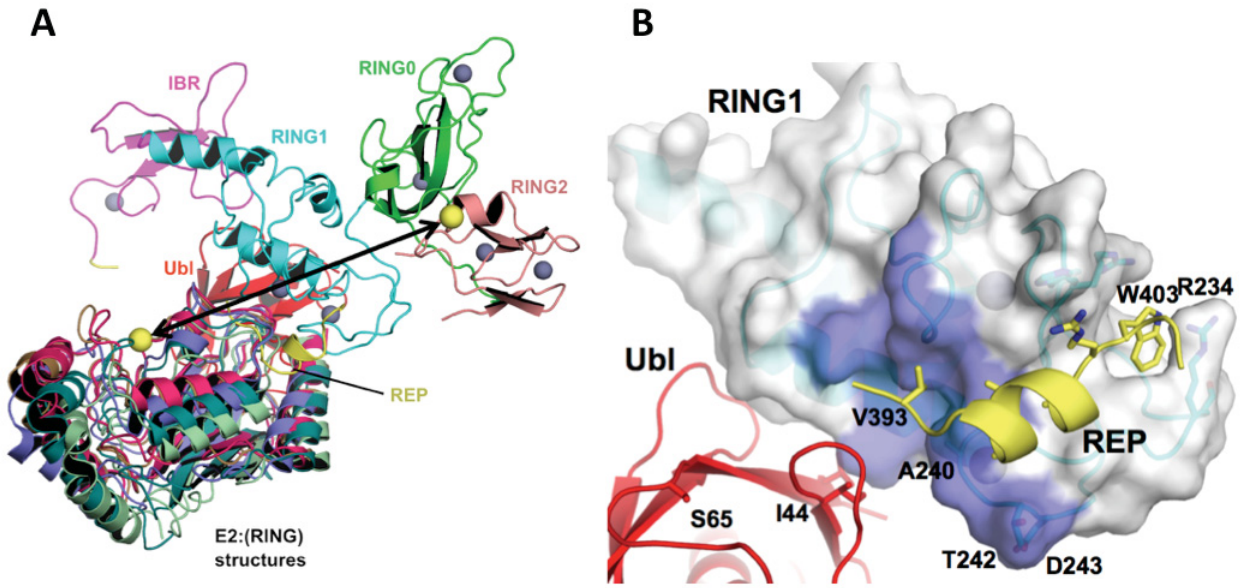

Figure 3.17 Modeling of the RING:E2 complexes show the E2 binding site on parkin. (A) The superposition of parkin RING1 (cyan) domain with the RING domains in RING/E2 complexes from c-Cbl:UbcH7 (orange, PDB 1fbv), CIAP2:UbcH5b (pale green, PDB 3eb6), TRAF6:Ubc13 (dark green, PDB 3hcu), Bmi1:UbcH5c (hot pink, PDB 3rp6) and RNF4:UbcH5a~Ub (brown, PDB 4ap4). This overlay shows that all E2 structures bind in the same orientation and to the same site on the RING1 domain of parkin. The double-headed arrow indicates the ~50 Å distance between the active site cysteine in E2 and C431 in RING2. (B) Surface view of RING1 (cyan) at the interface between RING1, Ubl (red) and the REP linker (yellow). The predicted UbcH7 binding site on RING1 is shown in blue. This binding site was determined by structural overlay with the cCbl-RING:UbcH7 crystal structure (PDB 1fbv) [274]. Figure from Trempe *et al.*, 2013 [203].

The deletion of the Ubl domain has been previously reported to affect parkin activity [195]. The position of this domain next to the E2 binding site also suggested this (Fig 3.17). In this work, we have shown that deletion of Ubl either alone or together with the following linker had very little effect on parkin activity (Fig 3.18). However, the additional deletion of the RING0 domain massively derepressed parkin activity (Fig 3.18), suggesting its auto-inhibitory role in parkin ligase activity. Supporting this notion, parkin point mutants F146A in RING0 and F463A in RING2 (predicted to disrupt the RING0:RING2 interface) both improved parkin ligase activity similarly to RBR deletion mutant lacking both Ubl and RING0 (Fig 17A).

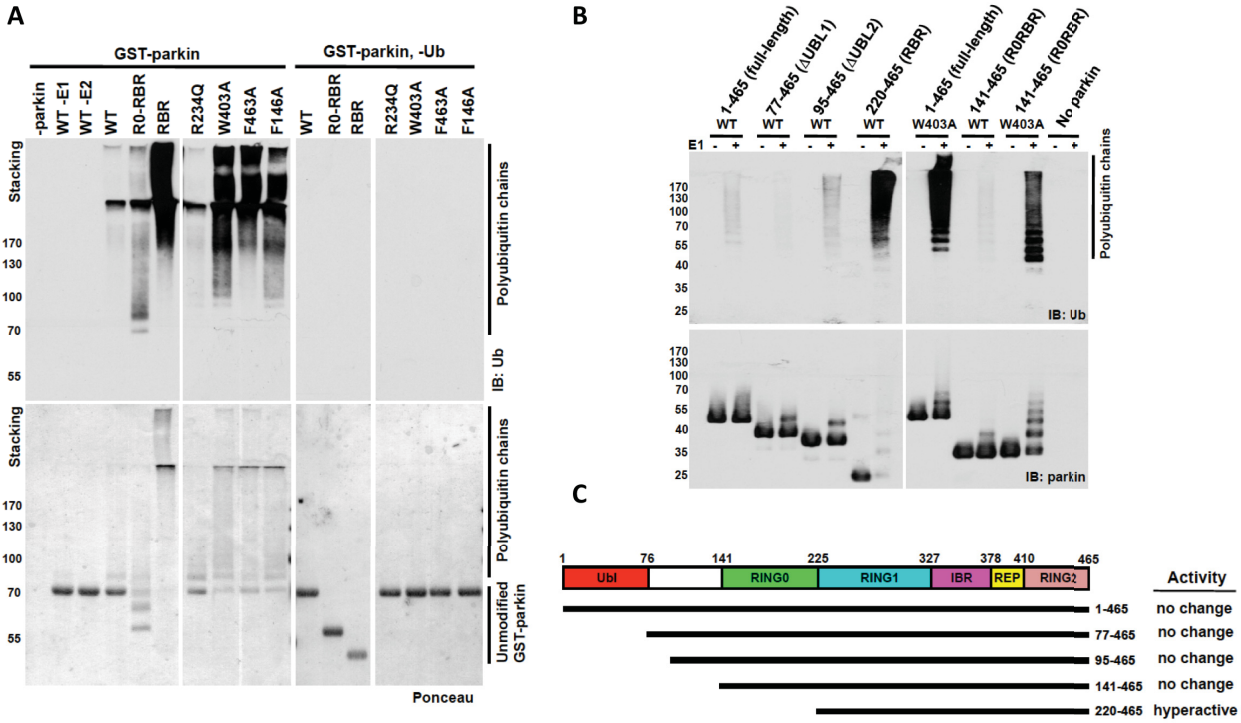

Figure 3.18 REP and RING0 regulate parkin autoinhibition. R0-RBR has similar activity to parkin, whereas additional removal of RING0 or disruption of the RING0:RING2 interface releases parkin autoinhibiton. W403A mutation activates parkin by removing REP from its position. (A) Autoubiquitination assays with GST-parkin. Assays were performed with 1 μM GST-parkin and 2 μM UbcH7 and incubated for 3 hours at 37°C. Autoubiquitination was followed by the appearance of high molecular weight poly-ubiquitin chains smear in both the stacking and resolving sections of the blots, and by the loss of unmodified parkin in the Ponceau. (B) Autoubiquitination assays with untagged parkin. Reactions were performed as described above for 2 hours. (C) Activity of different parkin deletion mutants. RING0 regulates parkin inhibition. Figure from Trempe *et al.*, 2013 [203].

To verify the role of the REP:RING1 interface, we mutated W403 to alanine to release REP from its position. As W403A R0-RBR has a similar shape to R0-RBR in solution in the SAXS experiment (Fig 3.13), we hypothesize that this mutation only releases REP and has no major effect on R0-RBR conformation. W403A parkin showed increased activity in autoubiquitination assay (Fig 3.18A), confirming that REP plays a prominent role in repressing parkin ligase activity.

To further confirm the E2 binding site on RING1, E2 binding to parkin was evaluated using NMR spectroscopy. In this experiment, ^{15}N-UbcH7 (an E2 enzyme) was titrated with a series of different parkin constructs. This binding led to different levels of line broadening and signal loss

from UbcH7 residues at the E2-RING1, including Arg5, Phe63, and Thr101 (Fig 3.19). In these experiments, mutation of A240, a residue in the predicted E2 binding site, to arginine abolished E2 binding, while the deletion of the Ubl domain and release of REP (using W403A mutant) both increased the affinity of E2 binding (Fig 3.19B). The highest affinity observed for W403A R0-RBR suggests that both REP and Ubl have inhibitory roles in E2 binding. Supporting this notion, A240R, T242A, D243A mutations in the predicted E2 binding site reduced parkin autoubiquitination activity (Fig 3.20).

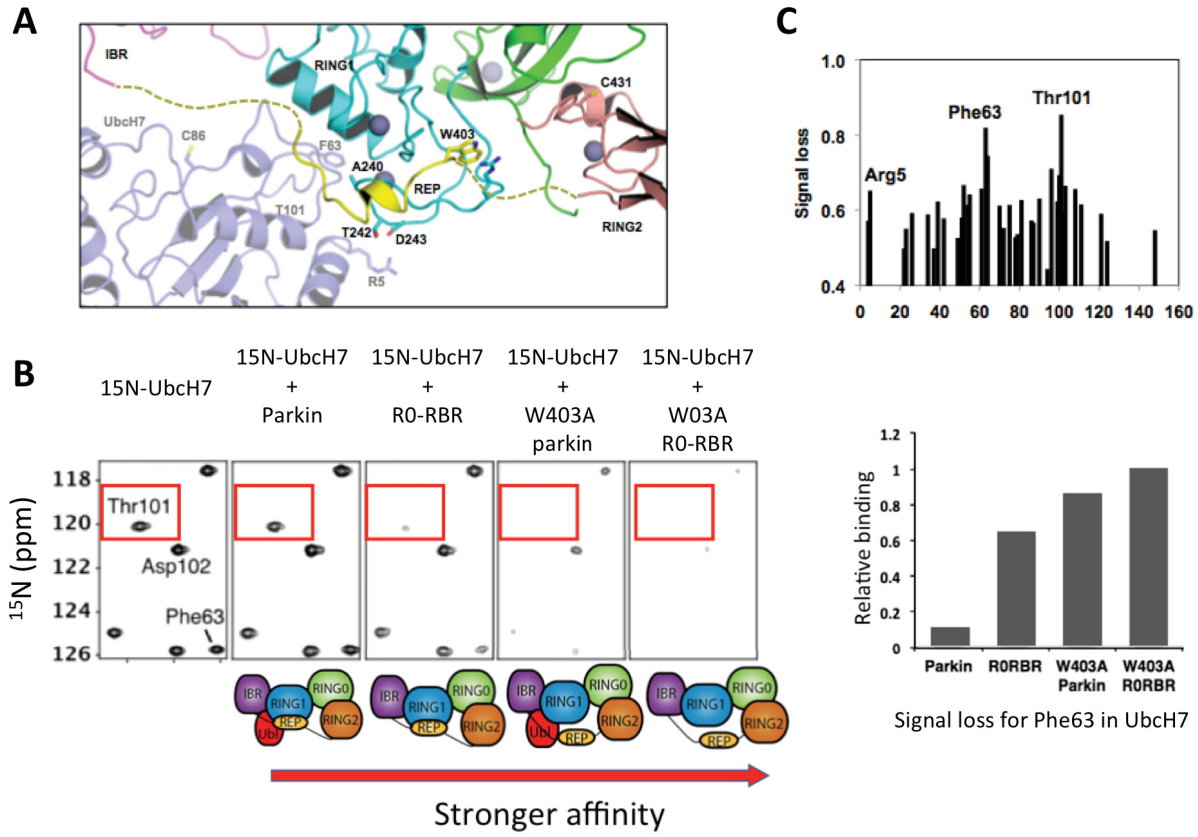

Figure 3.19 REP and Ubl block E2 binding site on parkin. (A) Close view of parkin/E2 model. E2 (blue) residues involved in R0-RBR binding are shown as sticks (B) NMR analysis of parkin binding to ^{15}N-labeled UbcH7. Changes in a portion of HSQC spectrum of UbcH7 (150 µM) caused by the addition of wild-type R0-RBR, W403A parkin, or W403A R0-RBR (70 µM). Peaks that undergo the most broadening (signal loss) correspond to the RING-binding site in UbcH7 including Thr101. (C) Quantification of NMR signal loss for Phe63 after addition of 216 µM parkin constructs. Spectra were normalized for dilution and the number of scans and the peak intensity lost relative to the free UbcH7 spectrum plotted.

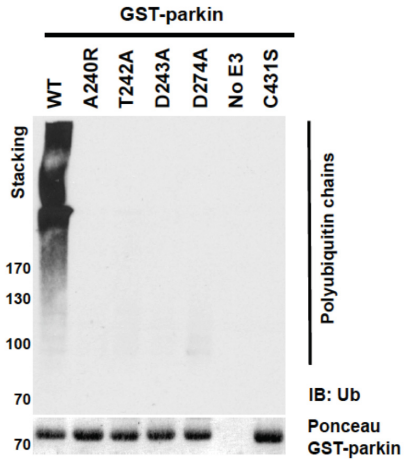

Figure 3.20 Mutations in the predicted E2 binding site reduced parkin activity. autoubiquitination assay with mutated GST-parkin constructs. Mutants at the E2 binding site reduce parkin activity. Reactions were performed with 1 μM GST-parkin and 2 μM UbcH7 and incubated for 3 hours at 37°C. Figure from Trempe *et al.*, 2013 [203].

We then addressed the role of REP in the regulation of parkin activity in cells. For this purpose, green fluorescent protein (GFP)-tagged parkin was expressed in HeLa cells and time-lapse microscopy was used to examine the kinetics of wild-type and mutant GFP-parkin recruitment to mitochondria following their depolarization with carbonyl cyanide m-chlorophenyl hydrazone (CCCP), a proton ionophore [275]. Wild-type parkin recruitment to mitochondria was observable 30 minutes after CCCP treatment, with half of the cells showing recruitment at 45 minutes, while the catalytically inactive C431S mutant did not recruit during the first hour (Fig 3.21 and 3.22), as previously reported [116, 275]. On the other hand, the W403A mutant showed earlier recruitment than wild-type parkin upon CCCP treatment (~10 minutes earlier) implying that REP release not only regulates parkin activity, but also accelerates parkin recruitment to the damaged organelle. Nevertheless, like wild-type parkin, W403A recruitment was still PINK1-dependent (Fig 3.23) [95, 97, 114].

3.4 Conclusion and discussion

Mutations in the *Parkin* gene lead to a recessive inherited form of the Parkinson's disease with an early onset. Heterozygous *Parkin* mutations have also been identified in sporadic PD [276], making it a promising target for future treatment of PD.

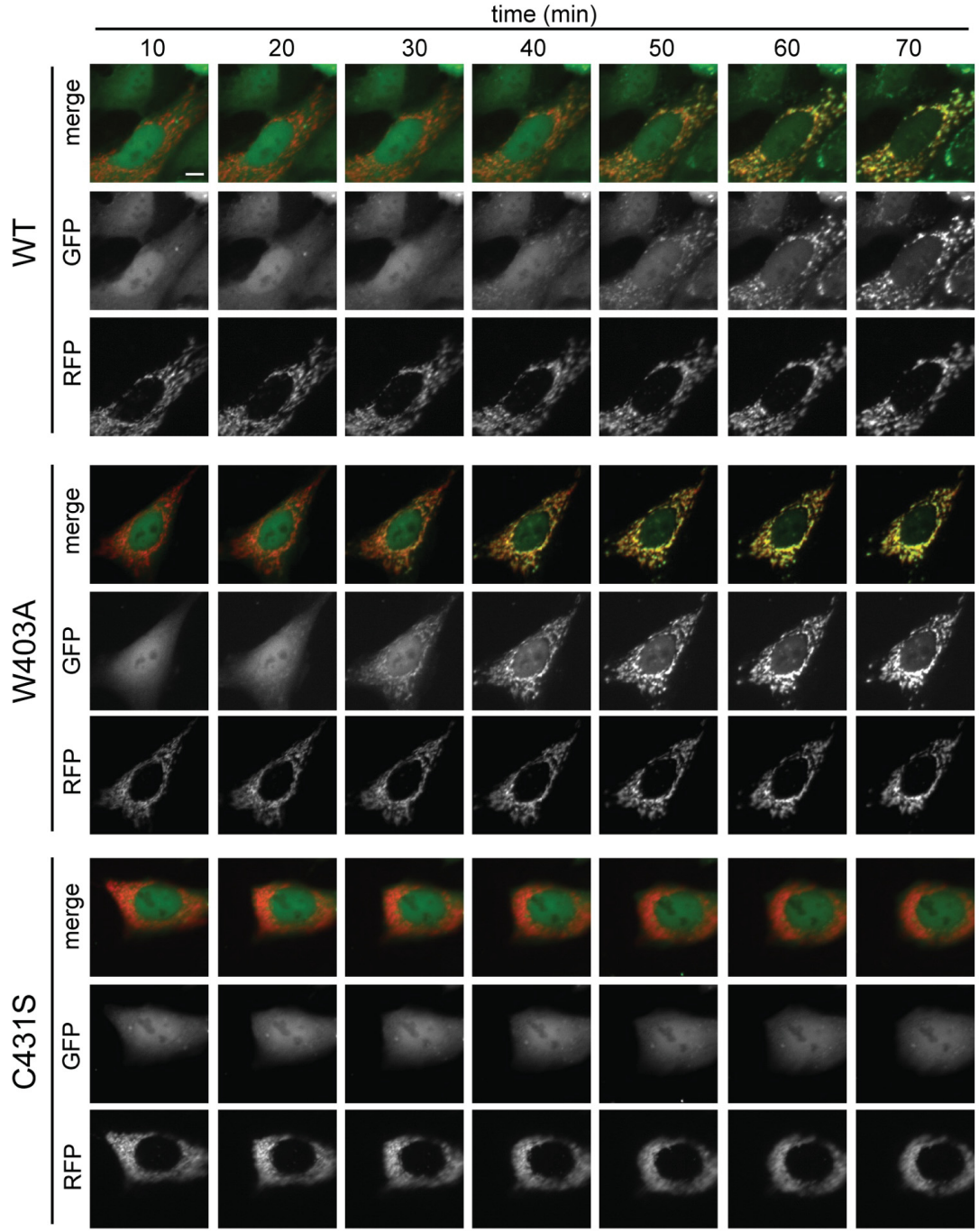

Figure 3.21 Recruitment of GFP-parkin mutants to mitochondria. Parkin recruitment to mitochondria upon membrane depolarization. HeLa cells were transduced with CellLight® mitochondria-RFP and transfected with equal amount of GFP-parkin wild-type, W403A or C431S. Cells were treated with 20 µM CCCP and visualized by time-lapse microscopy. Experiments were performed in a double-blinded fashion with n=4 and over 150 cells analyzed in each condition. Scale bar: 10 µm. Figure from Trempe *et al.*, 2013 [203].

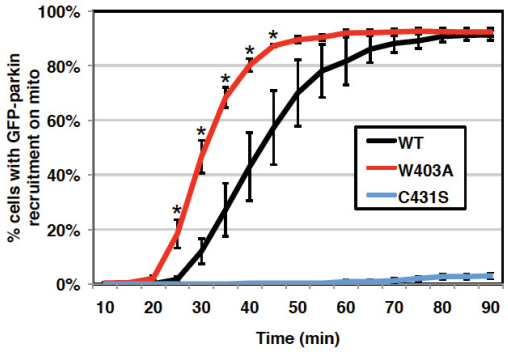

Figure 3.22 Quantification of GFP-parkin recruitment to mitochondria. The percentage of cells showing recruitment of GFP-parkin to mitochondria was determined every 5 min. Error bars indicate mean ± SEM (N=4). The asterisk indicates $P < 0.05$ (student t-test). [203]

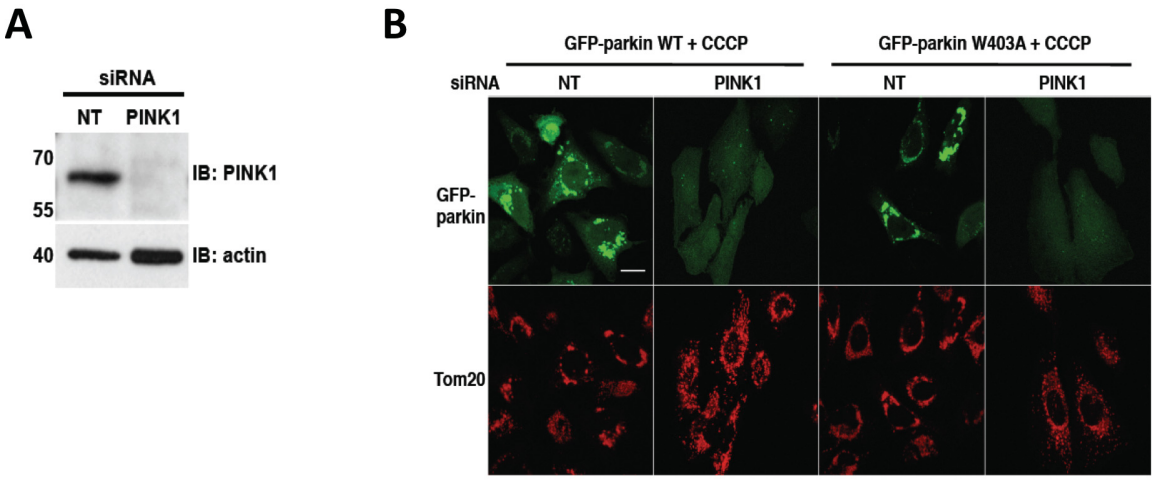

Figure 3.23 Parkin W403A recruitment to mitochondria is PINK1-dependent. (A) HeLa cells were transfected with non-targeting (NT) or PINK1 siRNAs for 24 hours and treated with CCCP for 3 hours. Whole-cell lysate proteins were immunoblotted for PINK1 and actin. (B) Parkin W403A recruitment to mitochondria is PINK1-dependent. HeLa cells were transfected with NT or PINK1 siRNAs prior to transfection of GFP-parkin WT or W403A (green). Cells were treated with 20 μM CCCP for 3 h and immunostained for Tom20 (red). Scale bar: 20 μm. Figure from Trempe *et al.*, 2013 [203].

Here, we solved the structure of parkin using X-ray crystallography. In the structure, parkin domains form a rigid core stabilized by several key hydrophobic interactions. In this conformation parkin catalytic Cys431 is occluded by the RING0-RING2 interactions, and E2-binding site on the RING1 domain is occluded by REP and Ubl domain. We believe that these interdomain interactions keep parkin in an autoinhibited state, as mutations that disrupt this hydrophobic

interdomain interactions increase parkin ligase activity. This autoinhibited conformation is in accordance with the low basal activity of parkin. Our hypothesis is that parkin should undergo large-scale conformational changes to bring ubiquitin, which is attached to the active cysteine of E2 ubiquitin conjugating enzyme, to the active cysteine on the RING2 domain. These conformational changes occur on the damaged mitochondria upon activation by PINK1.

To get a better understanding of parkin function and the molecular basis of ubiquitin transfer, more studies are required on the activated form of parkin. Illuminating the mechanism of parkin ligase activity is essential for understanding its biological function and may provide new avenues for therapeutic treatment of PD.

Chapter 4: Parkin Activation

4.1 Abstract

Mutations in *Parkin* and *PINK1* are the main causes of inherited early-onset form of Parkinson disease. The encoded proteins function together in a mitochondrial quality control pathway whereby PINK1 accumulates on damaged mitochondria and activates parkin to induce mitophagy. In this pathway, PINK1 kinase activity releases the auto-inhibited ubiquitin ligase activity of parkin by direct phosphorylation of the Ubl domain of parkin and by phosphorylating ubiquitin. How these two modifications affect parkin autoinhibition at the molecular level is not quite clear. Here, we found a binding switch between phospho-ubiquitin (pUb) and the ubiquitin-like domain (Ubl) domain of parkin as a key step. By mutagenesis and SAXS, we show that pUb binds to RING1 of parkin at a site formed by His302 and Arg305. pUb binding promotes disengagement of the Ubl domain from RING1 providing access to PINK1 for subsequent Ubl phosphorylation. Furthermore, the designed mutations that specifically release the Ubl domain from the RING1 domain mimic pUb binding and promote parkin phosphorylation. Parkin activity assays together with binding studies of E2 ubiquitin-conjugating enzyme UbcH7 to parkin suggest that parkin phosphorylation regulates E3 ligase activity downstream of pUb binding *in vitro*.

4.2 Rationales and hypothesis

Numerous studies over the last ten years have implicated *Parkin* and *PINK1* in a common mitochondrial quality control pathway [204]. In Drosophila, loss of PINK1 causes mitochondrial dysfunction that can be complemented by parkin [99, 100]. Parkin is a cytosolic E3 ubiquitin ligase that is recruited to mitochondria damaged by depolarization, reactive oxygen species (ROS), or accumulation of unfolded proteins [275, 277, 278]. Parkin then ubiquitinates mitochondrial outer membrane proteins such as Mitofusins or Miro to induce a wide range of outcomes, from proteasome degradation to vesicle formation, motility arrest and mitochondrial autophagy [73, 134, 275, 279-281]. Critically, all these parkin-dependent quality control processes require PINK1 (PTEN-induced putative kinase 1), a Ser/Thr kinase with a mitochondrial targeting sequence. PINK1 is normally imported into polarized mitochondria where it is cleaved by proteases and further degraded by the proteosome [98, 137, 138, 206]. When mitochondria are damaged, e.g.

upon depolarization, PINK1 accumulates on the cytosolic face of the outer membrane [208] where it can recruit and activate parkin [95, 97, 114].

The kinase activity of PINK1 is directly involved in parkin translocation and activation. First of all, PINK1 directly phosphorylates Ser65 located in the Ubl domain of parkin [112, 115]. This leads to an increase of parkin ligase activity. Secondly, PINK1 also phosphorylates ubiquitin on Ser65 [120-122]. Phosphorylated ubiquitin (pUb) interacts with parkin and also enhances its activity. Moreover, phosphorylated ubiquitin can act as a receptor for parkin translocation to mitochondria [282] in a feed-forward mechanism [199]. Thus, PINK1 phosphorylation of both ubiquitin and the Ubl are required for parkin's function in mitochondrial quality control, but their respective roles remain controversial.

Structural and biochemical studies have unveiled the molecular mechanisms underlying parkin's E3 ubiquitin ligase activity. Parkin is a member of the RBR (RING-in-between-RING) ligase family, which uses a RING/HECT hybrid mechanism to transfer ubiquitin from an E2 enzyme to a substrate via a thioester intermediate [190]. Crystal structures of full-length parkin (chapter 3) [203] showed that under basal conditions, the protein adopts a closed conformation where multiple intramolecular interactions inhibit key sites that are required for ubiquitin transfer. In particular, the E2-binding site on RING1 is occluded by the Repressor Element of Parkin (REP), and juxtaposed to the Ubl domain that was shown to play an important role in the regulation of its activity [195, 203]. However, the structural changes induced by Ubl phosphorylation and pUb binding to parkin, and the biochemical steps they regulate, remain obscure.

Given the importance of parkin in mitochondria quality control, it is crucial to gain insight into how parkin activation is regulated. We hypothesized that parkin activation is fully achieved by parkin phosphorylation at serine 65 in the Ubl domain and by binding to pUb. However, how these two steps are opening up parkin conformation and release parkin ligase activity are not clear. To gain insight into parkin activation mechanism, our objectives were to:

1. Determine how phosphorylation of the Ubl domain affects parkin autoinhibited conformation at the molecular level?
    a. Does parkin phosphorylation change the affinity of pUb binding to parkin?
    b. Determine how parkin phosphorylation affects UbcH7 binding to parkin and parkin E3 ligase activity

2. Determine how pUb binding affects parkin autoinhibited conformation at the molecular level?
    a. Does pUb binding affect the position of the Ubl domain in the autoinhibited conformation?
    b. Does pUb binding to parkin affect parkin phosphorylation?
    c. Determine how parkin binding to pUb affects UbcH7 binding to parkin and parkin E3 ligase activity?
3. Which one is the downstream signal for releasing parkin ligase activity: parkin phosphorylation or binding to pUb?

4.3 Results

4.3.1 The position of S65 in parkin autoinhibited conformation

A higher resolution crystal structure of Δ86-130 parkin, a deletion mutant that lacks the flexible linker between Ubl and RING0, at 2.54 Å confirmed our lower resolution structure of parkin at 6.5 Å. This structure superimposes well on the full-length parkin structure (backbone RMSD of 1.6 Å), showing that the reduced length of the linker does not perturb the conformation of parkin (Fig 4.1A and 4.1B).

This structure confirms that the Ubl mainly binds to a RING1 helix 261-274 as we previously reported in agreement with our results in chapter 3 that disruption of the Ubl-RING1 interface using L266K and N273K parkin mutants inhibits Ubl binding RING1. In this structure, Arg6 and His68 form hydrogen bonds with Asp274, a residue located at the end of the helix and preceding Arg275, a frequent mutation site in familial PD (R275W). Like ubiquitin, the Ubl has a hydrophobic patch centered on Ile44, which stacks against Leu266 of RING1 helix 261-274 (Fig 4.1C). Asn8, a residue conserved in parkin orthologs, binds RING1 helix 309-316 via a hydrogen bond with Gln311 and Arg314 (Fig 4.1D). This position is leucine in ubiquitin and may be a specificity determinant as ubiquitin does not bind the R0-RBR module. Ser65 of the Ubl domain, which is phosphorylated by PINK1 [115, 209] faces the disordered residues 382-391 preceding the REP helix and is located within 12 Å from RING1 (Fig 4.1B).

4.3.2 Parkin Ser65 phosphorylation releases the Ubl from RING1

The proximity of Ser65 to RING1 prompted us to test the role of its phosphorylation in regulating the Ubl:RING1 interaction. We used ITC to probe the interaction between the R0-RBR module and PINK1-phosphorylated Ubl (pUbl). A K_d of 16 μM was obtained for the unmodified Ubl binding to R0-RBR (Fig 4.2A), in agreement with previous measurements [195]. Strikingly, no signals were detected for the reaction of R0-RBR with pUbl.

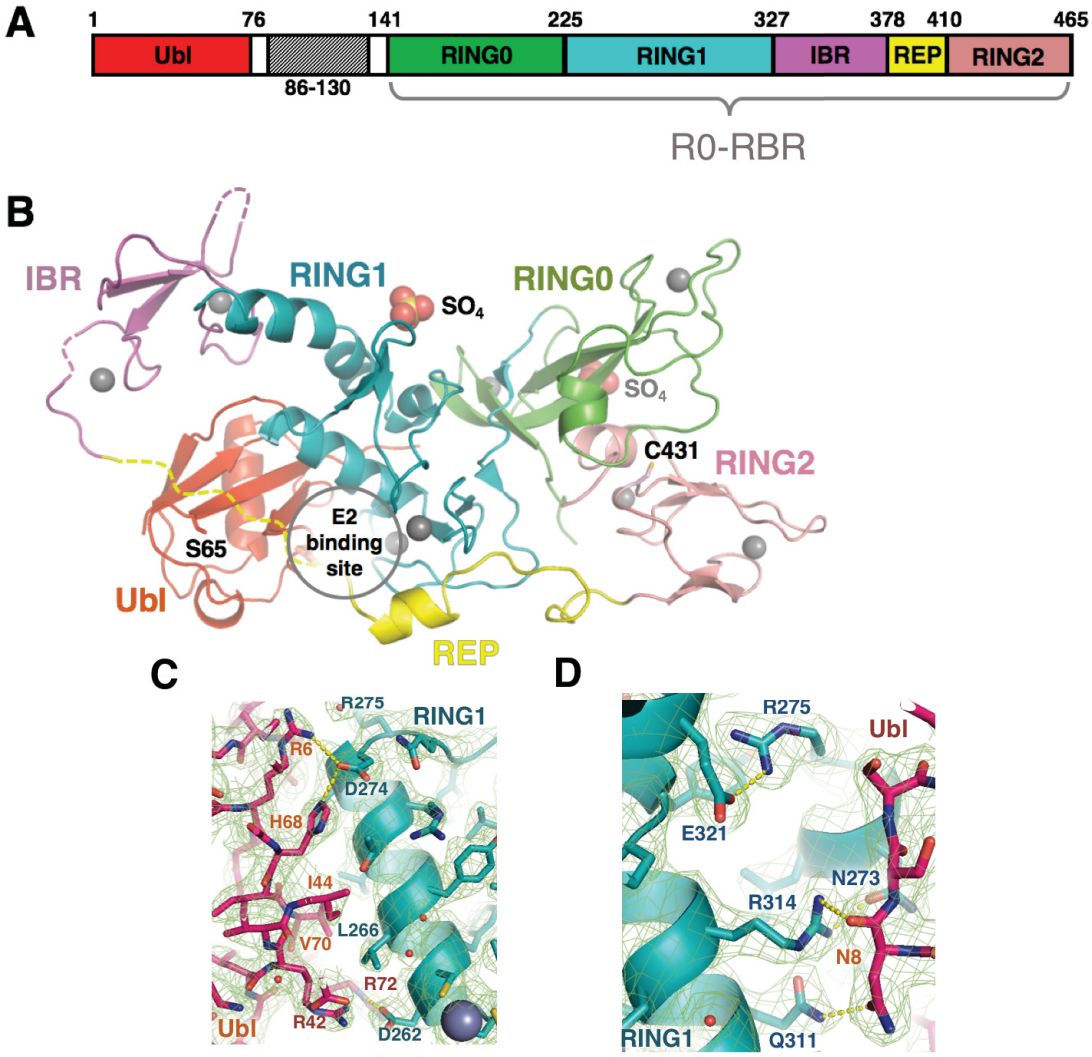

Figure 4.1 Structure of Δ86-130 parkin reveals details of Ubl binding. (A) Domain organization of parkin, showing location of Δ86-130 deletion and definition of R0-RBR module. (B) Structure of Δ86-130 parkin. The sites of phosphorylation on Ser 65 of the Ubl domain and the catalytic residue Cys 431 are indicated along with the bound sulfates. Intramolecular interactions between RING0 and RING2 block Cys431 in the catalytic site, and the E2-binding site is occluded by the Ubl domain and linker between the IBR and RING2 domains. (C and D) Close-up views of the interaction between the Ubl domain (red) with the RING1 domain (cyan). Figure from Sauvé *et al.*, 2015 [203].

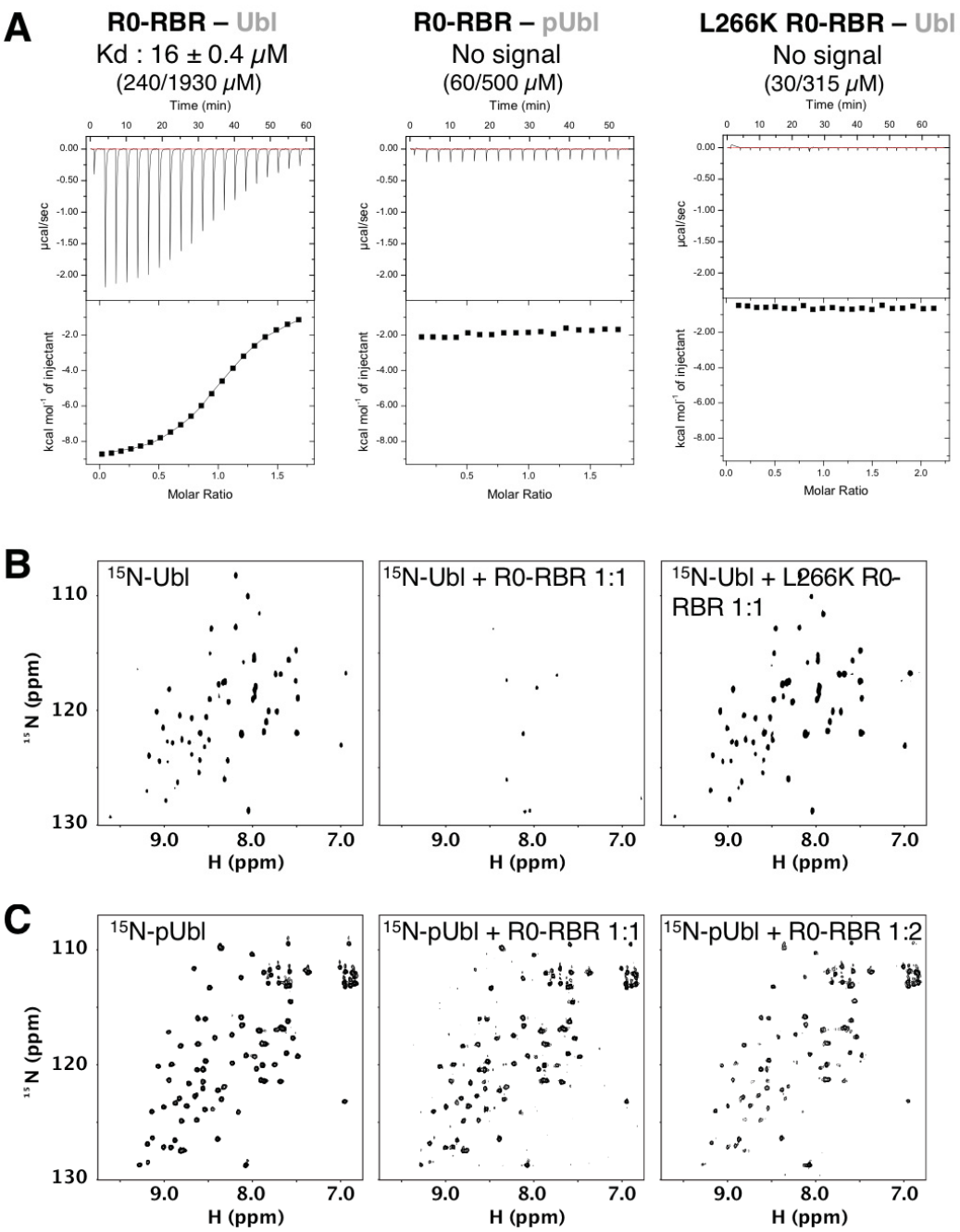

Figure 4.2 Phosphorylation of parkin disrupts the Ubl-RING1 interaction. (A) L266K mutation abrogates Ubl binding to R0-RBR. ITC measurement of the isolated parkin Ubl or phosphorylated Ubl domain with wild-type (WT) or L266K parkin R0-RBR fragments. The protein concentrations in the cell and syringe are indicated in parentheses. (B) pUbl interacts weakly with parkin R0-RBR. NMR ^{1}H-^{15}N correlation spectra of unmodified ^{15}N-Ubl (100 μM) titrated with wild-type or mutant L266K R0-RBR fragments. Binding results in a loss of NMR signals. (C) Spectra of phosphorylated ^{15}N-pUbl (30 μM) titrated with the parkin R0-RBR fragme nt. Figure from Sauvé *et al.*, 2015 [203].

To confirm that the lack of ITC signal was due to a loss of interaction and not the absence of an enthalpy change (ΔH), we performed an NMR titration experiment. As previously reported, ^{15}N-Ubl signals disappeared upon addition of R0-RBR due to the formation of a high molecular weight complex (Fig 4.2B middle panel) [195]. Addition of R0-RBR to the phosphorylated ^{15}N-Ubl domain led to only a small degree of signal loss consistent with a weaker interaction (Fig 4.2C middle pannel). No binding of the isolated Ubl to L266K R0-RBR could be observed by ITC or NMR (Fig 4.2A and 4.2B left panels). Overall, both techniques indicate that Ubl phosphorylation strongly decreases binding to the R0-RBR module.

We next asked whether Ser65 phosphorylation induces the dissociation of the Ubl domain in the context of the full-length protein. Dissociation of intramolecular interactions should increase the radius of gyration (R_g) and increase the number of long interatomic distances in the structure. SAXS measurements of unmodified full-length parkin yielded an R_g of 29.1 Å and a molecular weight estimations near its 52 kDa monomeric mass (Table 4.1). SAXS analysis of phosphorylated parkin (pParkin) showed a significantly greater R_g of 31.9 Å. The increased *Rg* was not caused by aggregation, because the estimated mass of the particle remained the same. The L266K parkin mutant also showed a larger *Rg* without evidence of aggregation. The *P(r)* pair-distance distribution functions calculated from the three samples confirmed more extended distances (r > 80 Å) in pParkin and L266K parkin (Fig 4.3A). Changes in parkin upon phosphorylation were also observed during sample preparation. We detected a significantly earlier elution of pParkin upon size-exclusion chromatography, suggesting an increased hydrodynamic size (Fig 4.3B). The L266K parkin mutant and a second mutation, N273K, that disrupts the Ubl-RING1 interface similarly eluted earlier than wild-type parkin (Fig 4.3C). In agreement with the experiments with the isolated Ubl domain, these measurements show that phosphorylation of parkin induces a structural rearrangement consistent with dissociation of the Ubl domain from RING1.

Table 4.1 SAXS-derived parameters for different parkin constructs. Table from Sauvé *et al.*, 2015 [203].

Parkin construct	Rg	Estimated Mass (kDa)	
		Porod	Qr
WT parkin	29.1 ± 0.1	54.4	48.9 ± 0.4
L266K parkin	34.1 ± 0.4	53.6	44.6 ± 1.1
Δ86-130 parkin	27.0 ± 0.1	45.5	39.8 ± 0.4
pParkin	31.9 ± 0.3	50.5	45.2 ± 0.8
pParkin + pUb	33.1 ± 0.3	54.7	55.0 ± 1.3
W403A parkin	30.1 ± 0.1	55.6	50.8 ± 0.4

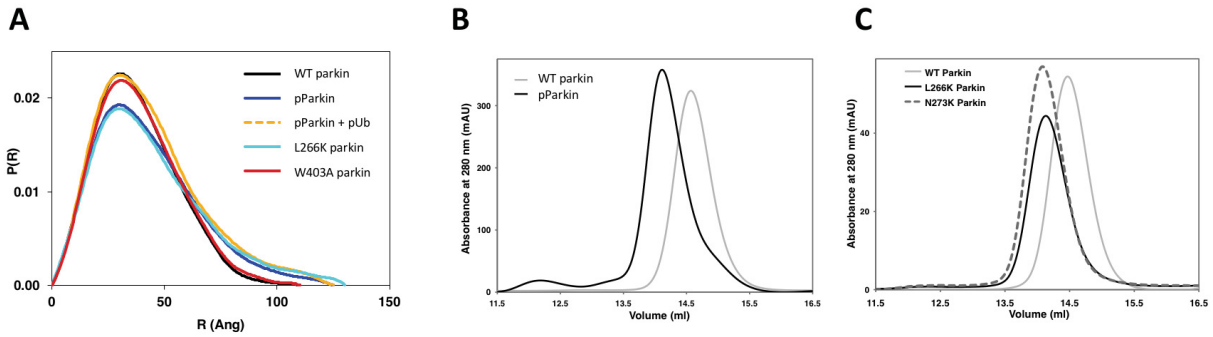

Figure 4.3 Phosphorylation of parkin induces a structural rearrangement consistent with dissociation of the Ubl domain from RING1. (A) Pair-distance distribution functions derived from SAXS curves for different parkin constructs. (B and C) Analytical size-exclusion chromatography of various parkin constructs. Concentrated protein solutions were injected on a Superdex 200 Increase 10/300 GL column at 1.0 mL/min, equilibrated in SAXS buffer. Figure from Sauvé *et al.*, 2015 [203].

We next performed NMR experiments to check whether the loss of binding induced by Ser65 phosphorylation could be attributed to an alternative conformation of the Ubl domain, as observed for pUb [251]. In the latter case, the C-terminal β5-strand of pUb was shown to adopt two different configurations in solution: a major conformation similar to unmodified ubiquitin and a minor conformation, unique to pUb, in which the β5-strand was shifted by two residues. We measured ^{15}N-^{1}H chemical shift differences between Ubl and pUbl (Fig 4.4A and 4.4B), and those perturbations were mapped on the Ubl domain of the structure of parkin (Fig 4.4C). The largest shifts were located in the region around Ser65: β-strand 65-70, its preceding loop 60-65 and its adjacent β-strand 2-6. All those regions face RING1 or the linker connecting the IBR to the REP. Interestingly, the backbone amide of Asn8, a residue unique to parkin and involved in the Ubl-RING1 interaction, is one of the most disturbed resonances despite being located 17 Å away from Ser65. Ubl phosphorylation thus seems to induce far-reaching perturbations in the structure of the Ubl. However, comparison of ^{15}N-NOESY-HSQC experiments acquired on Ubl and pUbl showed no major differences in cross-strands NOE patterns (Fig 4.4D), suggesting that no shift in beta-strand alignment occurs as observed in pUb [251]. The large perturbations in the amide chemical shifts probably reflect reconfiguration of the side-chains around the phosphorylation site. These different side-chain conformations affect surface residues further from the phosphorylation site such as Asn8 that in turn affect the interaction with RING1.

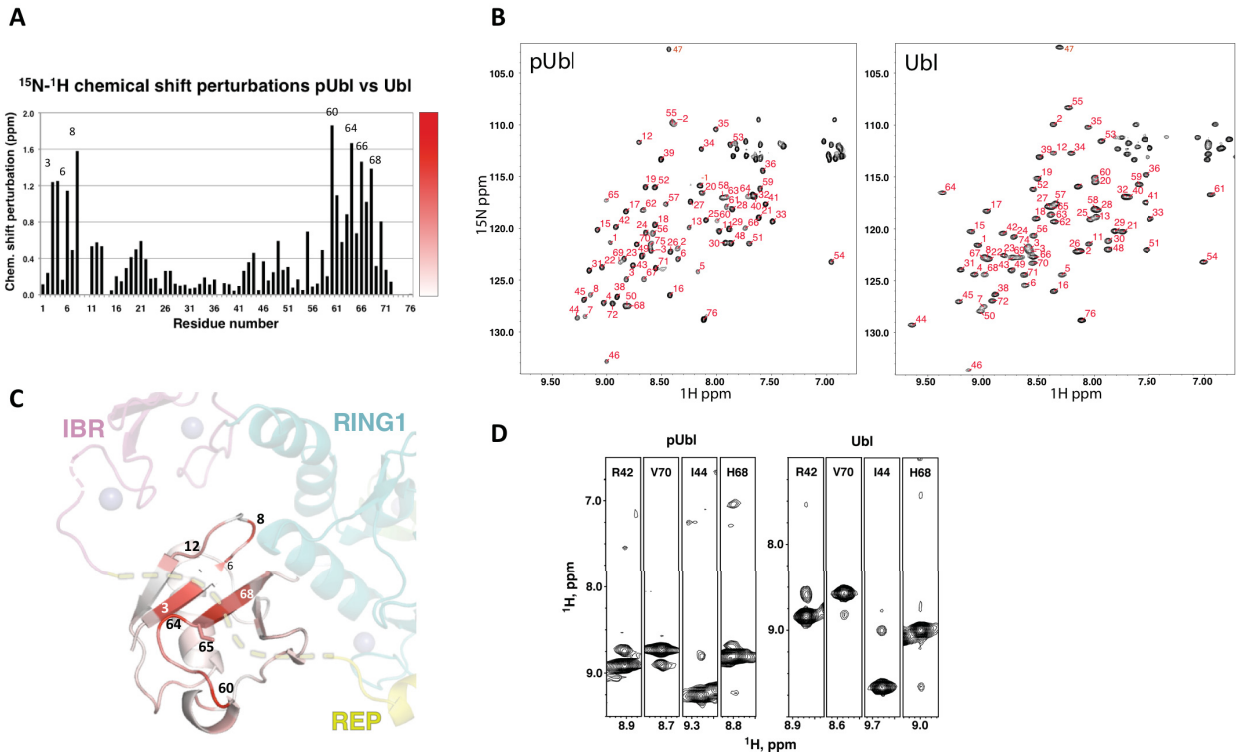

Figure 4.4 Conformational changes associated with Ubl phosphorylation. (A) Backbone amide NMR chemical shifts perturbations induced by Ser65 phosphorylation in the Ubl domain of parkin. (B) ^{15}N-HSQC NMR spectra of ^{15}N-labeled parkin pUbl and Ubl. (C) Backbone amide NMR chemical shifts perturbations induced by Ser65 phosphorylation in the Ubl domain of parkin. The magnitude of the perturbation is indicated by the intensity of the red color displayed on Ubl bound to RING1. (D) Comparison of strips from ^{15}N-NOESY-HSQC experiments on ^{15}N-labeled pUbl and Ubl. The H^N-H^N cross peaks between the pairs of residues Arg42-Val70 and Ile44-His68 located around the C-terminal β-strand are identical. Figure from Sauvé *et al.*, 2015 [203].

4.3.3 The Ubl domain and pUb compete for binding to parkin

Previous studies have demonstrated that the addition of pUb to parkin enhances ubiquitin ligase activity [120-122]; however, the molecular details of the interaction are unknown. We thus examined binding of different parkin constructs to pUb by ITC. We measured a 20-fold higher affinity for pUb binding to R0-RBR (22 nM) than to full-length parkin (431 nM) (Fig 4.4). This latter affinity is similar to that reported by another group using ITC and biolayer interferometry [199]. Therefore, deletion of the Ubl increases the affinity of pUb for parkin.

To test whether the inhibitory role of the Ubl was linked to its ability to bind RING1, we tested pUb binding to the L266K mutant. ITC measurements showed that full-length L266K parkin

binds pUb with an affinity comparable to the R0-RBR module (37 vs. 22 nM), confirming that the Ubl-RING1 interaction interferes with pUb binding (Table 4.2). Similar results were obtained by mutating Asn273, which is also located at the RING1:Ubl interface and required for Ubl binding. In the absence of the Ubl domain, the L266K mutation did not further increase the affinity of pUb binding, implying that the enhanced affinity observed with the L266K and N273K mutants was linked to the release of the Ubl domain (Table 4.2).

Table 4.2 The Ubl domain and pUb compete for binding to parkin. ITC-derived affinities of pUb binding to different parkin constructs. Table from Sauvé *et al.*, 2015 [203].

Parkin construct	Affinity for pUb (nM)
WT parkin	431 ± 25
R0-RBR	22 ± 5
L266K parkin	37 ± 7
L266K R0-RBR	41 ± 14
N273K parkin	57 ± 17
pParkin	17 ± 3

We next investigated the effect of the phosphorylation of parkin Ubl on pUb binding since it has already been demonstrated that both pUbl and pUb were required for optimal parkin activity [120-122]. Moreover, we have shown here that parkin phosphorylation releases the Ubl (Fig 4.5). We confirmed by ITC and NMR that pParkin binds pUb better than unphosphorylated parkin [199] (Table 4.2). We obtained a Kd of 17 nM for pParkin, which contrasts with the 431 nM found for unmodified parkin, but is similar to that measured for R0-RBR and L266K parkin. Parkin Ubl phosphorylation enhanced the binding of pUb to parkin to the same extent as deletion of the Ubl domain or release of the Ubl domain from its binding site on RING1. This confirms that the Ubl phosphorylation weakens the Ubl-R0-RBR interaction and facilitates access of pUb to parkin.

The competition between pUb and Ubl binding to parkin was tested by NMR spectroscopy. The loss of NMR signals from ^{15}N-Ubl in the presence of the R0-RBR module could be reversed by the subsequent addition of pUb (Fig 4.5). This indicates that pUb was able to displace the Ubl domain from the R0-RBR module

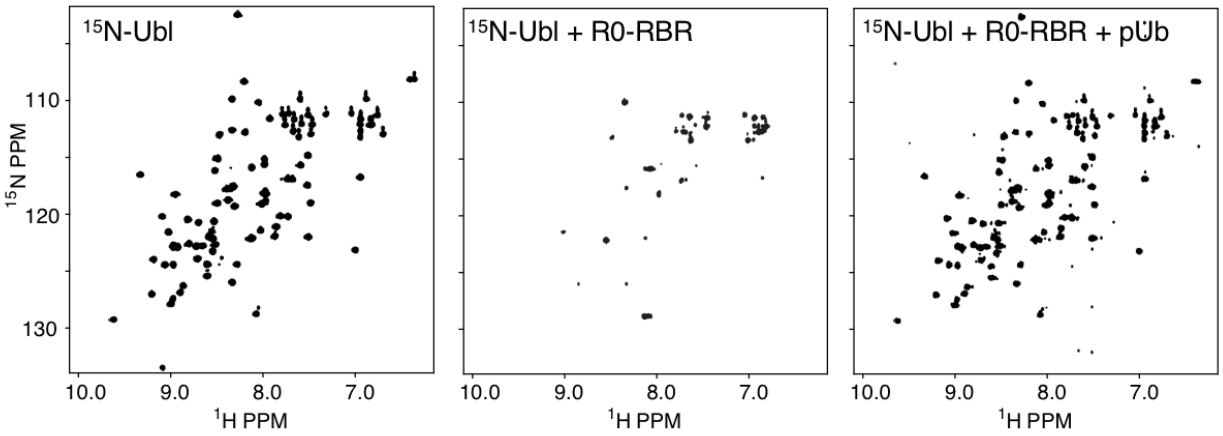

Figure 4.5 The Ubl domain and pUb compete for binding to parkin. NMR competition experiment. ^{1}H-^{15}N correlation spectra were acquired for ^{15}N-Ubl (100 μM) in the presence of equimolar R0-RBR and after addition of a molar equivalent of pUb. Figure from Sauvé *et al.*, 2015 [203].

PINK1 increases parkin activity by phosphorylating Ser65 in the Ubl domain [112]. In the basal state, the Ubl domain is bound to RING1 and Ser65 is poorly accessible for modification. We hypothesized that the release of the Ubl was necessary for efficient phosphorylation of Ser65 by PINK1. We thus measured the level of parkin phosphorylation by PINK1 in the presence of pUb using Phos-tag polyacrylamide gels. Under conditions where parkin is minimally phosphorylated by PINK1, the addition of pUb robustly led to phosphorylation of roughly 50% of Parkin. The L266K parkin mutant, where the Ubl domain is released from RING1, was also phosphorylated even in the absence of added pUb (Fig 4.6A). Moreover, the addition of pUb to L266K parkin did not lead to an increase in phosphorylation. The phosphate group of pUb was required for the stimulation of parkin phosphorylation. Addition of a non-phosphorylated ubiquitin (mutated to prevent its phosphorylation) did not increase the levels of parkin phosphorylation (Fig 4.6B). These results demonstrate that pUb binding to parkin facilitates its phosphorylation by PINK1 due to release of the Ubl domain. Through competition for binding RING1, pUb binding and Ubl phosphorylation reciprocally and synergistically lead to parkin activation.

4.3.4 pUb and the Ubl bind RING1 at distinct sites

The observation that the L266K mutation abrogates Ubl binding to R0-RBR (Fig 4.2) but not pUb binding (Table 4.2) suggests that the binding sites for pUb and Ubl are distinct. To identify the pUb-binding site on parkin, we mutated a series of residues in R0-RBR and performed a pull-

down assay with these mutants. We hypothesized the negatively-charged phosphate on Ser65 would bind to a positively charged patch on R0-RBR, and thus we selected basic residues that were either located adjacent to the Ubl domain (Arg271, Arg275, Arg314, Arg334, K369), or bound sulfates in the Δ86-130 structure (K161, K211, H302, R305) (Fig 4.1B). Only mutation of His302 and Arg305 compromised binding to pUb (Fig 4.7A and 4.7B), suggesting these two residues form the binding site for pUb. In the Δ86-130 structure, His302 and Arg305 are adjacent to the sulfate group with the lowest B-factor (Fig 4.8). ITC measurements confirmed that mutation of His302 to alanine dramatically reduced the affinity of R0-RBR for pUb by 60-fold (22 to 1333 nM), whereas mutation Lys211 in the other sulfate-binding site only reduced affinity by 2-fold (Fig 4.7C). Together, these results confirm that the phosphate group of pUb binds to a patch on RING1 formed by His302 and Arg305.

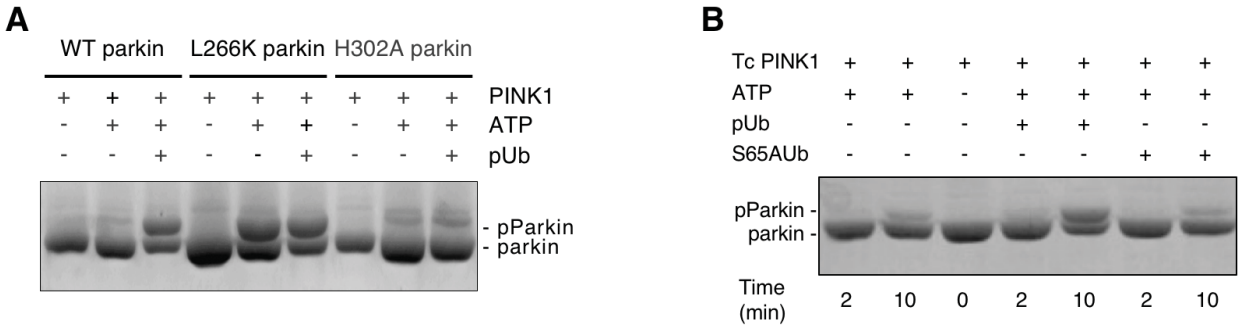

Figure 4.6 pUb binding facilitates parkin phosphorylation by PINK1. pUb binding to parkin facilitates its phosphorylation by PINK1 due to release of the Ubl domain**.** (A) Parkin phosphorylation assay showing increased phosphorylation in the presence of pUb. Wild-type (WT), L266K and H302A parkin were incubated 5 min with the *Tc*PINK1 kinase with and without ATP and pUb. Products were resolved by Phos-tag SDS-PAGE and stained with Coomassie Blue. (B) Parkin phosphorylation assay showing that unphosphorylated ubiquitin does not stimulate parkin phosphorylation by PINK1. The S65A mutant of ubiquitin was used to prevent the formation of pUb during the assay. Figure from Sauvé *et al.*, 2015 [203].

We next conducted SAXS experiments to model the structure of R0-RBR bound to pUb. Mass estimations from the Porod and Q_r analyses were consistent with the molecular weights of both R0-RBR (37 kDa) and the R0-RBR:pUb complex (46 kDa) (Fig 4.9A). The R_g values for both data sets were similar (Fig 4.9A), and the pair-distance distribution functions *P(r)* have similar shapes (Fig 4.9B), suggesting the R0-RBR:pUb complex retained a compact structure. We then modeled the SAXS data using two alternative approaches. First, we performed *ab initio* shape

determination to independently determine the location of the pUb-binding site. The shape determined from SAXS curves for the R0-RBR module alone fit well to the X-ray crystal structure thus validating the approach (Fig 4.9C). The shape calculated from SAXS data of R0-RBR:pUb revealed extra-density located between RING1 and RING0 (Fig 4.9D). The extra density could be accounted for by the placement of pUb with the phosphate in the sulfate-binding site next to His302 (Fig 4.9E).

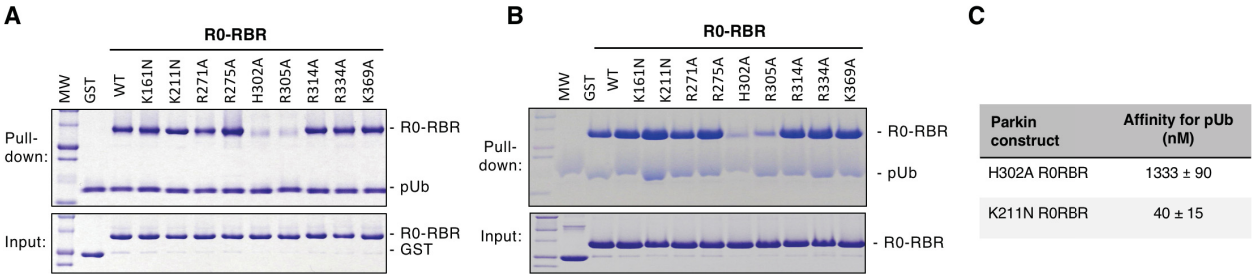

Parkin construct	Affinity for pUb (nM)
H302A R0RBR	1333 ± 90
K211N R0RBR	40 ± 15

Figure 4.7 pUb binds a RING1 site formed by His302 and Arg305. (A) Pull-down of R0-RBR mutants using His-tagged pUb, immobilized on Ni-NTA agarose. Bound proteins were eluted, resolved by SDS-PAGE and stained with Coomassie Blue. (B) Replicate of the pull-down of R0-RBR mutants using His-tagged pUb, immobilized on Ni-NTA agarose. Bound proteins were eluted, resolved by SDS-PAGE and stained with Coomassie Blue. (C) ITC-derived affinities of pUb binding to two different parkin R0-RBR mutants repressing the two major sulfate-binding sites. Figure from Sauvé *et al.*, 2015 [203].

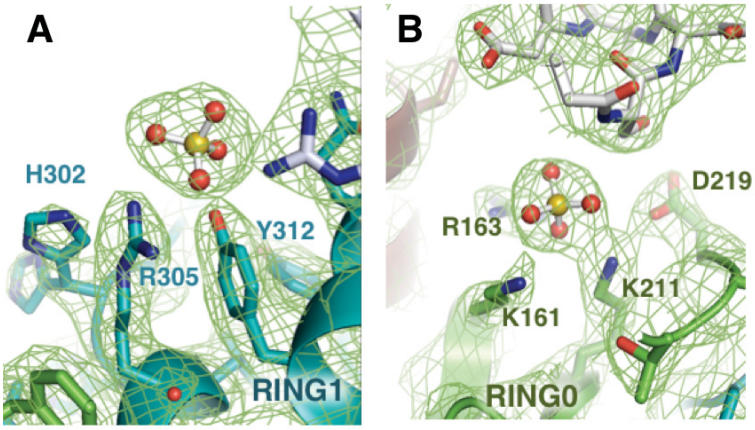

Figure 4.8 Polar contacts and residues around the bound sulfate ions in Δ86-130 parkin. structure (A and B) Polar contacts and residues around the bound sulfate ions. The sulfate in the first site has B-factor of 40 Å^2 and the second has a B-factor of 80 Å^2. Figure from Sauvé *et al.*, 2015 [203].

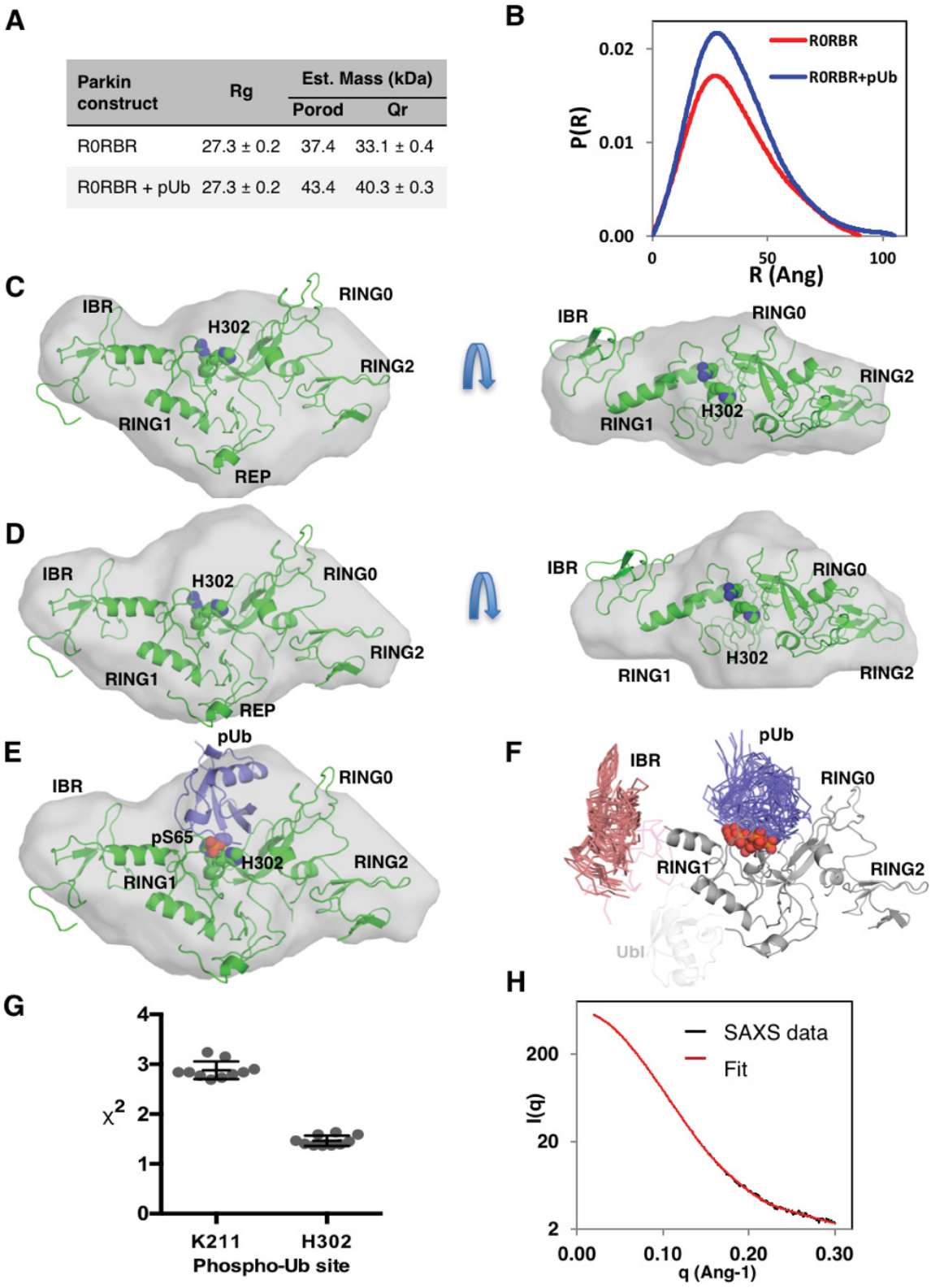

Figure 4.9 SAXS confirms that pUb binds a RING1 site formed by His302 and Arg305. (A)

SAXS-derived R_g and mass arameters for R0-RBR and the R0RBR:pUb complex. (B) Pair-distance distribution functions derived from SAXS curves for R0-RBR and the R0-RBR:pUb complex. (C) *Ab initio* shape determination for R0-RBR (light grey surface), superposed with the R0-RBR structure (green). The image on the right is a 90° rotation around the horizontal axis. (D) *Ab initio* shape determination for the R0-RBR:pUb complex (light grey surface), superposed with the R0-RBR structure (green). (E) *Ab initio* shape determination for the R0RBR:pUb complex (light grey surface), superposed with the R0-RBR structure (green) and pUb (blue) docked to the His302 phospho-binding site. (F) Overlay of the ten best R0RBR:pUb SAXS models where phospho-Ser65 (red spheres) is bound to His302 and Arg305. The flexible IBR and pUb domains are shown as Cα traces colored in coral and blue, respectively. The original position of the IBR in the R0-RBR structure is shown in light pink. For reference, the position of the Ubl domain in the Δ86-130 structure is shown in light grey. (G) χ^2 values for the ten best R0-RBR:pUb SAXS docking models for two potential phospho-Ser65 interaction sites. (H) Overlay of the experimental SAXS data from the R0-RBR:pUb complex [152] and the calculated scattering curve from the best rigid body model (red). Figure from Sauvé *et al.*, 2015 [203].

To confirm this model, we performed rigid-body modeling against the R0-RBR:pUb SAXS data using the structures of the parkin R0-RBR module [203] and pUb [251], while maintaining a short distance between Ser65 in pUb and His302/Arg305. This did not produce a docking model that satisfactorily fit the data (χ^2 above 10), so we introduced an additional degree of freedom by allowing the IBR domain to move within a distance set by the length of the disordered linkers located before (G328-G329) and after (M380-Y391) the IBR domain. The rationale stems from the intrinsic flexibility of the IBR domain observed in previous crystal structures. The docking calculations with IBR movement converged satisfactorily with an ensemble of models very similar to the *ab initio* model (Fig 4.9F) and χ^2 of 1.5 ± 0.2 (Fig 4.9G and 4.9H). Identical docking calculations with pUb docked in the vicinity of Lys211 (the alternative sulfate binding site) did not produce good fits.

These calculations suggest that pUb binds to the His302/Arg305 site, making contacts primarily with RING1 and RING0 (Fig 4.9E and 4.9F). The contacts on RING1 are opposite the Ubl-binding site and involve the helix that connects RING1 to the IBR domain (residues 309-327). That helix also contacts the Ubl domain (Fig 4.1D) and may mediate the allosteric coupling between pUb binding and Ubl release. The modeled pUb-binding site is also adjacent to RING1 residues Asp280-Gly284, which immediately follow the Ubl-binding helix (residues 261-274) (Fig 4.1C).

4.3.5 Phosphorylation of parkin stimulates its E3 ligase activity by increasing its affinity for the E2 enzyme

As an E3 ubiquitin ligase, parkin needs to interact with a ubiquitin-charged E2 enzyme to conduct the ubiquitination of its substrates. Superimposition of the RING-UbcH7 structure (cCbl RING:UbcH7, PDB: 1FBV) onto the Δ86-130 parkin structure predicts an overlap of both the Ubl domain and the REP with UbcH7 (Fig 4.10A). Therefore, we conducted ITC experiments to test how the phosphorylation of parkin Ubl domain affects UbcH7 binding to parkin. No binding and very weak binding (>700 μM) were measured for full-length parkin and the R0-RBR module respectively (Fig 4.10B), consistent with our previous findings [203]. As expected, mutation of Trp403 in R0-RBR to destabilize the REP:RING1 interaction, enhanced binding towards UbcH7 (K_d = 119 μM). Consistent with its reported increased activity, pParkin showed an increased affinity towards UbcH7 (161 μM) comparable to the R0-RBR-W403A mutant (Fig 4.10B and 4.10A). This suggests that phosphorylation of the Ubl facilitates binding of UbcH7. We also tested the binding of pUb-pParkin complex with UbcH7 and obtained an even higher affinity (31 μM) than for pParkin alone, consistent with both phosphorylation events being required for full E3 ligase activity [120-122].

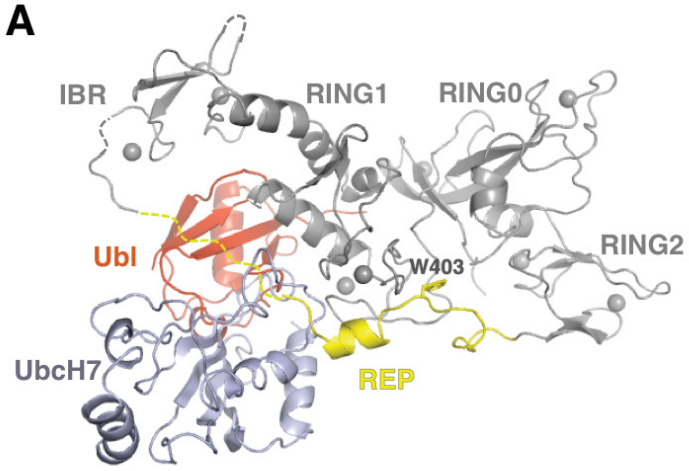

B

Parkin construct	Affinity for UbcH7 (μM)
WT Parkin	No signal
R0RBR	> 700
W403A	> 600
R0RBR-W403A	119
pParkin	161
pParkin + pUb	31

Figure 4.10 ITC measurements of UbcH7 binding to parkin. (A) UbcH7 (blue) modeled onto parkin Δ86-130 (grey) based on the cCbl-RING:UbcH7 complex. The Ubl and REP are colored in red and yellow, respectively. **(B)** ITC-derived affinities of different parkin constructs titrated with UbcH7. Figure from Sauvé *et al.*, 2015 [203].

NMR experiments were performed to validate our ITC results. Binding of parkin to the E2 enzyme was monitored by the loss of signal in the NMR spectra of ^{15}N-UbcH7 (Fig 4.11). Consistent with the previous results, no signal loss was observed for full-length parkin. The R0-RBR (Ubl deletion) or W403A mutants both showed increased binding to UbcH7 and their effects were additive, with the W403A R0-RBR mutant displaying a greater signal loss than either single mutation. Mutation of T240R in RING1 (A240R in rat parkin), prevented UbcH7 binding even in the context of activating mutations, thus confirming the model of E2 binding to RING1.

Titration with pParkin led to significant NMR signal loss comparable to the W403A R0-RBR double mutant. Binding of pParkin or parkin to UbcH7 could be further improved by the addition of pUb. However, the sole addition of pUb to R0-RBR didn't significantly affect binding to UbcH7, suggesting that the activating role of pUb is Ubl-dependent. Phosphorylation of the Ubl domain had a much larger effect than simply removal of the Ubl and following linker (Fig 4.11B and 4.11C).

To investigate the effect of Ubl and ubiquitin phosphorylation on the E3 ubiquitin ligase activity of parkin, we performed autoubiquitination assays with unmodified or pre-phosphorylated parkin in the presence of pUb. Addition of pUb mildly increased the low basal activity of wild-type parkin, as observed by the formation of monoubiquitinated parkin (Fig 4.12). In contrast, phosphorylation of the Ubl (pParkin) dramatically increased its activity, which were not further enhanced by pUb. These results are consistent with our affinity measurements for UbcH7, which show that phosphorylation of parkin leads to more significant E2 binding than pUb addition alone (Fig 4.10B and 4.11). The N273K mutant, which cannot bind the Ubl, behaves in a manner similar to wild-type in the unmodified form and is even more active in the phosphorylated form. The implication is that Ubl phosphorylation plays a positive role in the stimulation of parkin E3 ligase activity. Consistent with our pUb:parkin binding model, we find that the pUb-binding site mutants H302A and R305A showed wild-type activity when phosphorylated, but the unmodified H302A mutant could not be stimulated by pUb. This confirmed that the H302A mutation specifically abrogated the ability of parkin to bind pUb, but not its intrinsic E3 ligase activity.

4.4 Conclusion and discussion

Previous studies have shown that parkin is natively inhibited through interdomain interactions and stimulated through two parallel activation steps: phosphorylation of Ser65 in the

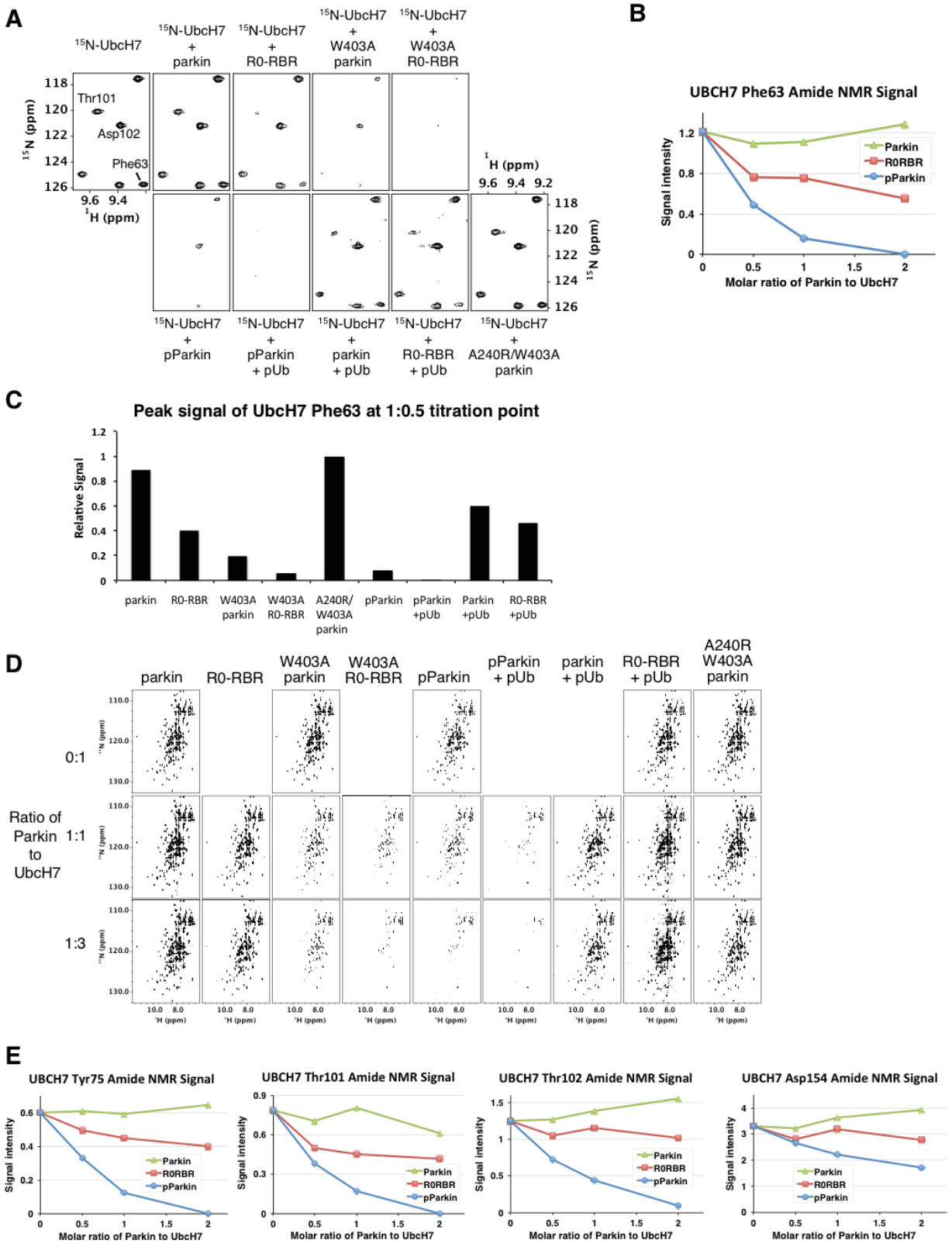

Figure 4.11 Phosphorylation of parkin and pUb binding increase parkin affinity for UbcH7. NMR titrations confirming that phosphorylation of parkin and pUb binding increase the affinity

of parkin for UbcH7. (A) NMR analysis of parkin binding to ^{15}N-labeled UbcH7. ^{1}H-^{15}N correlation spectra of UbcH7 (120 μM) were acquired in the presence of 120 μM of different parkin constructs ± pUb. Peaks that belong to the RING1-binding surface of UbcH7 undergo the most broadening (signal loss) and are labeled in the first panel. (B) Signal intensity of ^{15}N-UbcH7 the Phe63 backbone amide as a function of parkin added. UbcH7 and parkin concentrations were 1:0 (200 μM), 1:0.5 (120 μM:60 μM), 1:1 (120 μM:120 μM), 1:2 (90 μM:180 μM). Spectra were normalized for dilution of UbcH7 and the number of scans. (C) Relative signal intensity of ^{15}N-UbcH7 Phe63 amide in the presence of different parkin constructs and pUb complexes. UbcH7 concentration was 150 μM and the parkin constructs and pUb concentrations were 75 μM. Peaks heights were plotted relative to the UbcH7 spectrum with the E2 binding-deficient parkin mutant A240R/W403A. (D) NMR analysis of parkin binding to ^{15}N-labeled UbcH7. The UbcH7 and parkin concentrations were 1:0 (200 μM), 1:1 (120 μM:120 μM), and 1:3 (65 μM:195 μM). Spectra were adjusted to account for the number of transients and the concentration of ^{15}N-UbcH7. Reference spectra for free ^{15}N-UbcH7 are displayed above titrations with the parkin constructs. The spectra in Fig 4.11A are enlargements of the 1:1 titration spectra. (E) Signal intensity of ^{15}N-UbcH7 amides as a function of addition of parkin, R0-RBR and pParkin. Conditions were the same as in Fig 4.11B. Figure from Sauvé *et al.*, 2015 [203].

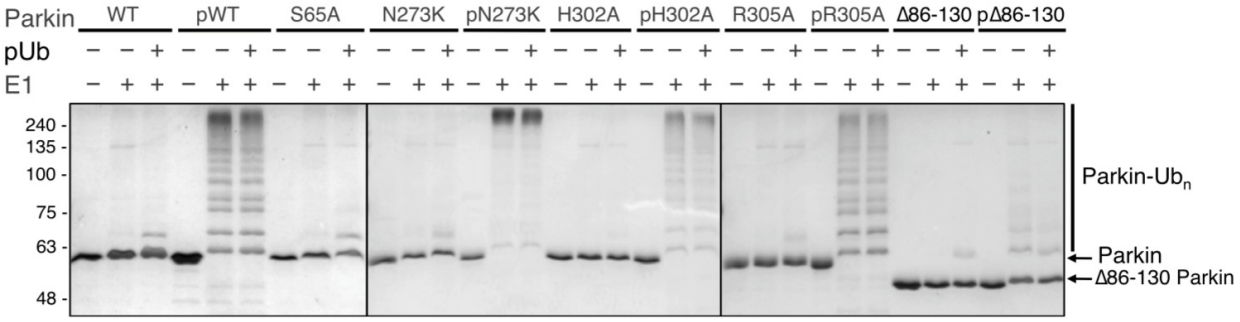

Figure 4.12 Phosphorylation of parkin and pUb binding increase parkin activity. Parkin autoubiquitination assay. Unmodified or phosphorylated parkin was incubated with ATP/Mg^{2+} and UbcH7, with and without E1 enzyme and pUb. Products were resolved by SDS-PAGE and stained with Coomassie Blue. Ligase activity can be monitored by the loss of unmodified parkin and the formation of higher molecular weight polyubiquitinated forms of parkin. Figure from Sauvé *et al.*, 2015 [203].

parkin Ubl domain and pUb binding. Here, we show that the steps involve a switch between pUb binding and Ubl release (Fig 4.13). Despite their structural and sequence similarity, the Ubl domain of parkin and ubiquitin are oppositely regulated by phosphorylation. Phosphorylation of the Ubl domain decreases its affinity for its binding site on RING1 while phosphorylation of ubiquitin increases its affinity.

Both activation steps involve conformational changes. The first is within the Ubl domain. The structure of Δ86-130 parkin shows a large interaction surface between the beta-sheet surface of the Ubl domain and the first alpha helix in RING1 (Fig 4.1). Phosphorylation of Ser65 induces NMR chemical shift changes in the two central strands of the beta-sheet surface and Asn8, which is more than 15 Å from the site of phosphorylation (Fig 4.4C). These changes destabilize the Ubl-RING1 interface by 20-fold. Although phosphorylation of ubiquitin was found to induce the formation of a second minor form [251], this does not appear to be the case for the Ubl domain. Analysis of NOESY spectra did not find evidence for a strand shift within the Ubl beta-sheet. Presciently, molecular dynamics simulations of parkin observed that phosphorylation of the Ubl domain led to its dissociation from RING1 as a result of changes in hydration and local structural changes [283].

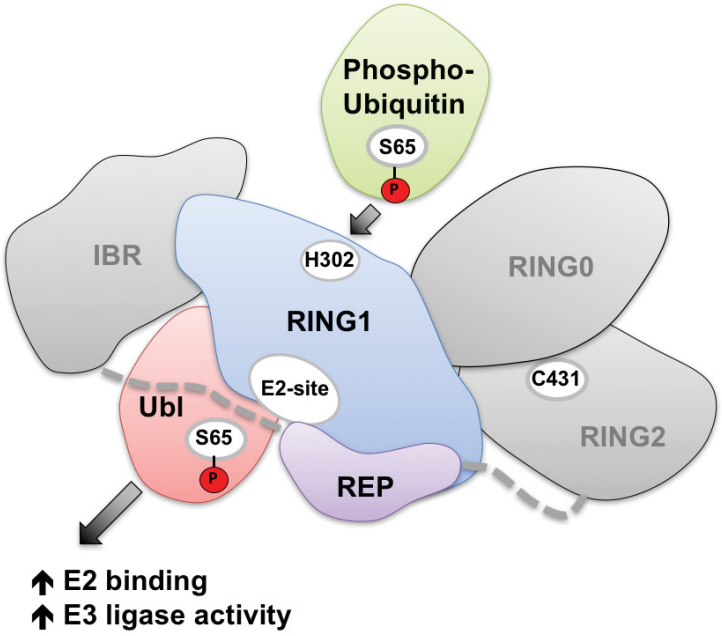

Figure 4.13 Schematic of the Ubl / ubiquitin switch in the activation of parkin. Phosphorylated ubiquitin binds to the H302 site on RING1 of parkin and promotes the dissociation of the parkin Ubl domain. The Ubl domain is in turn phosphorylated by PINK1 and activates parkin. Figure from Sauvé *et al.*, 2015 [203].

The second conformational change is mediated through the R0-RBR domain and gives rise to the antagonism between Ubl and pUb binding. As first observed by Ordureau et al. (2014), Ubl phosphorylation increases the affinity of parkin for pUb. Contrary to expectations, the two

phosphoproteins do not compete for binding; the non-phosphorylated form of one competes with the phosphorylated form of the other. Two pieces of evidence suggest that this competition is due to a conformational change rather than overlapping binding sites. The first is that mutations that disrupt the Ubl-RING1 association do not prevent pUb binding. The N273K and L266K mutations block Ubl binding and actually increase pUb binding by displacing the Ubl. In the context of the R0-RBR fragment, the L266K mutation has little effect on pUb binding (Fig 4.5). The second is that mutations of residues over 15 Å away from the Ubl-RING1 interaction site prevent pUb binding. Disruption of a sulfate ion-binding site on the opposite face of the RING1 domain decreases pUb binding by at least 30-fold (Fig 4.7C). Two other groups have recently reported the identification of the same pUb-binding site [251, 284].

We used SAXS to gain insight into the conformational change that couples Ubl and pUb binding. In the model structures, the pUb sits on the RING1 domain opposite the Ubl binding site on RING1. Alignment of the multiple structures of parkin show the IBR domain is flexible and varies in its position relative to the rest of parkin. We were able to obtain excellent agreement between observed and theoretical SAXS curves of the complex of pUb and R0-RBR but only when the IBR domain was allowed to move (Fig 4.9F and 4.9H). The IBR-RING1 interface is the site of several Parkinson disease missense mutations (R275W, Q311H, G328E), which may reflect a role in coupling pUb binding and Ubl release.

The catalysis by parkin requires a third and larger conformational change to bring the incoming E2-conjugated ubiquitin molecule in contact with the parkin catalytic residue, Cys431. Native parkin has very low affinity for E2 binding and low ubiquitin ligase activity. We previously showed that mutagenesis of the REP or deletion of the Ubl domain markedly increased UbcH7 binding and autoubiquitination activity [203]. Here, we observe that the physiological signal of Ubl phosphorylation has a stronger signal than either mutation alone. Parkin phosphorylation dramatically increases both UbcH7 binding and parkin autoubiquitination activity (Fig 4.10 and 4.11). The response from pUb binding was more muted in both assays. The concomitant increase in E2-binding and ligase activity under a wide variety of conditions suggests that the binding of ubiquitin-charged E2 is the rate-limiting step in catalysis. Mutations and stimuli (phosphorylation) that increase E2 binding invariably increase autoubiquitination activity in a parallel fashion.

Both pUb binding and Ubl phosphorylation have been suggested to be the key, initiating step in parkin activation on mitochondria [120-122, 199, 282]. Our switch model is evidence for

feed-forward regulation in which the signals synergize with each other to promote activation. Binding of pUb releases the Ubl domain and promotes its phosphorylation by PINK1, and conversely parkin phosphorylation on the Ubl domain increases parkin's affinity for pUb (Fig 4.13). However, the Ubl domain must do more than simply reduce pUb and E2 binding. Addition of isolated pUbl was shown to increase the activity of parkin [120] and Ubl phosphorylation leads to exposure of the active site cysteine while addition of pUb did not [199]. In cells, ΔUbl parkin does not recruit efficiently to mitochondria and, in patients, missense mutations that disrupt the Ubl domain lead to Parkinson disease. We observed that phosphorylation of the Ubl domain had a much stronger effect on E2 binding than its removal or addition of pUb (Fig 4.10 and 4.11). pUbl likely plays a role in stabilizing the parkin:E2 complex and the conformational change that allows the transfer of ubiquitin onto Cys431.

Thus, a model of parkin activation in mitophagy is emerging where pUb-binding plays a lead role in recruiting parkin to mitochondria and pUbl plays a larger role in regulating parkin activity. Following the initial phosphorylation by PINK1 of ubiquitin on mitochondrial proteins, parkin is recruited and the Ubl domain released through the switch-like mechanism described here. Phosphorylation of the Ubl by PINK1 locks parkin to the mitochondria surface by increasing the affinity for pUb and derepresses parkin ubiquitin ligase activity. The resulting ubiquitination of mitochondrial proteins leads to additional rounds of parkin recruitment and engagement of the autophagic machinery. More studies are needed to clarify the extent to which parkin is required for the initial ubiquitination of mitochondria and the residual activity of non-phosphorylatable S65A parkin in cellular recruitment assays [121, 285].

Chapter 5: Parkin inhibition

5.1 Abstract

Parkin is a cytosolic E3 ubiquitin ligase protein with low basal activity. Parkin autoinhibition stems from a compact arrangement of domains that buries the key elements involved in the ubiquitin transfer. Parkin is recruited to depolarized mitochondria and activated through action of the ubiquitin kinase, PINK1. PINK1 phosphorylates ubiquitin on mitochondria which acts as a receptor for parkin. PINK1 also directly phosphorylates parkin to generate an active conformation. The N-terminal Ubiquitin-like (Ubl) domain of parkin plays a central role in parkin activation, acting as both a regulator of phospho-ubiquitin binding and the site of parkin phosphorylation. Here, using NMR titrations and pull-down assays, we show that the Ubl-binding protein, endophilin A1, attenuates parkin activation by PINK1. Binding of the endophilin A1 SH3 domain to parkin is dependent on parkin activation and requires either phospho-ubiquitin binding or parkin phosphorylation. Parkin phosphorylation by PINK1 is modestly inhibited in the presence of endophilin A1 SH3 domain. Additionally, activity assays show that parkin ubiquitin ligases activity is attenuated by the SH3 domain of endophilin A1. In conclusion, our results show that endophilin A1 interacts with the open conformation of parkin to decrease its activity. This suggests endophilin may play a role in regulating mitophagy in neurons.

5.2 Rationales and hypothesis

In mitophagy, PINK1 recruits and activates parkin to depolarized mitochondria simultaneously by phosphorylating ubiquitin (likely residual phospho-ubiquitin (pUb) on outer mitochondrial membrane (OMM) proteins) and parkin [112, 115, 120-122]. pUb promotes the recruitment of cytosolic parkin to the mitochondrial surface by direct binding of parkin to pUb chains on mitochondria. PINK1 then phosphorylates recruited parkin and form phospho-parkin (pParkin) that enhances the ubiquitin-ligase activity of parkin. Active parkin then ubiquitinates MOM proteins and the added Ub chains on mitochondria by parkin act as further substrates for PINK1, promoting additional parkin recruitment in a feed-forward mechanism [199]. Massive ubiquitination of mitochondrial proteins ultimately promotes turnover of the impaired organelle by autophagy.

Parkin consists of Ubl domain domain at the N-terminus, a RING0 domain unique to parkin, and a RBR module at the C-terminus containing RING1, IBR and RING 2 domains (Fig 5.1A). RING2 domain harbors the catalytic cysteine Cys431 involved in ubiquitin transfer. Parkin Ubl domain plays a central role in regulating parkin activity [195]. The Ubl domain is phosphorylated on serine 65 (shown in Fig 5.1B) by PINK1, the same residue getting phosphorylated on Ub [112, 115]. Ubl phosphorylation not only derepresses parkin ubiquitin ligase activity, but also serves to increase parkin affinity for pUb, parkin receptor on mitochondria [199, 251, 286, 287]. Parkin binding to pUb and Ubl phosphorylation both promote disengagement of Ubl domain from RING1 and unleash parkin autoinhibition. The Ubl domain also interacts with numerous proteins and has been suggested to play a role in parkin trafficking and localization. The Ubl interacts with the proteasome subunit RPN10 [271] and ubiquitin interacting motifs in ataxin-3 and Eps15 [91, 288]. The Ubl domain of parkin also binds to the SH3 domains of endophilins, a family of BAR (Bin/amphiphysin/Rvs) domain membrane proteins [88]. The highest affinity binding was observed with the SH3 domain of endophilin A1, also called SH3GL2 (SH3 domain-containing GRB2-like 2). Endophilin A1 is a brain specific protein, highly concentrated in presynaptic terminals, and a key regulator of the endocytosis of synaptic vesicles [88]. The protein consists of a N-terminal dimeric BAR domain that binds curved membranes and a C-terminal SH3 domain (Fig 5.1 A) that binds to proline-rich motifs present in dynamin and synaptojanin 1 as well as to the Ubl domain of parkin [247, 248].

Binding of endophilin A1 to the parkin Ubl leads to constitutive endophilin A1 mono-ubiquitination by parkin in nerve terminals [122, 233]. However, the nature of the binding has been shown to be phosphorylation dependent [88]. This binding may also lead to ubiquitination of PRD-associated synaptic endophilin A1 binding partners including synaptojanin 1, dynamin, and ataxin-2 [233-235]. SH3 domain of endophilin A1 interacts with the hydrophobic patch surrounding Ile-44 in Ubl domain of parkin, with similar affinity that this patch has for binding to RING1 domain of parkin in the autoinhibited parkin conformation (Fig 5.1 C).

Given the importance of parkin Ubl domain in parkin activation and mitochondrial turnover, it is crucial to gain insight into how parkin Ubl interactors could affect parkin phosphorylation by PINK1 and parkin ligase activity. Moreover, Ubl phosphorylation has much greater effect than dissociation from the rest of the protein [120, 199, 209, 251, 263, 284, 286, 287, 289]. It has been suggested that phospho-Ubl (pUbl) modifies parkin hydrophobic core packing by exposing parkin

active cysteine and likely plays a role in stabilizing parkin-E2 complex by binding weakly back to parkin from another position. Thus, it is not surprising that high concentration of pUbl binding

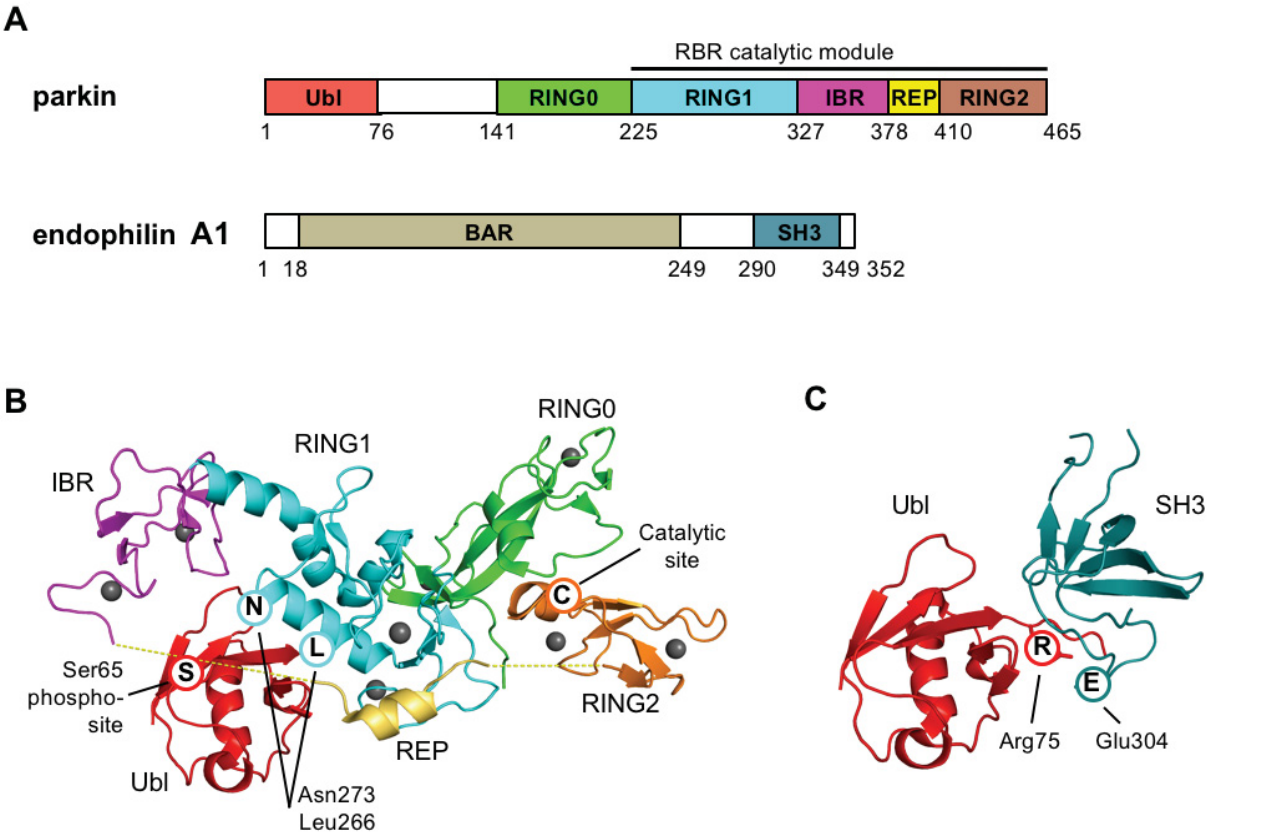

partners including SH3 domain of endophilin A1 suppresses parkin ligase activity by entangling Ubl domain.

Figure 5.1 Structures of parkin and endophilin A1. (A) Domain architecture of parkin and endophilin A1. (B) Schematic structure of parkin in autoinhibited conformation [203]. (C) Schematic representation of the complex of parkin Ubl with endophilin-A1 SH3 [88]. Key residues at the interface are labeled, and their side chains are displayed as sticks. The parkin Ubl domain binds endophilin A1 SH3 domain with the same surface that is involved in RING1 binding in the parkin autoinhibited structure.

Here, we hypothesized that parkin phosphorylation by PINK1 and binding to pUb (both of which release the Ubl domain from its position on RING1 domain in the autoinhibited parkin conformation) can affect parkin binding to endophilin A1 and parkin activity. Our objectives here were to:

4. Determine if parkin Ubl phosphorylation affects Ubl binding to SH3 domain?

5. Do parkin phosphorylation and binding to pUb drive the interaction between endogenous parkin and endophilin A1?
6. How does parkin phosphorylation by PINK1 is affected in the presence of SH3 domain of endophilin A1?
7. How does this binding regulate parkin ligase activity?

5.3 Results

5.3.1 pUbl interacts with endophilin A1 SH3 domain

Ubl domain of parkin interacts with SH3 domain of endophilin A1 with ~10 μM affinity, in a phosphorylation-dependent manner [88]. On the other hand, Ubl phosphorylation affects its binding to RING1 domain of parkin in the context of full-length protein. This prompted us to test whether this phosphorylation could affect Ubl binding to its binding partner endophilin A1. Using GST-SH3 as a bait, we were able to pull-down Ubl and pUbl (confirming that this phosphorylation does not affect its affinity for SH3 domain of endophilin A1 (Fig 5.2A). Strikingly, no signal was detected for full-length parkin (Fig 5.2A). To confirm the results, we performed NMR titration experiments. In consistent with previous results, ^{15}N-SH3 signals shifted upon addition of Ubl due to formation of a complex (Fig 5.2B). We got similar peak shifts upon addition of pUbl to ^{15}N-SH3 validating that Ubl and pUbl bind from the same surface of SH3 with similar affinities (Fig 5.2B). The perturbations were in the fast-intermediate exchange regime and enabled us to calculate a dissociation constant of 20 (±5) μM for Ubl and 37 (±9) μM for pUbl (Fig 5.2C). Interestingly, a similar titration experiment carried out with full-length parkin induced negligible chemical shift perturbations, which confirmed the absence of binding observed in pull-down assay (Fig 5.2B). Together, we discovered parkin does not bind endophilin A1 SH3 domain in the autoinhibited conformation where Ubl hydrophobic patch is buried in the Ubl:RING1 interface. Moreover, Ubl phosphorylation does not affect Ubl binding to endophilin A1 SH3 domain that can imply parkin Ubl domain may still bind to binding partners upon phosphorylation.

5.3.2 Activated parkin binds to endophilin A1 SH3 domain

Both parkin phosphorylation and binding to pUb are parkin activators in this pathway and has been shown to lead to Ubl disengagement from RING1 in the autoinhibited conformation. Endophilin A1 is an endocytic protein highly concentrated in nerve terminals, where mitophagy is of great importance. This prompted us to see how parkin activation by PINK1 affects endophilin

binding in the context of full-length protein as parkin phosphorylation and binding to pUb (which are parkin activators in this pathway) may lead to Ubl disengagement from RING1 in the autoinhibited parkin conformation.

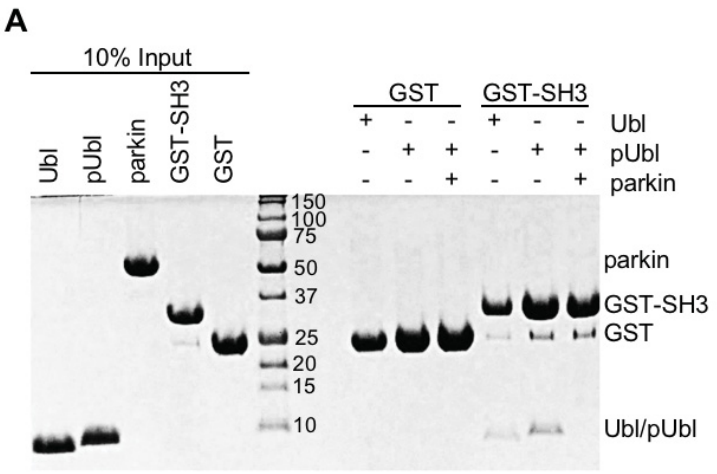

C

endophilin SH3 binding affinities

Parkin construct	K_D (μM)
Ubl	20 ± 5
pUbl	37 ± 9
parkin	No binding

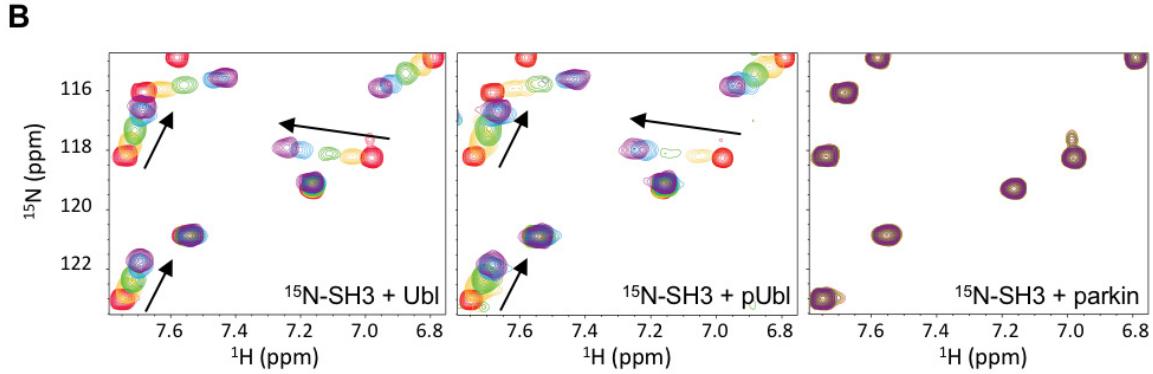

Figure 5.2 Ubl and pUbl, but not full-length parkin interact with SH3 domain of endophilin A1. (A) Pull-down of Ubl, pUbl, or parkin using GST-SH3 immobilized on glutathione–Sepharose resin. After washes, products were resolved by SDS–PAGE. (B) Part of 600 MHz ^{1}H-^{15}N HSQC NMR spectra of the SH3 domain of endophilin A1 upon addition of an increasing amount of Ubl domain of parkin (left), pUbl (middle), and parkin (right). The peak shifts indicate an interaction of the SH3 with Ubl and pUbl, but not parkin. Molar ratios were 0 (red), 0.5 (yellow), 1 (green), 2 (blue), and 3 (purple). (C) K_D of SH3 binding determined from fits of NMR chemical shift perturbations as a function of ligand concentration.

To answer this question, we thus performed pull-down assays using GST-SH3 as bait and were able to pull-down pParkin, parkin in the presence of 1:1 molar ratio pUb (parkin/pUb) and pParkin/pUb complex, but not full-length parkin (Fig 5.3A). The same pull-down experiment showed no binding between pUb and SH3 and confirmed the binding between parkin in the

presence of pUb and pParkin/pUb complex originates from parkin and not pUb (Fig 5.3B). To confirm that parkin phosphorylation and binding to pUb lead to parkin binding to endophilin A1, we next performed HSQC experiment of ^{15}N-SH3 domain of endophilin A1 in the presence of ATP•Mg^{2+}, parkin, pUb, and PINK1 and magnesium sulfate (Fig 5.3C and E). Very small spectral changes occurred upon addition of ATP•Mg^{2+} or parkin due to buffer changes or interaction of parkin with endophilin A1 SH3 domain. However, upon addition of catalytic amount of PINK1 (that leads to parkin phosphorylation), and addition of pUb (that leads to Ubl release), we observed peak shifts (with similar patterns observed for Ubl and pUbl) and peak disappearances that confirm the binding between pParkin and parkin in the presence of pUb to endophilin A1 SH3 domain (Fig 5.3C). Stronger binding was observed for parkin in the presence of pUb than for pParkin. Together, these data are consistent with a model, whereby parkin phosphorylation and binding to pUb disrupt Ubl:RING1 interface and disengage Ubl domain, (albeit the disengagement level could be more upon binding to pUb) which in return increase parkin binding to binding partners including endophilin A1 SH3 domain from Ile44 hydrophobic patch.

To confirm this model, we tested two parkin mutants, L266K and N273K, that are located in the Ubl-RING1 interface [286]. The mutations release the Ubl domain from its binding site on the RING1 domain and phenocopy pUb binding. Pull-down experiments showed that the mutants enhance SH3 binding to the same extent as activation by phosphorylation (Fig 5.3D). By opening the conformation of parkin, the mutants unmask its SH3-binding potential.

5.3.3 Parkin phosphorylation by PINK1 is decreased in the presence of endophilin A1 SH3 domain

We next investigated the efficiency of parkin phosphorylation by PINK1 in the presence of endophilin A1. We used Phos-tag polyacrylamide gels to measure the amount of phosphorylated parkin in the presence of PINK1 and ATP. As previously observed [286], pUb greatly enhanced phosphorylation by PINK1 (Fig 5.4A). While the amount of pParkin was barely detectable in the absence of activation, over half of the input parkin was phosphorylated in the presence of pUb. In contrast, parkin phosphorylation was inhibited by addition of the endophilin SH3 domain (Fig 5.4A, lanes 5 and 6). Quantification of the gels showed the amount was decreased by roughly one third (Fig 5.4B). These results confirm that endophilin hinders parkin activation by PINK1, most likely due to competition for Ubl binding.

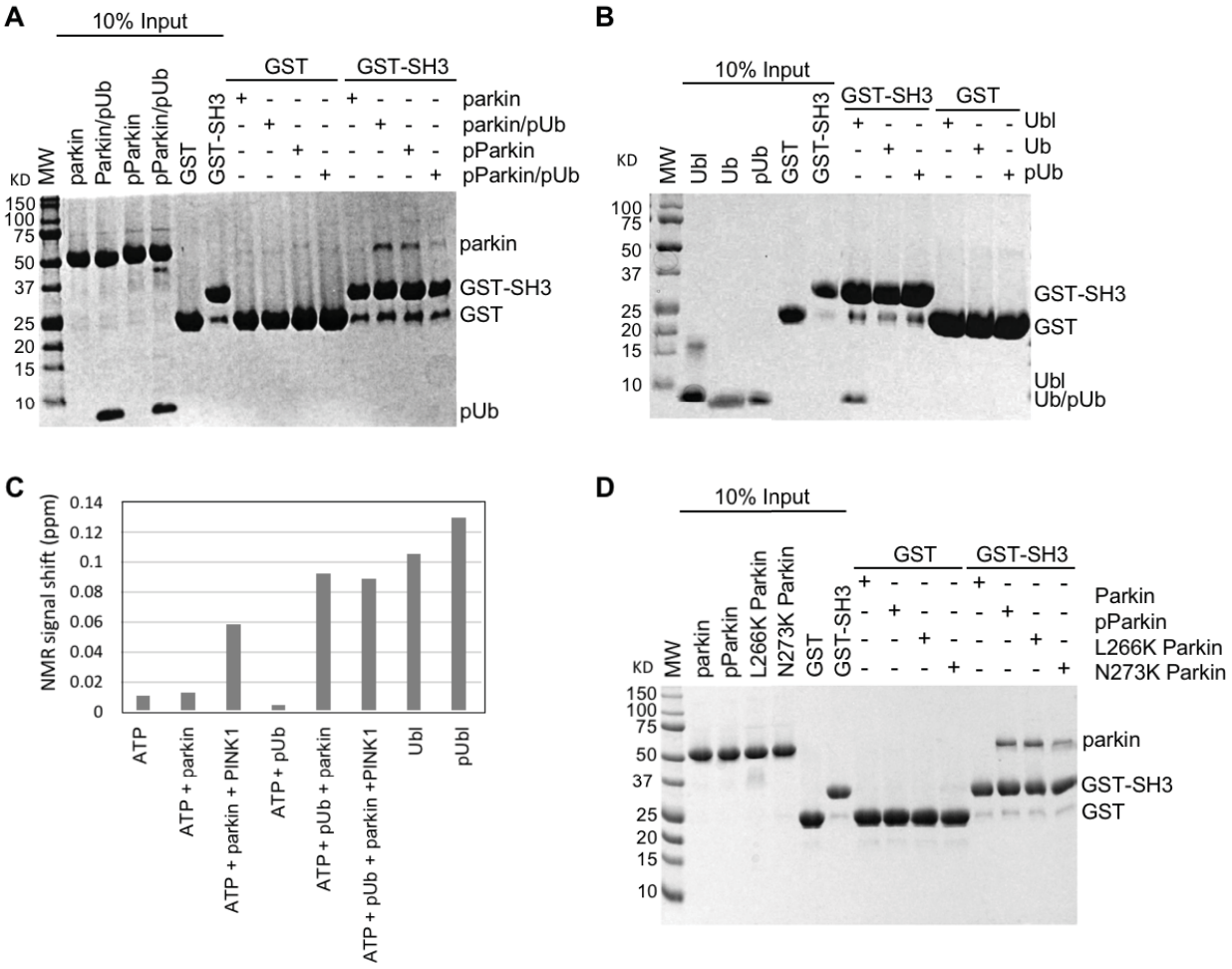

Figure 5.3 Ubl release is required for SH3 binding to Ubl and pUbl. (A) Pull-down of parkin in the presence of pUb and when phosphorylated by GST-tagged endophilin SH3 domain immobilized on glutathione–Sepharose. After washes, products were resolved using SDS–PAGE. (B) Pull-down of Ubl, Ub, or pUb using GST-SH3 construct immobilized on glutathione–Sepharose resin. After washes, products were resolved using SDS–PAGE. (C) NMR chemical shift changes (calculated as $((\delta^{1}\mathrm{H})^{2} + (0.2*\delta^{15}\mathrm{N})^{2})^{1/2}$) of the Phe 27 amide of ^{15}N-labeled endophilin A1 SH3 upon addition of the indicated components. Large shifts, indicative of binding, were observed with Ubl, pUbl, and activated forms of parkin. (D) Pull-down assay of parkin, pParkin, L266K parkin, or N273K parkin using GST-SH3 construct immobilized on glutathione–Sepharose resin. After washes, products were resolved using SDS–PAGE. L266K and N273K disrupt the Ubl-binding site on the parkin RING1 domain.

5.3.4 Addition of SH3 domain moderately decreases parkin activity *in vitro*

To investigate the effect of endophilin on the E3 ubiquitin ligase activity of parkin, we performed two types of assays – parkin autoubiquitination and an *in organello* assay – and

quantified the effects of adding the endophilin SH3 domain. Consistent with previous results, we observed low autoubiquitination activity with unactivated parkin and high levels of activity with the phosphorylated protein (Fig 5.4 C). Addition of the endophilin SH3 domain reproducibly decreased parkin ligase activity. The effect could be observed both in the decreased amount of unmodified parkin and increased amount of poly-ubiquitinated protein (Figs 5.4 C and D).

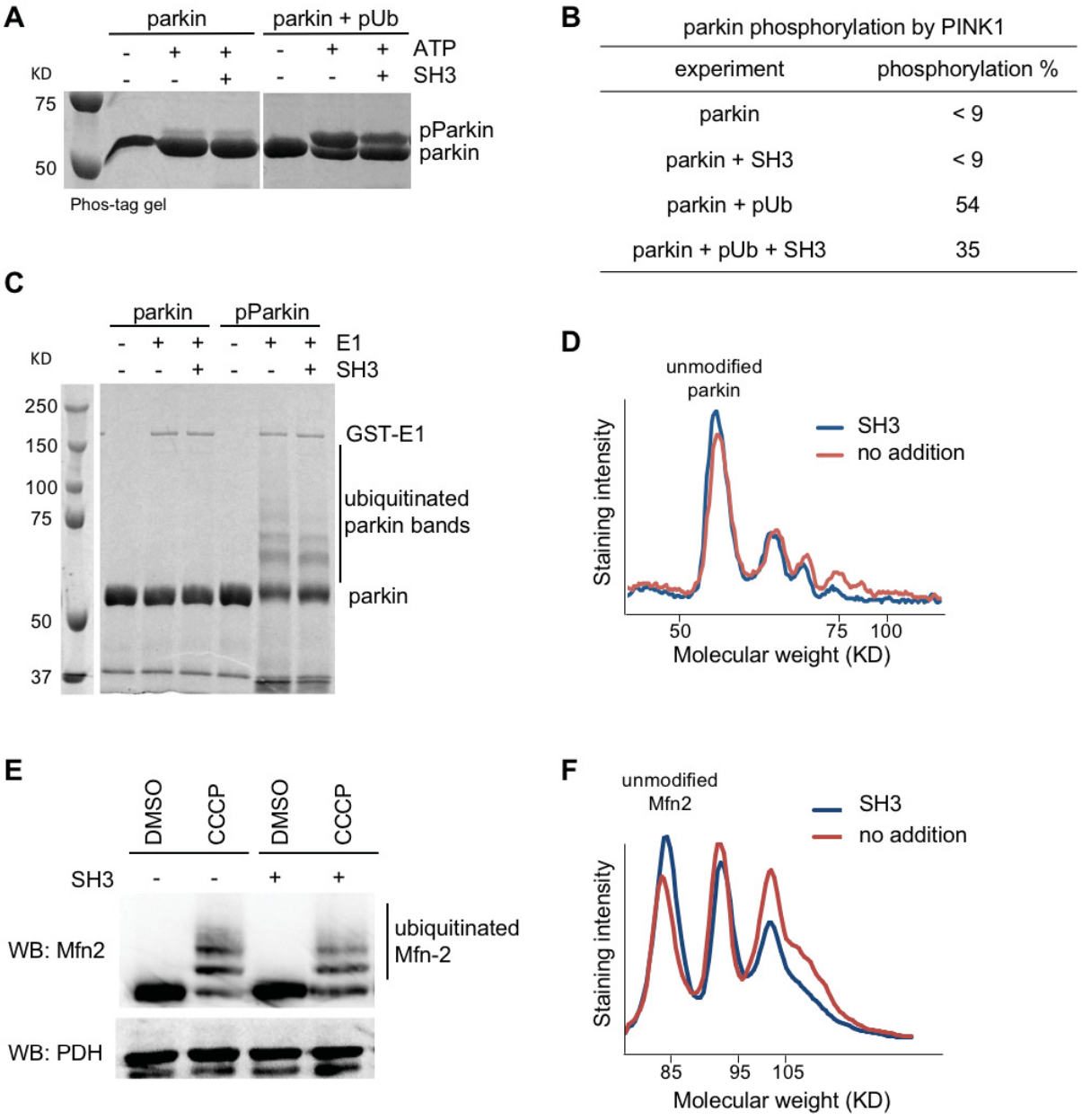

Figure 5.4 Parkin activity and phosphorylation are modestly decreased in the presence of SH3. (A) Parkin phosphorylation assay showing decreased parkin phosphorylation by PINK1 in the presence of pUb and endophilin A1 SH3 domain. Parkin was incubated for 3 minutes with the

*Tc*PINK1 kinase with and without ATP, pUb, and endophilin A1 SH3 domain. Products were resolved by Phos-tag SDS–PAGE and stained with Coomassie Blue. (B) Quantification of parkin phosphorylation in the gel in panel A. (C) Parkin autoubiquitination assay showing decreased parkin activity in the presence of endophilin A1 SH3 domain. Unmodified or phosphorylated parkin was incubated with ATP•Mg^{2+}, E2 ubiquitin-conjugating enzyme (UbcH7), with and without E1 ubiquitin-activating enzyme and endophilin A1 SH3 domain for 30 minutes. Products were resolved by SDS–PAGE and stained with Coomassie Blue. Ligase activity was monitored by the loss of unmodified parkin and the formation of higher molecular weight polyubiquitinated bands of parkin. (D) Comparison of autoubiquitination activity for the two right-hand lanes in the gel in panel C. (E) Western blot of *in organello* ubiquitination reactions showing parkin ubiquitination of Mfn2 is decreased in the presence of endophilin A1 SH3 domain. The *in organello* ubiquitination reactions were performed with DMSO and CCCP treated mitochondria for 30 minutes at 37 °C in the absence and presence of endophilin A1 SH3 domain. The reactions were stopped by addition of SDS-PAGE loading buffer and loaded directly on gel. (F) Comparison of Mfn2 ubiquitination in the gel lanes with CCCP in panel E.

To test this result in a more physiological system, we performed *in organello* ubiquitination assays and measured ubiquitination of the mitochondrial outer membrane protein, mitofusin 2 (Mfn2) [263]. As expected, no ubiquitination was observed in mitochondria treated with DMSO while carbonyl cyanide chlorophenyl hydrazone (CCCP) treated (depolarized) mitochondria showed significant ubiquitination of Mfn2 (Fig 5.4 E). Repeating the assay with the SH3 domain of endophilin revealed a small but meaningful decrease in the amount of ubiquitinated Mfn2 (Fig 5.4 F). These data demonstrate that endophilin A1 binding plays a negative role and represses parkin E3 ligase activity.

5.4 Conclusion and discussion

Synapses are metabolically active compartments packed with mitochondria that fuel numerous energy demanding steps of synaptic vesicle cycling and ion transport. Synapses are far from soma, and need to cope independently with mitochondrial dyshomeostasis to maintain a functional mitochondrial network. Not only are mitochondria more prone to accumulate damage throughout intense neuronal activity, but impaired mitochondria are themselves sources of reactive oxygen species and need to be removed rapidly [290]. Given the importance of healthy mitochondria in synapses, elaborate mitochondrial quality control processes are required to remove the damaged organelles. Parkin-PINK1 mediated mitophagy is one of the best-studied mitochondrial quality control pathways. Loss of function of parkin or PINK1 contribute to

neurodegeneration in PD. Parkin/PINK1 mitophagy has been shown to occur in the soma [291-294], as well as along the axons [295]. However, little is known about mitophagy at presynaptic terminals were most mitochondria are located.

Endophilin A1 is specifically present in presynaptic terminals and has major roles in calthrin-mediated [248, 296-298] and clathrin-independent endocytosis [299], and macroautophagy [300]. Endophilin A1 is a newly identified risk factor for PD [161] and linked to various PD-associated proteins. Endophilin A creates docking stations for autophagic proteins at synapses upon phosphorylation of its BAR domain by LRRK2 (a PD-linked protein) and is essential for autophagosome formation at presynaptic terminals [164, 300]. PD mutations in the endophilin binding partner, synaptojanin 1, impair clathrin uncoating [301]. Endophilin expression undergoes compensatory upregulation upon loss of synucleins [302]. Finally, parkin is upregulated in endophilin mutant mice [88, 233]. Parkin mediates ubiquitination of endophilin A1 and its binding partners, GTPase dynamin and phosphatase synaptojanin 1 [88, 233].

Our results reveal the molecular mechanisms of endophilin binding to parkin. In its autoinhibited structure [203], the Ubl domain of parkin is docked onto the RING1 domain and inaccessible for interacting with the endophilin SH3 domain. The Ubl domain is released by parkin activation and becomes accessible for endophilin binding. The *in vitro* pulldown experiments mirror results with brain extracts that showed a requirement for protein phosphorylation [88]. While pUb binding and parkin phosphorylation synergize to increase parkin ligase activity, surprisingly, we consistently observed a decrease in the amount of parkin pulldown by endophilin SH3 in the presence of both pUb and parkin phosphorylation (Fig 5.3 A). While the reason for this is not completely clear, it suggests that endophilin binds less well to the fully activated conformation of parkin. When phosphorylated, the Ubl domain plays a positive role in promoting parkin activity and would appear to be less available for binding endophilin. Biasing parkin toward an inactive conformation would also explain the inhibitory effect of endophilin on parkin ligase activity. As confirmed by the L266K mutant, release of the Ubl domain from RING1 is sufficient to expose all of the endophilin-parkin interaction (Fig 5.3 D).

Given the importance of mitophagy and endophilin in neural presynaptic terminals, we had expected to see endophilin would enhance PINK1 activation of parkin in *in vitro* assays. Instead, we observed modest inhibition of both PINK1 phosphorylation of parkin and parkin ubiquitin ligase activity. This may reflect fine-tuning by endophilin of the PINK1-parkin pathway on

mitochondria. Depletion of endophilin from the cytosol by recruitment to plasma membranes during intense neuronal activity could act to upregulate mitophagy. But the size of the effect also suggests heightened importance of non-mitochondrial functions. As we first reported [88], the binding of parkin to endophilin in brain synaptosomes leads to parkin relocalization to membrane and increased ubiquitination of polyproline rich proteins. The principal function of the endophilin-parkin interaction is most likely related to vesicle trafficking and macroautophagy. That we see decreased binding of endophilin fully activated by PINK1 and pUb binding suggests that there may be other mechanisms in synapses to activate parkin without inhibiting the endophilin binding.

Beside parkin-endophilin A1 binding consequence on parkin activity and mitophagy, this binding may lead to enhanced ubiquitination of endophilin A1 and its major binding partners, including dynamin (a GTPase implicated in the fission of the bud neck) and synaptojanin 1 (a phosphatase involved in rapid clathrin uncoating after fission). These ubiquitinations may also play additional roles in endocytosis, and autophagy that needs further investigation.

Three endophilin A isoforms have been found in human that all interact with Ubl domain of parkin (A1 and A3 with higher affinity than A2) [88]. While endophilin A1 is brain specific, endophilin A3 is mainly found in the brain and testis, and endophilin A2 is expressed in multiple tissues [163]. More studies are required to clarify the role of these interactions in different organs.

Together, our findings represent additional evidence of the central role of the parkin Ubl domain in mediating protein-protein interactions and regulating parkin activity. We show that endophilin binding by parkin is promoted by treatments that release the Ubl domain from the inhibited conformation. By competing with Ubl binding to the PINK1 kinase and the active parkin, endophilin A1 moderates activation of parkin by PINK1.

Chapter 6: General Discussion

Structural biologists are mostly concerned with the molecular structure of biological macromolecules and how alterations in these structures affect their function. This subject is of great importance to biologists as macromolecules carry out various functions in cells by folding into specific three-dimensional forms. Structural biology studies contribute to understanding and treatment of human diseases. The work described in this thesis mainly focuses on the structure and function of the protein parkin. Parkin has many functions in cell, and mutations in the encoding gene is a great contributor to genetic form of Parkinson's disease (PD) leading to the loss of dopamine-producing neurons in the brain. Why these neurons die is not completely clear and there is currently no therapy for treating or preventing Parkinson's disease.

A prevailing hypothesis is that mitochondrial dysfunction plays a central role in PD neuronal demise. A breakthrough in the field was the discovery of a mitochondrial quality control mechanism regulated by parkin and another PD-linked protein PINK1. Loss of function mutations of parkin and PINK1 are the most common causes of autosomal recessive form of PD. In this pathway, protein kinase PINK1 senses mitochondrial depolarization, and recruits and activates the basally inactive E3 ubiquitin-ligase parkin to the damaged organelle. Activated parkin clears the damaged organelle by catalyzing ubiquitin transfer onto mitochondrial proteins and induces autophagy. Mutations in parkin and PINK1 stimulated interest in their roles in this pathway. When I started my project, the mechanism of parkin autoinhibition and how this autoinhibition can be released by PINK1 at the molecular level were not clear. The main goals of the research presented in this thesis were to obtain a molecular view of parkin autoinhibition and activation.

6.1 Lessons from parkin structure

As described above, in 2013, we solved the structure of full-length and a truncated fragment of parkin by X-ray crystallography technique at resolutions of 6.5 Å and 2.8 Å, respectively. From the structures, we found that parkin is autoinhibited due to intra-molecular contacts. SAXS experiments validated these structures in solution. In the same year, two other groups reported very similar high-resolution crystal structures of truncated parkin consisting of the RING0, RING1, IBR, and RING2 domains (4I1H, 4I1F, 4BM9) [201, 202]. Parkin crystal

structures shed light on parkin regulation mechanism of autoinhibition. In the structures, parkin adopts a compact arrangement of domains, stabilized by multiple hydrophobic inter-domain interactions including the specific contacts between RING2/RING0, as well as Ubl/RING1, and REP/RING1 (Fig 6.1A).

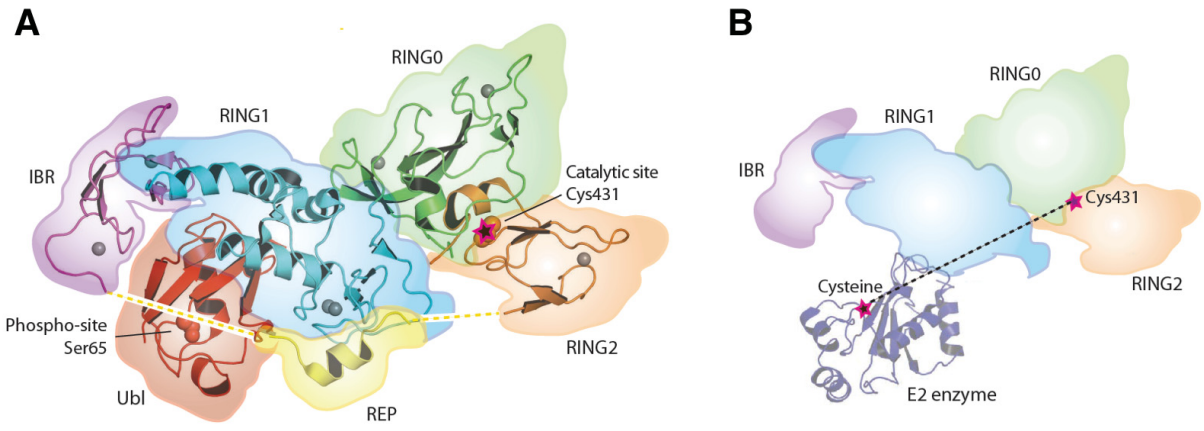

Figure 6.1 The structure of parkin reveals the mechanism of its autoinhibition. (A) Cartoon representation of parkin (pdb: 4K95, [203]). The RING0 domain partially covers the catalytic cysteine on the RING2 domain. The eight structural zinc ions in parkin are shown as gray spheres. Dashed lines indicate portions of the IBR and RING2 linker that were not observed in the crystal structure. (B) Model of an E2 enzyme bound to parkin with Ubl and REP linker removed. An additional structural rearrangement must occur to allow ubiquitin on the E2 enzyme to transfer to the catalytic cysteine of parkin. The E2 and parkin catalytic cysteines are ~50 Å apart in the model. Figure from Seirafi *et al.,*2015 [86].

Parkin activity depends on two functional sites: a binding site for ubiquitin conjugated E2 enzyme on the RING1 of parkin and a catalytic site with a cysteine that forms a transient covalent linkage with ubiquitin on the RING2 domain (Figure 6.2). Remarkably, in our parkin crystal structure, both required elements of ubiquitin transfer were blocked by intra-molecular interactions; the Ubl domain and Repressor Element of Parkin (REP) linker prevent the E2 from binding (Figure 6.1B), whereas parkin catalytic cysteine is occluded by RING0 domain (Fig 6.1). Furthermore, the large distance between the E2 binding site and catalytic site on RING2 prevents transfer of ubiquitin from the ubiquitin~E2 conjugate to the parkin catalytic cysteine. (Fig 6.1B).

Based on the crystal structures, we designed mutations that prevent inter-domain interactions. The designed mutations that prevent RING0/RING2 and REP/RING1 binding greatly enhanced parkin activity in autoubiquitination assays, whereas the designed mutations that prevent

Ubl/RING1 binding had very small effect suggesting different roles played by these domains. Designed mutations that prevent RING1/REP and RING1/Ubl binding also enabled us to confirm our parkin/E2 model, in that these mutations led to increased binding to E2 enzyme UbcH7 in NMR binding studies.

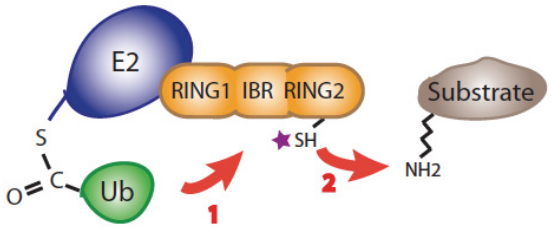

Figure 6.2 Mechanism of ubiquitin transfer in RBR family of E3 ubiquitin ligases. RBRs bind to ubiquitin-charged E2 enzymes through their RING domain, transfer ubiquitin to their catalytic cysteine first and then to the substrate molecules. Figure from Seirafi *et al.,* 2015 [86].

Parkin structure also confirmed the stoichiometry of eight zinc ions per molecule [272] and depicted the topology of four zinc finger domains, RING0, RING1, IBR and RING2 (collectively referred to as R0-RBR), each coordinating two zinc ions. Even though RING0 and RING2 were originally predicted as RING domains based on the primary amino acid sequence, their structural topologies in the structures revealed that they differ from a classical RING fold; the RING0 domain presented a hairpin arrangement unique to parkin, while the RING2 and IBR domains show a sequential arrangement of zinc-coordinating residues. In parkin structure, the RING1 domain is the only RING domain with the classical cross-brace zinc coordination topology observed in other RING-type E3 ubiquitin ligases.

Parkin crystal structure also provide rationales for many of the mutations associated with PD as certain mutations compromise the structural integrity of the protein, while others interfere with binding of substrates or directly affect the enzyme catalysis.

Two other structures of members of RBR E3 ubiquitin ligases were also solved within the same year [303, 304]. HHARI, a member of the Ariadne family, and HOIP, a component of the linear ubiquitination assembly complex (LUBAC), both revealed similar mechanism of autoinhibition regulated by blocking the catalytic RING2 domain by Ariadne domain and the UBA domain, respectively. Moreover, the catalytic cysteine residue in the RING2 domain is conserved in all the members of the RBR family, as are the residues involved in zinc coordination (Fig 6.3A).

Following the catalytic cysteine, there is partial conservation of a histidine residue and an acidic residue. In parkin, these residues have been proposed to act as a catalytic triad, where the histidine acts as a general base to promote catalysis [201-203] (Fig 6.3B). In parkin, HHARI and HOIP crystal structures [203, 303, 304], the RING2 domains are highly conserved and share the linear arrangement of the three residues (Fig 6.3B). Nonetheless, the results of mutagenesis are ambiguous about the importance of the catalytic triad. The effect of the loss of the histidine is substrate dependent and can be suppressed *in vitro* by raising the pH [201, 304]. In cultured cells, mutation of the histidine only moderately slows parkin mediated mitophagy and while the E444Q mutation reduces autoubiquitination [203] and may be implicated in PD [305], it has no effect on parkin activity in cells [201].

Additional insight into the catalytic mechanism comes from the crystal structure of HOIP, which contains two ubiquitin molecules in contact with the catalytic RING2 domain (Fig 6.3C). The C-terminus of one ubiquitin molecule is positioned to mimic the thioester linkage with the catalytic cysteine while the amino group of the second ubiquitin molecule approaches the cysteine from the other side and occupies the position of the acceptor molecule. Transposition of the two ubiquitin molecules onto the parkin crystal structure generates a hypothetical model of the active site with a thioester intermediate prior to acyl transfer. While the donor ubiquitin can be accommodated to fit in a groove on the surface of the RING2 domain, the position of the acceptor ubiquitin or substrate protein clashes with the RING0 domain, implying that this domain must move in order for a substrate amino group to access the active site.

6.2 Activation mechanism of parkin

PINK1 acts upstream of parkin and is required for parkin activation and recruitment to depolarized mitochondria [95-97, 114, 279]. In 2012, Kondapally *et. al* showed that PINK1 phosphorylates parkin Ubl domain on residue Ser65 to activate parkin [112, 113, 306]. Although the phosphomimetic S65E mutation stimulates parkin ligase activity *in vitro*, this mutation is not able to bypass the PINK1 requirement for mitochondrial recruitment in cells and the non-phosphorylatable S65A mutation is not completely impaired [306]. These observations led to the search for an additional PINK1 substrate involved in the parkin activation and the breakthrough discovery that ubiquitin can be phosphorylated by PINK1 [120-122].

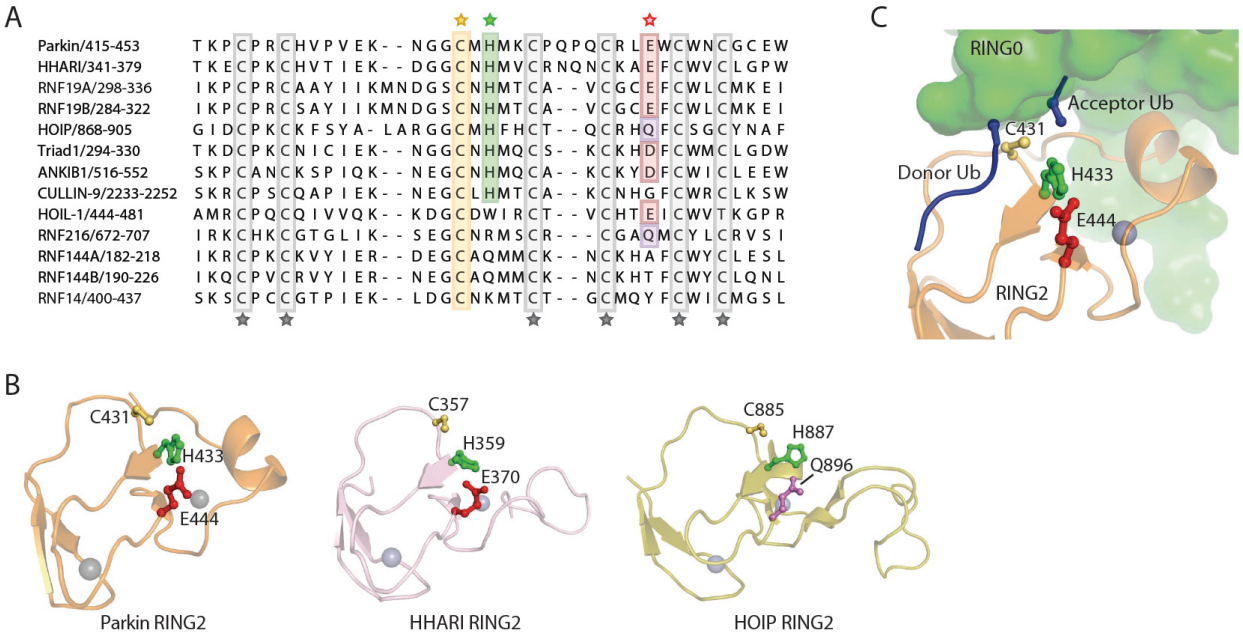

Figure 6.3 Mechanism of ubiquitin ligase activity of RBR E3 ubiquitin ligases. (A) Sequence alignment of RBR E3 ubiquitin ligases shows conservation in the catalytic RING2 domains. The catalytic cysteine (highlighted in yellow) is invariant across RBR proteins, whereas histidine (green) and glutamate residues (red) that play secondary roles in catalysis are less conserved. Grey indicates zinc-coordinating residues. (B) Structural comparison of catalytic domains of parkin, HHARI, and HOIP (pdb: 4K7D, [203]; 4KBL, [303]; 4LJO, [304]). The alignment of the catalytic cysteine, histidine and glutamate/glutamine is suggestive of catalytic triad where the histidine acts as a general base to promote transesterification of ubiquitin onto the substrate. (C) Model of the positions of the donor and acceptor ubiquitin molecules in the catalytic site of parkin based on crystal structure of HOIP [304]. The C-terminus of the donor ubiquitin lies in a groove of the RING2 domain and terminates next to the catalytic cysteine, mimicking the thioester intermediate. The amino group of the acceptor ubiquitin approaches Cys431 from the opposite side but would be sterically blocked by the parkin RING0 domain in the absence of a conformational change. Figure from Seirafi *et al.,* 2015 [86].

In 2014, three groups concurrently observed that PINK1 can phosphorylate ubiquitin on Ser65, the same position that is phosphorylated in the parkin Ubl domain. Further, they showed that phosphorylated ubiquitin or phospho-mimetic ubiquitin mutants (S65D/E) directly activate parkin by enhancing the rate of E2~ubiquitin discharge [120-122]. Parkin binds strongly to phospho-ubiquitin with an affinity of 400 nM. Phosphorylation of Ser65 of parkin further increases the affinity 20 fold. In cells, expression of the non-phosphorylatable S65A ubiquitin delays parkin recruitment to the depolarized mitochondria, and mutation of both parkin and ubiquitin at Ser65 abolishes parkin activation [121]. Further studies have revealed that PINK1 is not only a ubiquitin

kinase but is also capable of phosphorylating ubiquitin in ubiquitin chains [199, 307, 308]. While phosphoubiquitin (pUb) can still become activated by E1 and charged onto E2 enzymes, its activity in ubiquitination assays is E3 dependent [308]. Parkin shows somewhat less activity with phospho-ubiquitin~E2 than with ubiquitin~E2 [122]. Potentially more relevant is the observation that phosphorylated ubiquitin chains were more resistant to hydrolysis by 10 out of 12 deubiquitinases tested [308]. One possible explanation is the presence of a minor conformation of phospho-ubiquitin that was detected by nuclear magnetic resonance [308]. The minor conformation, corresponding to about 30% of molecules, shows a β-strand slippage that disrupts the Ile44 hydrophobic patch involved in many ubiquitin interactions.

To get a better understanding of parkin activation by phosphorylation and binding to pUb in Chapter 4, we designed experiments to get a better view of these two activators at the molecular level. The site of parkin phosphorylation is in close proximity to the REP linker between IBR and RING2 domain in the autoinhibited conformation (Fig 6.1A). Surprisingly, we found that despite the sequential and structural similarities between Ubl and ubiquitin, their phosphorylations lead to opposite outcomes. While Ubl phosphorylation decreases affinity for the R0-RBR core, ubiquitin phosphorylation greatly enhances this affinity.

We used NMR technique to verify the conformational changes in Ubl upon phosphorylation. Interestingly, we found that in contrast to ubiquitin phosphorylation, Ubl phosphorylation leads to small local changes, and pUbl has only one conformation in solution with no strand shifts in the β-sheet. We believe that these small changes destabilize Ubl/RING1 interface and decrease pUbl affinity for R0-RBR, as first observed by Ordureau *et al.* [199].

We next addressed the question of where pUb binds on parkin. We performed NMR titration experiments and unexpectedly discovered a competition between pUb and Ubl in binding the R0-RBR module. However, we have shown that this competition is not due to overlapping binding sites, but due to a conformational change occur in R0-RBR upon binding to pUb, as disruption of Ubl binding site on RING1 did not affect pUb binding to R0-RBR. In order to find the position of pUb in pUb/ parkin complex, we used the information from sulfates bound to positively charged pockets in different parkin crystal structures and designed parkin mutants; we also mutated positively charged residues near Ubl binding site. ITC and pull-down assays on these mutants strongly suggests that one of the sulfate-bound positions (around residue H302) is likely to be the pUb binding site as mutating residues in this pocket prevents pUb binding by 30-fold.

Whilst this position is 15 Å away from Ubl/RING1 site, we believe that binding to pUb from this surface leads to conformational changes in RING1 that destabilize Ubl binding. We modeled this position using SAXS data to gain insight into the conformational change occurring upon pUb binding. In our model, pUb binds to the opposite site of RING1 domain, while position of flexible IBR domain was adjusted. Concurrently, two other groups identified the same binding site on parkin RING1 [120, 251]. One of these groups crystallized covalently attached pUb/parkin complex. In their structure, pUb binding to RING1 led to straightening of a helix in RING1 [251]. This helix is kinked at Gly319 in RING1 of previous autoinhibited parkin crystal structures as well as in RING1 of HHARI ubiquitin ligase.

In line with our SAXS results, Wauer *et al.* have also shown that IBR domain rotates and moves over 20 Å when pUb binds to parkin in phosphoubiquitin/parkin crystal structure. Nevertheless, the purpose of this rearrangement is still unclear. Keeping in mind that pathogenic mutations are present in IBR domain as well as every other domain of parkin, it would be important to uncover the role of the IBR domain in parkin function. Kumar *et al.* recently suggested a new ubiquitin-binding site produced in IBR domain upon binding to phospho-ubiquitin as this position was occupied by a Ubl domain of another parkin molecule and mutating this surface negatively affects parkin ligase activity. More binding studies are required to confirm this ubiquitin binding site on parkin.

Lastly, we showed that parkin phosphorylation, similarly to REP release, enhances parkin binding to the E2 enzyme UbcH7. We also found that pUb binding to parkin is not sufficient to open up the E2 binding site on parkin. Thus, we believe the large conformational change in parkin occurs upon parkin phosphorylation and not binding to pUb. Our activity assays correlated well with E2 binding affinities, suggesting that the rate limiting step in catalysis is E2 binding. Again, parkin phosphorylation has more impact on parkin activity in our assays than pUb binding to parkin.

Most of the evidence is compatible with a simple two-state system. Inputs that activate parkin shift the equilibrium between an inactive and active conformation. There is no evidence of multiple steps in the pathway: disruption of the RING0-RING2 interface increases ligase activity as does disruption of the REP-RING1 interaction. The conformational change between the two states has been suggested to be a "butterfly" movement in which parkin folds along the axis between the RING0 and RING1 domains to bring the two functional sites together [201].

Alternatively, the active conformation could consist of an ensemble of structures where the E2 binding and catalytic sites transiently interact like beads on a string. The release of the inhibitory interactions would suffice to activate the RING1 and RING2 domains to carry out the ubiquitin ligase activity. Taken together, our experiments provide significant insights into the activation of parkin. We propose a switch model which is regulated in a feed-forward manner. We believe that pUb is the parkin receptor on mitochondria. Upon binding parkin, it releases the Ubl domain of parkin. Ubl release enhances parkin binding to pUb and locks parkin on to the damaged organelle. In parallel, Ubl release promotes its phosphorylation by PINK1. Phosphorylation of Ubl subsequently leads to large conformational change in parkin, opening the E2 binding site on RING1 similar to displacement of the REP linker.

Figure 6.4 Conformational changes in RING1 domain due to pUb binding. pUBH helix straighten in RING1 upon binding to pUb. Straight helix in parkin/pUb complex (left) versus kinked helix in our previous parkin full-length structure (pdb: 4K95). pUb is not shown in the left structure. Figure from Wauer *et al.,* 2015 [251].

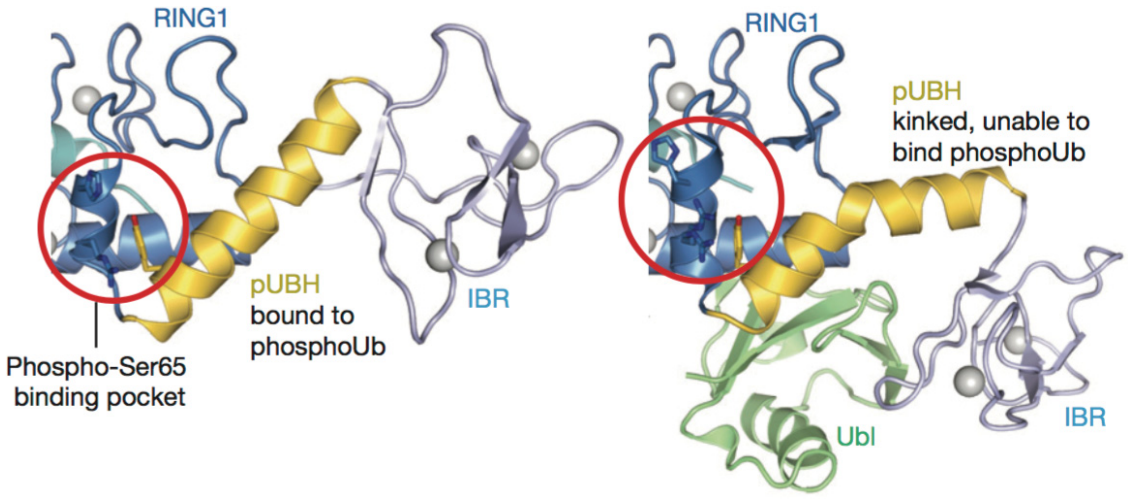

A further enigma in the field for years was the requirement of parkin ubiquitin ligase activity for its recruitment to mitochondria. Catalytically inactive mutants of parkin do not show detectable recruitment following mitochondrial depolarization [97, 116]. The solution to this puzzle is now emerging with a model of the events leading to the recruitment and activation of parkin by phosphoubiquitin (Fig 1.10). In the first step, the selective accumulation of PINK1 on depolarized mitochondria leads to the phosphorylation of low, basal levels of ubiquitin or parkin present on mitochondria [120-122, 199]. The system exhibits feedforward control as both ubiquitin

and parkin phosphorylation are positive effectors of parkin ubiquitin ligase activity [120-122, 199]. Phosphorylation of ubiquitin chains was recently shown to inhibit the action of deubiquitinases [308], which would act as an additional feedforward mechanism. Full activation of the system requires a positive feedback loop where activation of parkin increases the amount of mitochondrially conjugated ubiquitin, which is then phosphorylated by PINK1 to recruit more parkin. The positive feedback explains the requirement for both PINK1 and parkin catalytic activities as well as how high levels of parkin can be recruited and depleted from the cytosol by low, endogenous levels of PINK1. In agreement with the model, the requirement for parkin ligase activity can be bypassed by using overexpressed tetra-ubiquitin chains artificially targeted to mitochondria [309]. The requirement for PINK1 activity can further be bypassed by the use of phosphomimetic chains for S65E tetraubiquitin [307]. Our data provides insights into the relative importance of the feedforward pathway.

Another question to address is how parkin phosphorylation activates parkin. A recent study shows the crystal structure of pUb/phosphomimetic parkin deletion mutant (no linker between Ubl and RING1) complex [251]. The phosphomimetic structure is very similar to wild-type parkin, and Ubl still binds to the similar surface of RING1. This is unlikely, as we showed by SAXS that phosphorylated parkin has a more elongated conformation than parkin and parkin activity is greatly enhanced upon parkin phosphorylation. Moreover, parkin phosphorylation opens up the E2 binding site of parkin, which is not reflected in their structure. While this could be the case of crystallization bias, a more likely explanation is that aspartic acid is not a good replacement for phosphoserine as we and other groups observed that phosphomimetic parkin does not act similarly to parkin in ligase activity assays, and NMR and SAXS experiments. On the other hand, a very short linker in their construct between Ubl and RING0 domain might have imposed little mobility to the Ubl domain upon phosphorylation. Our unpublished data show that Ubl domain interacts with RING0 and may release the autoinhibition by REP and RING0 domain. More studies are required to get a better understanding of parkin activation at the molecular level. In future studies, co-crystallization attempts between phosphorylated parkin and E2s and ubiquitin-charged E2s can be attempted, to uncover how parkin phosphorylation regulates E2 binding to parkin.

6.3 Parkin/PINK1 mediated mitophagy in neurons

Although parkin recruitment to depolarized mitochondria is a robust phenomenon in diverse mammalian cell lines, it has been controversial whether mitophagy is applicable in neurons

and in PD pathogenesis. Concerns are that most of these experiments use overexpressed parkin and that CCCP treatment leads to complete depolarization of mitochondria, which is probably never the case in PD. In experiments in primary neurons, parkin recruitment to depolarized mitochondria is modest and only happens after prolonged CCCP treatment or in the presence of lysosomal or apoptosis inhibitors or special culture conditions [294, 310]. In part, this could arise from the fact that most cell lines are glycolytic while neurons are strictly dependent on oxidative phosphorylation for mitochondrial ATP production; neuronal mitophagy studies may require more physiological methods for induction of depolarized mitochondria. In a recent paper, the mitochondrial ARF protein was shown to induce mitochondrial depolarization and parkin/PINK1 autophagy both in cell lines and in neurons [311]. Moreover, light-activated ROS-induced mitochondrial depolarization was also shown to initiate parkin and PINK1 dependent mitochondrial degradation by autophagy in axonal mitochondria [277]. This confirms that parkin recruitment and activation on mitochondria is relevant for PD.

6.4 Endophilin A1 may regulate mitophagy in neurons

A 2009 study showed binding between parkin Ubl domain and endophilin A proteins [88]. Endophilins have major roles in synaptic vesicle cycling. Among three endophilin A isoforms, endophilin A1 is mainly brain specific and highly concentrated in nerve terminals. More interestingly, it is among newly identified PD risk factors and is linked to two other PD-associate proteins LRRK2 and synaptojanin [161, 164, 237, 245]. The 2009 study showed that the endophilin A1-parkin interaction occurs through the hydrophobic patch of the Ubl domain around Ile44. However, the interaction between full-length parkin and endophilin A1 in brain extracts was only observed in the presence of phosphatase inhibitors, suggesting that the interaction is phosphorylation dependent. The structural basis for these observations was unknown at the time. We know now that the interacting site of Ubl is involved in binding to RING1 domain in autoinhibited parkin. We also know that parkin phosphorylation and binding to phospho-ubiquitin are parkin activators that release the Ubl domain from this position in parkin active conformation. Our pull-down assays mirror results with brain extracts that show the requirement of parkin phosphorylation. The functional relevance of these interactions has not been explored or validated yet, but it implicates parkin in ubiquitination of endophilin A1 and its binding partners in synaptic vesicle cycling. However, we showed that parkin ligase activity is inhibited by the presence of endophilin A1 *in vitro*. More studies are required in cells and brain extracts to validate this result.

6.5 Is parkin a good therapeutic target?

The recent progress in understanding the regulation of parkin activity is appealing for new routes in treating diseases liked to mitochondrial dysfunction. Parkin displays low basal activity and a small increase in the activation of parkin could be sufficient to slow the progression of PD in sporadic forms of the disease where the wild-type protein is present [264]. Although simplistic, small molecules that mimic phospho-ubiquitin or disrupt autoinhibitory interactions might enhance its neuroprotective action. In cultured cells, mutation of Trp403 or Phe463 speeds up recruitment of parkin to mitochondria in a regulated process that remains dependent on PINK1 and mitochondrial depolarization [203]. A small molecule that binds tightly to the pocket normally occupied by amino acid side chains would be expected to have similar effect. Alternatively, the deubiquitinating (DUB) enzymes USP30 and USP15 were recently found to oppose parkin/PINK1 in mitophagy, making inhibitors of these DUBs prime candidates for drug design [312, 313]. In contrast, USP8 promotes parkin-mediated mitophagy and, thus, agonists of this DUB could be developed [200]. While it remains speculative and with many challenges, the quality control pathway mediated by PINK1 and parkin appears to offer multiple therapeutic targets for the treatment of PD and other diseases caused by dysfunctional mitochondria.

6.6 Overall conclusions

In this thesis, with the help of structural biology methodologies and biophysical techniques, we addressed the molecular basis of low basal activity of parkin in cells and shed light on parkin structure and activation by PINK1 at the molecular level. The crystal structure of parkin, which is complemented with mutational and *in vitro* functional assays, validates that parkin's autoinhibition is rooted in its inter-domain interactions that occlude the required elements of ubiquitin transfer. This work also suggests that endophilin A1, a PD risk factor, may regulate parkin ligase activity in nerve terminals. The thesis provides a framework for future structural and biochemical analysis to develop novel therapeutics for patients with PD by targeting parkin.

References

1. Sveinbjornsdottir S. The clinical symptoms of Parkinson's disease. J Neurochem. 2016;139 Suppl 1:318-324.
2. Massano J, Bhatia KP. Clinical approach to Parkinson's disease: features, diagnosis, and principles of management. Cold Spring Harb Perspect Med. 2012;2:a008870.
3. de Lau LM, Breteler MM. Epidemiology of Parkinson's disease. Lancet Neurol. 2006;5:525-535.
4. Jankovic J. Parkinson's disease: clinical features and diagnosis. J Neurol Neurosurg Psychiatry. 2008;79:368-376.
5. Bhattacharyya KB. Hallmarks of Clinical Aspects of Parkinson's Disease Through Centuries. Int Rev Neurobiol. 2017;132:1-23.
6. Kalia LV, Kalia SK, McLean PJ, Lozano AM, Lang AE. alpha-Synuclein oligomers and clinical implications for Parkinson disease. Ann Neurol. 2013;73:155-169.
7. Braak H, Del Tredici K, Rub U, de Vos RA, Jansen Steur EN, Braak E. Staging of brain pathology related to sporadic Parkinson's disease. Neurobiol Aging. 2003;24:197-211.
8. Dong A, Xu X, Edwards AM, Midwest Center for Structural G, Structural Genomics C, Chang C, et al. In situ proteolysis for protein crystallization and structure determination. Nat Methods. 2007;4:1019-1021.
9. Poewe W, Seppi K, Tanner CM, Halliday GM, Brundin P, Volkmann J, et al. Parkinson disease. Nat Rev Dis Primers. 2017;3:17013.
10. Parkinson J. An essay on the shaking palsy. 1817. J Neuropsychiatry Clin Neurosci. 2002;14:223-236; discussion 222.
11. Goetz CG. Charcot on Parkinson's disease. Mov Disord. 1986;1:27-32.
12. Parent M, Parent A. Substantia nigra and Parkinson's disease: a brief history of their long and intimate relationship. Can J Neurol Sci. 2010;37:313-319.
13. Greenfield JG, Bosanquet FD. The brain-stem lesions in Parkinsonism. J Neurol Neurosurg Psychiatry. 1953;16:213-226.
14. Holdorff B. Friedrich Heinrich Lewy (1885-1950) and his work. J Hist Neurosci. 2002;11:19-28.
15. Walden H, Muqit MM. Ubiquitin and Parkinson's disease through the looking glass of genetics. Biochem J. 2017;474:1439-1451.
16. Carlsson A, Lindqvist M, Magnusson T, Waldeck B. On the presence of 3-hydroxytyramine in brain. Science. 1958;127:471.
17. Hornykiewicz O. [Dopamine (3-hydroxytyramine) in the central nervous system and its relation to the Parkinson syndrome in man]. Dtsch Med Wochenschr. 1962;87:1807-1810.
18. Ehringer H, Hornykiewicz O. [Distribution of noradrenaline and dopamine (3-hydroxytyramine) in the human brain and their behavior in diseases of the extrapyramidal system]. Klin Wochenschr. 1960;38:1236-1239.
19. Barbeau A. L-dopa therapy in Parkinson's disease: a critical review of nine years' experience. Can Med Assoc J. 1969;101:59-68.
20. Cotzias GC, Van Woert MH, Schiffer LM. Aromatic amino acids and modification of parkinsonism. N Engl J Med. 1967;276:374-379.

21. Cotzias GC, Papavasiliou PS, Gellene R. Modification of Parkinsonism--chronic treatment with L-dopa. N Engl J Med. 1969;280:337-345.
22. Sprenger F, Poewe W. Management of motor and non-motor symptoms in Parkinson's disease. CNS Drugs. 2013;27:259-272.
23. Olanow CW, Schapira AH. Therapeutic prospects for Parkinson disease. Ann Neurol. 2013;74:337-347.
24. Connolly BS, Lang AE. Pharmacological treatment of Parkinson disease: a review. JAMA. 2014;311:1670-1683.
25. Glover V, Sandler M, Owen F, Riley GJ. Dopamine is a monoamine oxidase B substrate in man. Nature. 1977;265:80-81.
26. Benabid AL, Koudsie A, Benazzouz A, Piallat B, Krack P, Limousin-Dowsey P, et al. Deep brain stimulation for Parkinson's disease. Adv Neurol. 2001;86:405-412.
27. Kringelbach ML, Jenkinson N, Owen SL, Aziz TZ. Translational principles of deep brain stimulation. Nat Rev Neurosci. 2007;8:623-635.
28. Klein C, Westenberger A. Genetics of Parkinson's disease. Cold Spring Harb Perspect Med. 2012;2:a008888.
29. Hernandez DG, Reed X, Singleton AB. Genetics in Parkinson disease: Mendelian versus non-Mendelian inheritance. J Neurochem. 2016;139 Suppl 1:59-74.
30. Trinh J, Farrer M. Advances in the genetics of Parkinson disease. Nat Rev Neurol. 2013;9:445-454.
31. Polymeropoulos MH, Lavedan C, Leroy E, Ide SE, Dehejia A, Dutra A, et al. Mutation in the alpha-synuclein gene identified in families with Parkinson's disease. Science. 1997;276:2045-2047.
32. George S, Rey NL, Reichenbach N, Steiner JA, Brundin P. alpha-Synuclein: the long distance runner. Brain Pathol. 2013;23:350-357.
33. Nemani VM, Lu W, Berge V, Nakamura K, Onoa B, Lee MK, et al. Increased expression of alpha-synuclein reduces neurotransmitter release by inhibiting synaptic vesicle reclustering after endocytosis. Neuron. 2010;65:66-79.
34. Burre J, Sharma M, Tsetsenis T, Buchman V, Etherton MR, Sudhof TC. Alpha-synuclein promotes SNARE-complex assembly in vivo and in vitro. Science. 2010;329:1663-1667.
35. Yavich L, Tanila H, Vepsalainen S, Jakala P. Role of alpha-synuclein in presynaptic dopamine recruitment. J Neurosci. 2004;24:11165-11170.
36. Singleton AB, Farrer M, Johnson J, Singleton A, Hague S, Kachergus J, et al. alpha-Synuclein locus triplication causes Parkinson's disease. Science. 2003;302:841.
37. Ibanez P, Bonnet AM, Debarges B, Lohmann E, Tison F, Pollak P, et al. Causal relation between alpha-synuclein gene duplication and familial Parkinson's disease. Lancet. 2004;364:1169-1171.
38. Bartels T, Choi JG, Selkoe DJ. alpha-Synuclein occurs physiologically as a helically folded tetramer that resists aggregation. Nature. 2011;477:107-110.
39. Fauvet B, Mbefo MK, Fares MB, Desobry C, Michael S, Ardah MT, et al. alpha-Synuclein in central nervous system and from erythrocytes, mammalian cells, and Escherichia coli exists predominantly as disordered monomer. J Biol Chem. 2012;287:15345-15364.
40. Wang W, Perovic I, Chittuluru J, Kaganovich A, Nguyen LT, Liao J, et al. A soluble alpha-synuclein construct forms a dynamic tetramer. Proc Natl Acad Sci U S A. 2011;108:17797-17802.
41. Irizarry MC, Growdon W, Gomez-Isla T, Newell K, George JM, Clayton DF, et al. Nigral and cortical Lewy bodies and dystrophic nigral neurites in Parkinson's disease and cortical Lewy

body disease contain alpha-synuclein immunoreactivity. J Neuropathol Exp Neurol. 1998;57:334-337.
42. Spillantini MG, Schmidt ML, Lee VM, Trojanowski JQ, Jakes R, Goedert M. Alpha-synuclein in Lewy bodies. Nature. 1997;388:839-840.
43. Luk KC, Song C, O'Brien P, Stieber A, Branch JR, Brunden KR, et al. Exogenous alpha-synuclein fibrils seed the formation of Lewy body-like intracellular inclusions in cultured cells. Proc Natl Acad Sci U S A. 2009;106:20051-20056.
44. Serpell LC, Berriman J, Jakes R, Goedert M, Crowther RA. Fiber diffraction of synthetic alpha-synuclein filaments shows amyloid-like cross-beta conformation. Proc Natl Acad Sci U S A. 2000;97:4897-4902.
45. Zimprich A, Biskup S, Leitner P, Lichtner P, Farrer M, Lincoln S, et al. Mutations in LRRK2 cause autosomal-dominant parkinsonism with pleomorphic pathology. Neuron. 2004;44:601-607.
46. Shulman JM, De Jager PL, Feany MB. Parkinson's disease: genetics and pathogenesis. Annu Rev Pathol. 2011;6:193-222.
47. Sheng Z, Zhang S, Bustos D, Kleinheinz T, Le Pichon CE, Dominguez SL, et al. Ser1292 autophosphorylation is an indicator of LRRK2 kinase activity and contributes to the cellular effects of PD mutations. Sci Transl Med. 2012;4:164ra161.
48. Greggio E, Taymans JM, Zhen EY, Ryder J, Vancraenenbroeck R, Beilina A, et al. The Parkinson's disease kinase LRRK2 autophosphorylates its GTPase domain at multiple sites. Biochem Biophys Res Commun. 2009;389:449-454.
49. Xiong Y, Coombes CE, Kilaru A, Li X, Gitler AD, Bowers WJ, et al. GTPase activity plays a key role in the pathobiology of LRRK2. PLoS Genet. 2010;6:e1000902.
50. Guo L, Gandhi PN, Wang W, Petersen RB, Wilson-Delfosse AL, Chen SG. The Parkinson's disease-associated protein, leucine-rich repeat kinase 2 (LRRK2), is an authentic GTPase that stimulates kinase activity. Exp Cell Res. 2007;313:3658-3670.
51. Li X, Tan YC, Poulose S, Olanow CW, Huang XY, Yue Z. Leucine-rich repeat kinase 2 (LRRK2)/PARK8 possesses GTPase activity that is altered in familial Parkinson's disease R1441C/G mutants. J Neurochem. 2007;103:238-247.
52. Daniels V, Vancraenenbroeck R, Law BM, Greggio E, Lobbestael E, Gao F, et al. Insight into the mode of action of the LRRK2 Y1699C pathogenic mutant. J Neurochem. 2011;116:304-315.
53. Tong Y, Pisani A, Martella G, Karouani M, Yamaguchi H, Pothos EN, et al. R1441C mutation in LRRK2 impairs dopaminergic neurotransmission in mice. Proc Natl Acad Sci U S A. 2009;106:14622-14627.
54. Matta S, Van Kolen K, da Cunha R, van den Bogaart G, Mandemakers W, Miskiewicz K, et al. LRRK2 controls an EndoA phosphorylation cycle in synaptic endocytosis. Neuron. 2012;75:1008-1021.
55. Lee S, Liu HP, Lin WY, Guo H, Lu B. LRRK2 kinase regulates synaptic morphology through distinct substrates at the presynaptic and postsynaptic compartments of the Drosophila neuromuscular junction. J Neurosci. 2010;30:16959-16969.
56. Parisiadou L, Yu J, Sgobio C, Xie C, Liu G, Sun L, et al. LRRK2 regulates synaptogenesis and dopamine receptor activation through modulation of PKA activity. Nat Neurosci. 2014;17:367-376.

57. Imai Y, Gehrke S, Wang HQ, Takahashi R, Hasegawa K, Oota E, et al. Phosphorylation of 4E-BP by LRRK2 affects the maintenance of dopaminergic neurons in Drosophila. EMBO J. 2008;27:2432-2443.
58. Kanao T, Venderova K, Park DS, Unterman T, Lu B, Imai Y. Activation of FoxO by LRRK2 induces expression of proapoptotic proteins and alters survival of postmitotic dopaminergic neuron in Drosophila. Hum Mol Genet. 2010;19:3747-3758.
59. Heo HY, Kim KS, Seol W. Coordinate Regulation of Neurite Outgrowth by LRRK2 and Its Interactor, Rab5. Exp Neurobiol. 2010;19:97-105.
60. Berwick DC, Harvey K. LRRK2 functions as a Wnt signaling scaffold, bridging cytosolic proteins and membrane-localized LRP6. Hum Mol Genet. 2012;21:4966-4979.
61. Dorval V, Hebert SS. LRRK2 in Transcription and Translation Regulation: Relevance for Parkinson's Disease. Front Neurol. 2012;3:12.
62. Gardet A, Benita Y, Li C, Sands BE, Ballester I, Stevens C, et al. LRRK2 is involved in the IFN-gamma response and host response to pathogens. J Immunol. 2010;185:5577-5585.
63. Parisiadou L, Cai H. LRRK2 function on actin and microtubule dynamics in Parkinson disease. Commun Integr Biol. 2010;3:396-400.
64. Gomez-Suaga P, Luzon-Toro B, Churamani D, Zhang L, Bloor-Young D, Patel S, et al. Leucine-rich repeat kinase 2 regulates autophagy through a calcium-dependent pathway involving NAADP. Hum Mol Genet. 2012;21:511-525.
65. Orenstein SJ, Kuo SH, Tasset I, Arias E, Koga H, Fernandez-Carasa I, et al. Interplay of LRRK2 with chaperone-mediated autophagy. Nat Neurosci. 2013;16:394-406.
66. Schapansky J, Nardozzi JD, Felizia F, LaVoie MJ. Membrane recruitment of endogenous LRRK2 precedes its potent regulation of autophagy. Hum Mol Genet. 2014;23:4201-4214.
67. Vilarino-Guell C, Wider C, Ross OA, Dachsel JC, Kachergus JM, Lincoln SJ, et al. VPS35 mutations in Parkinson disease. Am J Hum Genet. 2011;89:162-167.
68. Zimprich A, Benet-Pages A, Struhal W, Graf E, Eck SH, Offman MN, et al. A mutation in VPS35, encoding a subunit of the retromer complex, causes late-onset Parkinson disease. Am J Hum Genet. 2011;89:168-175.
69. Gokool S, Tattersall D, Reddy JV, Seaman MN. Identification of a conserved motif required for Vps35p/Vps26p interaction and assembly of the retromer complex. Biochem J. 2007;408:287-295.
70. Collins BM, Norwood SJ, Kerr MC, Mahony D, Seaman MN, Teasdale RD, et al. Structure of Vps26B and mapping of its interaction with the retromer protein complex. Traffic. 2008;9:366-379.
71. Wang X, Huang T, Bu G, Xu H. Dysregulation of protein trafficking in neurodegeneration. Mol Neurodegener. 2014;9:31.
72. Braschi E, Goyon V, Zunino R, Mohanty A, Xu L, McBride HM. Vps35 mediates vesicle transport between the mitochondria and peroxisomes. Curr Biol. 2010;20:1310-1315.
73. McLelland GL, Soubannier V, Chen CX, McBride HM, Fon EA. Parkin and PINK1 function in a vesicular trafficking pathway regulating mitochondrial quality control. EMBO J. 2014;33:282-295.
74. Kitada T, Asakawa S, Hattori N, Matsumine H, Yamamura Y, Minoshima S, et al. Mutations in the parkin gene cause autosomal recessive juvenile parkinsonism. Nature. 1998;392:605-608.
75. Lucking CB, Abbas N, Durr A, Bonifati V, Bonnet AM, de Broucker T, et al. Homozygous deletions in parkin gene in European and North African families with autosomal recessive juvenile

parkinsonism. The European Consortium on Genetic Susceptibility in Parkinson's Disease and the French Parkinson's Disease Genetics Study Group. Lancet. 1998;352:1355-1356.
76. Abbas N, Lucking CB, Ricard S, Durr A, Bonifati V, De Michele G, et al. A wide variety of mutations in the parkin gene are responsible for autosomal recessive parkinsonism in Europe. French Parkinson's Disease Genetics Study Group and the European Consortium on Genetic Susceptibility in Parkinson's Disease. Hum Mol Genet. 1999;8:567-574.
77. Lucking CB, Durr A, Bonifati V, Vaughan J, De Michele G, Gasser T, et al. Association between early-onset Parkinson's disease and mutations in the parkin gene. N Engl J Med. 2000;342:1560-1567.
78. Periquet M, Latouche M, Lohmann E, Rawal N, De Michele G, Ricard S, et al. Parkin mutations are frequent in patients with isolated early-onset parkinsonism. Brain. 2003;126:1271-1278.
79. Nuytemans K, Theuns J, Cruts M, Van Broeckhoven C. Genetic etiology of Parkinson disease associated with mutations in the SNCA, PARK2, PINK1, PARK7, and LRRK2 genes: a mutation update. Hum Mutat. 2010;31:763-780.
80. Pramstaller PP, Schlossmacher MG, Jacques TS, Scaravilli F, Eskelson C, Pepivani I, et al. Lewy body Parkinson's disease in a large pedigree with 77 Parkin mutation carriers. Ann Neurol. 2005;58:411-422.
81. Shimura H, Hattori N, Kubo S, Mizuno Y, Asakawa S, Minoshima S, et al. Familial Parkinson disease gene product, parkin, is a ubiquitin-protein ligase. Nat Genet. 2000;25:302-305.
82. Hershko A, Ciechanover A. The ubiquitin system. Annual review of biochemistry. 1998;67:425-479.
83. Randow F, Youle RJ. Self and nonself: how autophagy targets mitochondria and bacteria. Cell host & microbe. 2014;15:403-411.
84. Komander D, Rape M. The ubiquitin code. Annual review of biochemistry. 2012;81:203-229.
85. Dye BT, Schulman BA. Structural mechanisms underlying posttranslational modification by ubiquitin-like proteins. Annu Rev Bioph Biomol Struct. 2007;36:131-150.
86. Seirafi M, Kozlov G, Gehring K. Parkin structure and function. FEBS J. 2015;282:2076-2088.
87. Cruts M, Theuns J, Van Broeckhoven C. Locus-specific mutation databases for neurodegenerative brain diseases. Hum Mutat. 2012;33:1340-1344.
88. Trempe JF, Chen CX, Grenier K, Camacho EM, Kozlov G, McPherson PS, et al. SH3 domains from a subset of BAR proteins define a Ubl-binding domain and implicate parkin in synaptic ubiquitination. Mol Cell. 2009;36:1034-1047.
89. Kalia SK, Lee S, Smith PD, Liu L, Crocker SJ, Thorarinsdottir TE, et al. BAG5 inhibits parkin and enhances dopaminergic neuron degeneration. Neuron. 2004;44:931-945.
90. Fallon L, Moreau F, Croft BG, Labib N, Gu WJ, Fon EA. Parkin and CASK/LIN-2 associate via a PDZ-mediated interaction and are co-localized in lipid rafts and postsynaptic densities in brain. J Biol Chem. 2002;277:486-491.
91. Fallon L, Belanger CML, Corera AT, Kontogiannea M, Regan-Klapisz E, Moreau F, et al. A regulated interaction with the UIM protein Eps15 implicates parkin in EGF receptor trafficking and PI(3) K-Akt signalling. Nat Cell Biol. 2006;8:834-842.
92. Yang Y, Nishimura I, Imai Y, Takahashi R, Lu B. Parkin suppresses dopaminergic neuron-selective neurotoxicity induced by Pael-R in Drosophila. Neuron. 2003;37:911-924.

93. Corti O, Hampe C, Koutnikova H, Darios F, Jacquier S, Prigent A, et al. The p38 subunit of the aminoacyl-tRNA synthetase complex is a Parkin substrate: linking protein biosynthesis and neurodegeneration. Hum Mol Genet. 2003;12:1427-1437.
94. Ko HS, von Coelln R, Sriram SR, Kim SW, Chung KK, Pletnikova O, et al. Accumulation of the authentic parkin substrate aminoacyl-tRNA synthetase cofactor, p38/JTV-1, leads to catecholaminergic cell death. J Neurosci. 2005;25:7968-7978.
95. Geisler S, Holmstrom KM, Skujat D, Fiesel FC, Rothfuss OC, Kahle PJ, et al. PINK1/Parkin-mediated mitophagy is dependent on VDAC1 and p62/SQSTM1. Nat Cell Biol. 2010;12:119-131.
96. Vives-Bauza C, Zhou C, Huang Y, Cui M, de Vries RLA, Kim J, et al. PINK1-dependent recruitment of Parkin to mitochondria in mitophagy. Proceedings of the National Academy of Sciences of the United States of America. 2010;107:378-383.
97. Narendra DP, Jin SM, Tanaka A, Suen DF, Gautier CA, Shen J, et al. PINK1 is selectively stabilized on impaired mitochondria to activate Parkin. PLoS Biol. 2010;8:e1000298.
98. Greene AW, Grenier K, Aguileta MA, Muise S, Farazifard R, Haque ME, et al. Mitochondrial processing peptidase regulates PINK1 processing, import and Parkin recruitment. EMBO Rep. 2012;13:378-385.
99. Clark IE, Dodson MW, Jiang C, Cao JH, Huh JR, Seol JH, et al. Drosophila pink1 is required for mitochondrial function and interacts genetically with parkin. Nature. 2006;441:1162-1166.
100. Park J, Lee SB, Lee S, Kim Y, Song S, Kim S, et al. Mitochondrial dysfunction in Drosophila PINK1 mutants is complemented by parkin. Nature. 2006;441:1157-1161.
101. Yang Y, Gehrke S, Imai Y, Huang Z, Ouyang Y, Wang JW, et al. Mitochondrial pathology and muscle and dopaminergic neuron degeneration caused by inactivation of Drosophila Pink1 is rescued by Parkin. Proc Natl Acad Sci U S A. 2006;103:10793-10798.
102. Whitworth AJ, Lee JR, Ho VMW, Flick R, Chowdhury R, McQuibban GA. Rhomboid-7 and HtrA2/Omi act in a common pathway with the Parkinson's disease factors Pink1 and Parkin. Dis Model Mech. 2008;1:168-174.
103. Greene JC, Whitworth AJ, Kuo I, Andrews LA, Feany MB, Pallanck LJ. Mitochondrial pathology and apoptotic muscle degeneration in Drosophila parkin mutants. Proc Natl Acad Sci U S A. 2003;100:4078-4083.
104. Palacino JJ, Sagi D, Goldberg MS, Krauss S, Motz C, Wacker M, et al. Mitochondrial dysfunction and oxidative damage in parkin-deficient mice. J Biol Chem. 2004;279:18614-18622.
105. Gautier CA, Kitada T, Shen J. Loss of PINK1 causes mitochondrial functional defects and increased sensitivity to oxidative stress. Proc Natl Acad Sci U S A. 2008;105:11364-11369.
106. Kitada T, Pisani A, Karouani M, Haburcak M, Martella G, Tscherter A, et al. Impaired dopamine release and synaptic plasticity in the striatum of parkin-/- mice. J Neurochem. 2009;110:613-621.
107. Valente EM, Abou-Sleiman PM, Caputo V, Muqit MM, Harvey K, Gispert S, et al. Hereditary early-onset Parkinson's disease caused by mutations in PINK1. Science. 2004;304:1158-1160.
108. Kumazawa R, Tomiyama H, Li Y, Imamichi Y, Funayama M, Yoshino H, et al. Mutation analysis of the PINK1 gene in 391 patients with Parkinson disease. Arch Neurol. 2008;65:802-808.
109. Cookson MR. Parkinsonism due to mutations in PINK1, parkin, and DJ-1 and oxidative stress and mitochondrial pathways. Cold Spring Harb Perspect Med. 2012;2:a009415.

110. Trempe JF, Fon EA. Structure and Function of Parkin, PINK1, and DJ-1, the Three Musketeers of Neuroprotection. Front Neurol. 2013;4:38.
111. Sim CH, Gabriel K, Mills RD, Culvenor JG, Cheng HC. Analysis of the regulatory and catalytic domains of PTEN-induced kinase-1 (PINK1). Hum Mutat. 2012;33:1408-1422.
112. Kondapalli C, Kazlauskaite A, Zhang N, Woodroof HI, Campbell DG, Gourlay R, et al. PINK1 is activated by mitochondrial membrane potential depolarization and stimulates Parkin E3 ligase activity by phosphorylating Serine 65. Open Biol. 2012;2:120080.
113. Okatsu K, Oka T, Iguchi M, Imamura K, Kosako H, Tani N, et al. PINK1 autophosphorylation upon membrane potential dissipation is essential for Parkin recruitment to damaged mitochondria. Nat Commun. 2012;3:1016.
114. Matsuda N, Sato S, Shiba K, Okatsu K, Saisho K, Gautier CA, et al. PINK1 stabilized by mitochondrial depolarization recruits Parkin to damaged mitochondria and activates latent Parkin for mitophagy. J Cell Biol. 2010;189:211-221.
115. Shiba-Fukushima K, Imai Y, Yoshida S, Ishihama Y, Kanao T, Sato S, et al. PINK1-mediated phosphorylation of the Parkin ubiquitin-like domain primes mitochondrial translocation of Parkin and regulates mitophagy. Sci Rep. 2012;2:1002.
116. Lazarou M, Narendra DP, Jin SM, Tekle E, Banerjee S, Youle RJ. PINK1 drives Parkin self-association and HECT-like E3 activity upstream of mitochondrial binding. J Cell Biol. 2013;200:163-172.
117. Pridgeon JW, Olzmann JA, Chin LS, Li L. PINK1 protects against oxidative stress by phosphorylating mitochondrial chaperone TRAP1. PLoS Biol. 2007;5:e172.
118. Plun-Favreau H, Klupsch K, Moisoi N, Gandhi S, Kjaer S, Frith D, et al. The mitochondrial protease HtrA2 is regulated by Parkinson's disease-associated kinase PINK1. Nat Cell Biol. 2007;9:1243-1252.
119. Morais VA, Haddad D, Craessaerts K, De Bock PJ, Swerts J, Vilain S, et al. PINK1 loss-of-function mutations affect mitochondrial complex I activity via NdufA10 ubiquinone uncoupling. Science. 2014;344:203-207.
120. Kazlauskaite A, Kondapalli C, Gourlay R, Campbell DG, Ritorto MS, Hofmann K, et al. Parkin is activated by PINK1-dependent phosphorylation of ubiquitin at Ser65. Biochem J. 2014;460:127-139.
121. Kane LA, Lazarou M, Fogel AI, Li Y, Yamano K, Sarraf SA, et al. PINK1 phosphorylates ubiquitin to activate Parkin E3 ubiquitin ligase activity. J Cell Biol. 2014;205:143-153.
122. Koyano F, Okatsu K, Kosako H, Tamura Y, Go E, Kimura M, et al. Ubiquitin is phosphorylated by PINK1 to activate parkin. Nature. 2014;510:162-166.
123. Deng H, Dodson MW, Huang H, Guo M. The Parkinson's disease genes pink1 and parkin promote mitochondrial fission and/or inhibit fusion in Drosophila. Proc Natl Acad Sci U S A. 2008;105:14503-14508.
124. Yang Y, Ouyang Y, Yang L, Beal MF, McQuibban A, Vogel H, et al. Pink1 regulates mitochondrial dynamics through interaction with the fission/fusion machinery. Proc Natl Acad Sci U S A. 2008;105:7070-7075.
125. Poole AC, Thomas RE, Andrews LA, McBride HM, Whitworth AJ, Pallanck LJ. The PINK1/Parkin pathway regulates mitochondrial morphology. Proc Natl Acad Sci U S A. 2008;105:1638-1643.
126. Liu W, Acin-Perez R, Geghman KD, Manfredi G, Lu B, Li C. Pink1 regulates the oxidative phosphorylation machinery via mitochondrial fission. Proc Natl Acad Sci U S A. 2011;108:12920-12924.

127. Heeman B, Van den Haute C, Aelvoet SA, Valsecchi F, Rodenburg RJ, Reumers V, et al. Depletion of PINK1 affects mitochondrial metabolism, calcium homeostasis and energy maintenance. J Cell Sci. 2011;124:1115-1125.
128. Gandhi S, Wood-Kaczmar A, Yao Z, Plun-Favreau H, Deas E, Klupsch K, et al. PINK1-associated Parkinson's disease is caused by neuronal vulnerability to calcium-induced cell death. Mol Cell. 2009;33:627-638.
129. Marongiu R, Spencer B, Crews L, Adame A, Patrick C, Trejo M, et al. Mutant Pink1 induces mitochondrial dysfunction in a neuronal cell model of Parkinson's disease by disturbing calcium flux. J Neurochem. 2009;108:1561-1574.
130. Exner N, Treske B, Paquet D, Holmstrom K, Schiesling C, Gispert S, et al. Loss-of-function of human PINK1 results in mitochondrial pathology and can be rescued by parkin. J Neurosci. 2007;27:12413-12418.
131. Amo T, Sato S, Saiki S, Wolf AM, Toyomizu M, Gautier CA, et al. Mitochondrial membrane potential decrease caused by loss of PINK1 is not due to proton leak, but to respiratory chain defects. Neurobiol Dis. 2011;41:111-118.
132. Morais VA, Verstreken P, Roethig A, Smet J, Snellinx A, Vanbrabant M, et al. Parkinson's disease mutations in PINK1 result in decreased Complex I activity and deficient synaptic function. EMBO Mol Med. 2009;1:99-111.
133. Vilain S, Esposito G, Haddad D, Schaap O, Dobreva MP, Vos M, et al. The yeast complex I equivalent NADH dehydrogenase rescues pink1 mutants. PLoS Genet. 2012;8:e1002456.
134. Wang X, Winter D, Ashrafi G, Schlehe J, Wong YL, Selkoe D, et al. PINK1 and Parkin target Miro for phosphorylation and degradation to arrest mitochondrial motility. Cell. 2011;147:893-906.
135. Matenia D, Hempp C, Timm T, Eikhof A, Mandelkow EM. Microtubule affinity-regulating kinase 2 (MARK2) turns on phosphatase and tensin homolog (PTEN)-induced kinase 1 (PINK1) at Thr-313, a mutation site in Parkinson disease: effects on mitochondrial transport. J Biol Chem. 2012;287:8174-8186.
136. Liu S, Sawada T, Lee S, Yu W, Silverio G, Alapatt P, et al. Parkinson's disease-associated kinase PINK1 regulates Miro protein level and axonal transport of mitochondria. PLoS Genet. 2012;8:e1002537.
137. Meissner C, Lorenz H, Weihofen A, Selkoe DJ, Lemberg MK. The mitochondrial intramembrane protease PARL cleaves human Pink1 to regulate Pink1 trafficking. J Neurochem. 2011;117:856-867.
138. Deas E, Plun-Favreau H, Gandhi S, Desmond H, Kjaer S, Loh SHY, et al. PINK1 cleavage at position A103 by the mitochondrial protease PARL. Hum Mol Genet. 2011;20:867-879.
139. Thomas RE, Andrews LA, Burman JL, Lin WY, Pallanck LJ. PINK1-Parkin pathway activity is regulated by degradation of PINK1 in the mitochondrial matrix. PLoS Genet. 2014;10:e1004279.
140. Yamano K, Youle RJ. PINK1 is degraded through the N-end rule pathway. Autophagy. 2013;9:1758-1769.
141. Nagakubo D, Taira T, Kitaura H, Ikeda M, Tamai K, Iguchi-Ariga SM, et al. DJ-1, a novel oncogene which transforms mouse NIH3T3 cells in cooperation with ras. Biochem Biophys Res Commun. 1997;231:509-513.
142. Bonifati V, Rizzu P, Squitieri F, Krieger E, Vanacore N, van Swieten JC, et al. DJ-1(PARK7), a novel gene for autosomal recessive, early onset parkinsonism. Neurol Sci. 2003;24:159-160.

143. Tao X, Tong L. Crystal structure of human DJ-1, a protein associated with early onset Parkinson's disease. J Biol Chem. 2003;278:31372-31379.
144. Wilson MA, Collins JL, Hod Y, Ringe D, Petsko GA. The 1.1-A resolution crystal structure of DJ-1, the protein mutated in autosomal recessive early onset Parkinson's disease. Proc Natl Acad Sci U S A. 2003;100:9256-9261.
145. Honbou K, Suzuki NN, Horiuchi M, Niki T, Taira T, Ariga H, et al. The crystal structure of DJ-1, a protein related to male fertility and Parkinson's disease. J Biol Chem. 2003;278:31380-31384.
146. Chen J, Li L, Chin LS. Parkinson disease protein DJ-1 converts from a zymogen to a protease by carboxyl-terminal cleavage. Hum Mol Genet. 2010;19:2395-2408.
147. Lee JY, Song J, Kwon K, Jang S, Kim C, Baek K, et al. Human DJ-1 and its homologs are novel glyoxalases. Hum Mol Genet. 2012;21:3215-3225.
148. Gautier V, Le HT, Malki A, Messaoudi N, Caldas T, Kthiri F, et al. YajL, the prokaryotic homolog of the Parkinsonism-associated protein DJ-1, protects cells against protein sulfenylation. J Mol Biol. 2012;421:662-670.
149. Bonifati V, Rizzu P, van Baren MJ, Schaap O, Breedveld GJ, Krieger E, et al. Mutations in the DJ-1 gene associated with autosomal recessive early-onset parkinsonism. Science. 2003;299:256-259.
150. Kamp F, Exner N, Lutz AK, Wender N, Hegermann J, Brunner B, et al. Inhibition of mitochondrial fusion by alpha-synuclein is rescued by PINK1, Parkin and DJ-1. EMBO J. 2010;29:3571-3589.
151. Irrcher I, Aleyasin H, Seifert EL, Hewitt SJ, Chhabra S, Phillips M, et al. Loss of the Parkinson's disease-linked gene DJ-1 perturbs mitochondrial dynamics. Hum Mol Genet. 2010;19:3734-3746.
152. Thomas KJ, McCoy MK, Blackinton J, Beilina A, van der Brug M, Sandebring A, et al. DJ-1 acts in parallel to the PINK1/parkin pathway to control mitochondrial function and autophagy. Hum Mol Genet. 2011;20:40-50.
153. Kim RH, Smith PD, Aleyasin H, Hayley S, Mount MP, Pownall S, et al. Hypersensitivity of DJ-1-deficient mice to 1-methyl-4-phenyl-1,2,3,6-tetrahydropyrindine (MPTP) and oxidative stress. Proc Natl Acad Sci U S A. 2005;102:5215-5220.
154. Menzies FM, Yenisetti SC, Min KT. Roles of Drosophila DJ-1 in survival of dopaminergic neurons and oxidative stress. Curr Biol. 2005;15:1578-1582.
155. Yang Y, Gehrke S, Haque ME, Imai Y, Kosek J, Yang L, et al. Inactivation of Drosophila DJ-1 leads to impairments of oxidative stress response and phosphatidylinositol 3-kinase/Akt signaling. Proc Natl Acad Sci U S A. 2005;102:13670-13675.
156. Lavara-Culebras E, Paricio N. Drosophila DJ-1 mutants are sensitive to oxidative stress and show reduced lifespan and motor deficits. Gene. 2007;400:158-165.
157. Guzman JN, Sanchez-Padilla J, Wokosin D, Kondapalli J, Ilijic E, Schumacker PT, et al. Oxidant stress evoked by pacemaking in dopaminergic neurons is attenuated by DJ-1. Nature. 2010;468:696-700.
158. Joselin AP, Hewitt SJ, Callaghan SM, Kim RH, Chung YH, Mak TW, et al. ROS-dependent regulation of Parkin and DJ-1 localization during oxidative stress in neurons. Hum Mol Genet. 2012;21:4888-4903.
159. Meulener M, Whitworth AJ, Armstrong-Gold CE, Rizzu P, Heutink P, Wes PD, et al. Drosophila DJ-1 mutants are selectively sensitive to environmental toxins associated with Parkinson's disease. Curr Biol. 2005;15:1572-1577.

160. Meulener MC, Xu K, Thomson L, Ischiropoulos H, Bonini NM. Mutational analysis of DJ-1 in Drosophila implicates functional inactivation by oxidative damage and aging. Proc Natl Acad Sci U S A. 2006;103:12517-12522.
161. Chang D, Nalls MA, Hallgrimsdottir IB, Hunkapiller J, van der Brug M, Cai F, et al. A meta-analysis of genome-wide association studies identifies 17 new Parkinson's disease risk loci. Nat Genet. 2017;49:1511-1516.
162. Pakkenberg B, Pelvig D, Marner L, Bundgaard MJ, Gundersen HJ, Nyengaard JR, et al. Aging and the human neocortex. Exp Gerontol. 2003;38:95-99.
163. Kjaerulff O, Brodin L, Jung A. The structure and function of endophilin proteins. Cell Biochem Biophys. 2011;60:137-154.
164. Soukup SF, Kuenen S, Vanhauwaert R, Manetsberger J, Hernandez-Diaz S, Swerts J, et al. A LRRK2-Dependent EndophilinA Phosphoswitch Is Critical for Macroautophagy at Presynaptic Terminals. Neuron. 2016;92:829-844.
165. DePaolo J, Goker-Alpan O, Samaddar T, Lopez G, Sidransky E. The association between mutations in the lysosomal protein glucocerebrosidase and parkinsonism. Mov Disord. 2009;24:1571-1578.
166. Sidransky E, Lopez G. The link between the GBA gene and parkinsonism. Lancet Neurol. 2012;11:986-998.
167. Sun Y, Grabowski GA. Impaired autophagosomes and lysosomes in neuronopathic Gaucher disease. Autophagy. 2010;6:648-649.
168. Sardi SP, Singh P, Cheng SH, Shihabuddin LS, Schlossmacher MG. Mutant GBA1 expression and synucleinopathy risk: first insights from cellular and mouse models. Neurodegener Dis. 2012;10:195-202.
169. MacLeod DA, Rhinn H, Kuwahara T, Zolin A, Di Paolo G, McCabe BD, et al. RAB7L1 interacts with LRRK2 to modify intraneuronal protein sorting and Parkinson's disease risk. Neuron. 2013;77:425-439.
170. Kieburtz K, Wunderle KB. Parkinson's disease: evidence for environmental risk factors. Mov Disord. 2013;28:8-13.
171. Winklhofer KF, Haass C. Mitochondrial dysfunction in Parkinson's disease. Biochim Biophys Acta. 2010;1802:29-44.
172. Nunnari J, Suomalainen A. Mitochondria: in sickness and in health. Cell. 2012;148:1145-1159.
173. Gao J, Wang L, Liu J, Xie F, Su B, Wang X. Abnormalities of Mitochondrial Dynamics in Neurodegenerative Diseases. Antioxidants (Basel). 2017;6.
174. Karbowski M, Youle RJ. Regulating mitochondrial outer membrane proteins by ubiquitination and proteasomal degradation. Curr Opin Cell Biol. 2011;23:476-482.
175. Matsushima Y, Kaguni LS. Matrix proteases in mitochondrial DNA function. Biochim Biophys Acta. 2012;1819:1080-1087.
176. Baker BM, Haynes CM. Mitochondrial protein quality control during biogenesis and aging. Trends Biochem Sci. 2011;36:254-261.
177. van der Bliek AM, Shen Q, Kawajiri S. Mechanisms of mitochondrial fission and fusion. Cold Spring Harb Perspect Biol. 2013;5.
178. Twig G, Elorza A, Molina AJ, Mohamed H, Wikstrom JD, Walzer G, et al. Fission and selective fusion govern mitochondrial segregation and elimination by autophagy. EMBO J. 2008;27:433-446.

179. Soubannier V, Rippstein P, Kaufman BA, Shoubridge EA, McBride HM. Reconstitution of mitochondria derived vesicle formation demonstrates selective enrichment of oxidized cargo. PLoS One. 2012;7:e52830.
180. Youle RJ, Narendra DP. Mechanisms of mitophagy. Nat Rev Mol Cell Biol. 2011;12:9-14.
181. Ding WX, Yin XM. Mitophagy: mechanisms, pathophysiological roles, and analysis. Biol Chem. 2012;393:547-564.
182. Chan CS, Gertler TS, Surmeier DJ. Calcium homeostasis, selective vulnerability and Parkinson's disease. Trends Neurosci. 2009;32:249-256.
183. Tanner CM, Kamel F, Ross GW, Hoppin JA, Goldman SM, Korell M, et al. Rotenone, paraquat, and Parkinson's disease. Environ Health Perspect. 2011;119:866-872.
184. Richardson JR, Caudle WM, Guillot TS, Watson JL, Nakamaru-Ogiso E, Seo BB, et al. Obligatory role for complex I inhibition in the dopaminergic neurotoxicity of 1-methyl-4-phenyl-1,2,3,6-tetrahydropyridine (MPTP). Toxicol Sci. 2007;95:196-204.
185. Schapira AH, Cooper JM, Dexter D, Clark JB, Jenner P, Marsden CD. Mitochondrial complex I deficiency in Parkinson's disease. J Neurochem. 1990;54:823-827.
186. Bender A, Krishnan KJ, Morris CM, Taylor GA, Reeve AK, Perry RH, et al. High levels of mitochondrial DNA deletions in substantia nigra neurons in aging and Parkinson disease. Nat Genet. 2006;38:515-517.
187. Kraytsberg Y, Kudryavtseva E, McKee AC, Geula C, Kowall NW, Khrapko K. Mitochondrial DNA deletions are abundant and cause functional impairment in aged human substantia nigra neurons. Nat Genet. 2006;38:518-520.
188. Dolle C, Flones I, Nido GS, Miletic H, Osuagwu N, Kristoffersen S, et al. Defective mitochondrial DNA homeostasis in the substantia nigra in Parkinson disease. Nat Commun. 2016;7:13548.
189. Berndsen CE, Wolberger C. New insights into ubiquitin E3 ligase mechanism. Nat Struct Mol Biol. 2014;21:301-307.
190. Wenzel DM, Lissounov A, Brzovic PS, Klevit RE. UBCH7 reactivity profile reveals parkin and HHARI to be RING/HECT hybrids. Nature. 2011;474:105-108.
191. Spratt DE, Walden H, Shaw GS. RBR E3 ubiquitin ligases: new structures, new insights, new questions. Biochem J. 2014;458:421-437.
192. Marin I, Ferrus A. Comparative genomics of the RBR family, including the Parkinson's disease-related gene parkin and the genes of the ariadne subfamily. Mol Biol Evol. 2002;19:2039-2050.
193. Marin I, Lucas JI, Gradilla AC, Ferrus A. Parkin and relatives: the RBR family of ubiquitin ligases. Physiol Genomics. 2004;17:253-263.
194. Morett E, Bork P. A novel transactivation domain in parkin. Trends Biochem Sci. 1999;24:229-231.
195. Chaugule VK, Burchell L, Barber KR, Sidhu A, Leslie SJ, Shaw GS, et al. Autoregulation of Parkin activity through its ubiquitin-like domain. EMBO J. 2011;30:2853-2867.
196. Ikeda F, Deribe YL, Skanland SS, Stieglitz B, Grabbe C, Franz-Wachtel M, et al. SHARPIN forms a linear ubiquitin ligase complex regulating NF-kappaB activity and apoptosis. Nature. 2011;471:637-641.
197. Chan NC, Salazar AM, Pham AH, Sweredoski MJ, Kolawa NJ, Graham RL, et al. Broad activation of the ubiquitin-proteasome system by Parkin is critical for mitophagy. Hum Mol Genet. 2011;20:1726-1737.

198. Sarraf SA, Raman M, Guarani-Pereira V, Sowa ME, Huttlin EL, Gygi SP, et al. Landscape of the PARKIN-dependent ubiquitylome in response to mitochondrial depolarization. Nature. 2013;496:372-376.
199. Ordureau A, Sarraf SA, Duda DM, Heo JM, Jedrychowski MP, Sviderskiy VO, et al. Quantitative proteomics reveal a feedforward mechanism for mitochondrial PARKIN translocation and ubiquitin chain synthesis. Mol Cell. 2014;56:360-375.
200. Durcan TM, Tang MY, Perusse JR, Dashti EA, Aguileta MA, McLelland GL, et al. USP8 regulates mitophagy by removing K6-linked ubiquitin conjugates from parkin. EMBO J. 2014;33:2473-2491.
201. Riley BE, Lougheed JC, Callaway K, Velasquez M, Brecht E, Nguyen L, et al. Structure and function of Parkin E3 ubiquitin ligase reveals aspects of RING and HECT ligases. Nat Commun. 2013;4:1982.
202. Wauer T, Komander D. Structure of the human Parkin ligase domain in an autoinhibited state. EMBO J. 2013;32:2099-2112.
203. Trempe JF, Sauve V, Grenier K, Seirafi M, Tang MY, Menade M, et al. Structure of Parkin Reveals Mechanisms for Ubiquitin Ligase Activation. Science. 2013;340:1451-1455.
204. Narendra D, Walker JE, Youle R. Mitochondrial Quality Control Mediated by PINK1 and Parkin: Links to Parkinsonism. Cold Spring Harb Perspect Biol. 2012;4:pii: a011338.
205. Lazarou M, Jin SM, Kane LA, Youle RJ. Role of PINK1 Binding to the TOM Complex and Alternate Intracellular Membranes in Recruitment and Activation of the E3 Ligase Parkin. Dev Cell. 2012;22:320-333.
206. Jin SM, Lazarou M, Wang CX, Kane LA, Narendra DP, Youle RJ. Mitochondrial membrane potential regulates PINK1 import and proteolytic destabilization by PARL. J Cell Biol. 2010;191:933-942.
207. Lin W, Kang UJ. Characterization of PINK1 processing, stability, and subcellular localization. J Neurochem. 2008;106:464-474.
208. Zhou C, Huang Y, Shao YF, May J, Prou D, Perier C, et al. The kinase domain of mitochondrial PINK1 faces the cytoplasm. P Natl Acad Sci USA. 2008;105:12022-12027.
209. Kazlauskaite A, Kelly V, Johnson C, Baillie C, Hastie CJ, Peggie M, et al. Phosphorylation of Parkin at Serine65 is essential for activation: elaboration of a Miro1 substrate-based assay of Parkin E3 ligase activity. Open Biol. 2014;4:130213.
210. Scarffe LA, Stevens DA, Dawson VL, Dawson TM. Parkin and PINK1: much more than mitophagy. Trends Neurosci. 2014;37:315-324.
211. Soubannier V, McLelland GL, Zunino R, Braschi E, Rippstein P, Fon EA, et al. A vesicular transport pathway shuttles cargo from mitochondria to lysosomes. Curr Biol. 2012;22:135-141.
212. Vincow ES, Merrihew G, Thomas RE, Shulman NJ, Beyer RP, MacCoss MJ, et al. The PINK1-Parkin pathway promotes both mitophagy and selective respiratory chain turnover in vivo. Proceedings of the National Academy of Sciences of the United States of America. 2013;110:6400-6405.
213. Kuroda Y, Mitsui T, Kunishige M, Shono M, Akaike M, Azuma H, et al. Parkin enhances mitochondrial biogenesis in proliferating cells. Hum Mol Genet. 2006;15:883-895.
214. Rothfuss O, Fischer H, Hasegawa T, Maisel M, Leitner P, Miesel F, et al. Parkin protects mitochondrial genome integrity and supports mitochondrial DNA repair. Hum Mol Genet. 2009;18:3832-3850.
215. Shin JH, Ko HS, Kang H, Lee Y, Lee YI, Pletinkova O, et al. PARIS (ZNF746) repression of PGC-1alpha contributes to neurodegeneration in Parkinson's disease. Cell. 2011;144:689-702.

216. Lee Y, Karuppagounder SS, Shin JH, Lee YI, Ko HS, Swing D, et al. Parthanatos mediates AIMP2-activated age-dependent dopaminergic neuronal loss. Nat Neurosci. 2013;16:1392-1400.
217. Ekholm-Reed S, Goldberg MS, Schlossmacher MG, Reed SI. Parkin-dependent degradation of the F-box protein Fbw7beta promotes neuronal survival in response to oxidative stress by stabilizing Mcl-1. Molecular and cellular biology. 2013;33:3627-3643.
218. Muller-Rischart AK, Pilsl A, Beaudette P, Patra M, Hadian K, Funke M, et al. The E3 Ligase Parkin Maintains Mitochondrial Integrity by Increasing Linear Ubiquitination of NEMO. Mol Cell. 2013;49:908-921.
219. Hwang S, Kim D, Choi G, An SW, Hong YK, Suh YS, et al. Parkin Suppresses c-Jun N-Terminal Kinase-Induced Cell Death via Transriptional Regulation in Drosophila. Mol Cells. 2010;29:575-580.
220. Jiang HB, Ren Y, Zhao JH, Feng J. Parkin protects human dopaminergic neuroblastoma cells against dopamine-induced apoptosis. Hum Mol Genet. 2004;13:1745-1754.
221. Ren Y, Jiang H, Yang F, Nakaso K, Feng J. Parkin Protects Dopaminergic Neurons against Microtubule-depolymerizing Toxins by Attenuating Microtubule-associated Protein Kinase Activation. J Biol Chem. 2009;284:4009-4017.
222. Hollville E, Carroll RG, Cullen SP, Martin SJ. Bcl-2 family proteins participate in mitochondrial quality control by regulating Parkin/PINK1-dependent mitophagy. Mol Cell. 2014;55:451-466.
223. Johnson BN, Berger AK, Cortese GP, LaVoie MJ. The ubiquitin E3 ligase parkin regulates the proapoptotic function of Bax. Proceedings of the National Academy of Sciences of the United States of America. 2012;109:6283-6288.
224. Berger AK, Cortese GP, Amodeo KD, Weihofen A, Letai A, LaVoie MJ. Parkin selectively alters the intrinsic threshold for mitochondrial cytochrome c release. Hum Mol Genet. 2009;18:4317-4328.
225. Zhang C, Lee S, Peng Y, Bunker E, Giaime E, Shen J, et al. PINK1 Triggers Autocatalytic Activation of Parkin to Specify Cell Fate Decisions. Curr Biol. 2014;24:1854-1865.
226. Zhang C, Lin M, Wu R, Wang X, Yang B, Levine AJ, et al. Parkin, a p53 target gene, mediates the role of p53 in glucose metabolism and the Warburg effect. Proceedings of the National Academy of Sciences of the United States of America. 2011;108:16259-16264.
227. Cesari R, Martin ES, Calin GA, Pentimalli F, Bichi R, McAdams H, et al. Parkin, a gene implicated in autosomal recessive juvenile parkinsonism, is a candidate tumor suppressor gene on chromosome 6q25-q27. Proc Natl Acad Sci U S A. 2003;100:5956-5961.
228. Fujiwara M, Marusawa H, Wang HQ, Iwai A, Ikeuchi K, Imai Y, et al. Parkin as a tumor suppressor gene for hepatocellular carcinoma. Oncogene. 2008;27:6002-6011.
229. Gong Y, Zack TI, Morris LG, Lin K, Hukkelhoven E, Raheja R, et al. Pan-cancer genetic analysis identifies PARK2 as a master regulator of G1/S cyclins. Nature Genetics. 2014;46:588-594.
230. Veeriah S, Taylor BS, Meng S, Fang F, Yilmaz E, Vivanco I, et al. Somatic mutations of the Parkinson's disease-associated gene PARK2 in glioblastoma and other human malignancies. Nature Genetics. 2010;42:77-82.
231. Mira MT, Alcais A, Nguyen VT, Moraes MO, Di Flumeri C, Vu HT, et al. Susceptibility to leprosy is associated with PARK2 and PACRG. Nature. 2004;427:636-640.
232. Manzanillo PS, Ayres JS, Watson RO, Collins AC, Souza G, Rae CS, et al. The ubiquitin ligase parkin mediates resistance to intracellular pathogens. Nature. 2013;501:512-516.

233. Cao M, Milosevic I, Giovedi S, De Camilli P. Upregulation of Parkin in endophilin mutant mice. J Neurosci. 2014;34:16544-16549.
234. Huynh DP, Nguyen DT, Pulst-Korenberg JB, Brice A, Pulst SM. Parkin is an E3 ubiquitin-ligase for normal and mutant ataxin-2 and prevents ataxin-2-induced cell death. Exp Neurol. 2007;203:531-541.
235. Nonis D, Schmidt MH, van de Loo S, Eich F, Dikic I, Nowock J, et al. Ataxin-2 associates with the endocytosis complex and affects EGF receptor trafficking. Cell Signal. 2008;20:1725-1739.
236. Chen H, Antonarakis SE. The SH3D1A gene maps to human chromosome 21q22.1-->q22.2. Cytogenet Cell Genet. 1997;78:213-215.
237. Micheva KD, Kay BK, McPherson PS. Synaptojanin forms two separate complexes in the nerve terminal. Interactions with endophilin and amphiphysin. J Biol Chem. 1997;272:27239-27245.
238. Giachino C, Lantelme E, Lanzetti L, Saccone S, Bella Valle G, Migone N. A novel SH3-containing human gene family preferentially expressed in the central nervous system. Genomics. 1997;41:427-434.
239. Huttner WB, Schmidt A. Lipids, lipid modification and lipid-protein interaction in membrane budding and fission--insights from the roles of endophilin A1 and synaptophysin in synaptic vesicle endocytosis. Curr Opin Neurobiol. 2000;10:543-551.
240. Cuddeback SM, Yamaguchi H, Komatsu K, Miyashita T, Yamada M, Wu C, et al. Molecular cloning and characterization of Bif-1. A novel Src homology 3 domain-containing protein that associates with Bax. J Biol Chem. 2001;276:20559-20565.
241. Pierrat B, Simonen M, Cueto M, Mestan J, Ferrigno P, Heim J. SH3GLB, a new endophilin-related protein family featuring an SH3 domain. Genomics. 2001;71:222-234.
242. Dittman J, Ryan TA. Molecular circuitry of endocytosis at nerve terminals. Annu Rev Cell Dev Biol. 2009;25:133-160.
243. Frost A, Unger VM, De Camilli P. The BAR domain superfamily: membrane-molding macromolecules. Cell. 2009;137:191-196.
244. Peter BJ, Kent HM, Mills IG, Vallis Y, Butler PJ, Evans PR, et al. BAR domains as sensors of membrane curvature: the amphiphysin BAR structure. Science. 2004;303:495-499.
245. Perera RM, Zoncu R, Lucast L, De Camilli P, Toomre D. Two synaptojanin 1 isoforms are recruited to clathrin-coated pits at different stages. Proc Natl Acad Sci U S A. 2006;103:19332-19337.
246. Ferguson SM, Raimondi A, Paradise S, Shen H, Mesaki K, Ferguson A, et al. Coordinated actions of actin and BAR proteins upstream of dynamin at endocytic clathrin-coated pits. Dev Cell. 2009;17:811-822.
247. de Heuvel E, Bell AW, Ramjaun AR, Wong K, Sossin WS, McPherson PS. Identification of the major synaptojanin-binding proteins in brain. J Biol Chem. 1997;272:8710-8716.
248. Ringstad N, Gad H, Low P, Di Paolo G, Brodin L, Shupliakov O, et al. Endophilin/SH3p4 is required for the transition from early to late stages in clathrin-mediated synaptic vesicle endocytosis. Neuron. 1999;24:143-154.
249. Svergun DI. Determination of the Regularization Parameter in Indirect-Transform Methods Using Perceptual Criteria. J Appl Crystallogr. 1992;25:495-503.
250. Mylonas E, Svergun DI. Accuracy of molecular mass determination of proteins in solution by small-angle X-ray scattering. J Appl Crystallogr. 2007;40:S245-S249.

251. Wauer T, Simicek M, Schubert A, Komander D. Mechanism of phospho-ubiquitin-induced PARKIN activation. Nature. 2015.
252. Read RJ, Sussman JL, SpringerLink (Online service). Evolving Methods for Macromolecular Crystallography The Structural Path to the Understanding of the Mechanism of Action of CBRN Agents. Dordrecht: Springer Science+Business Media B.V.; 2007.
253. Winn MD, Ballard CC, Cowtan KD, Dodson EJ, Emsley P, Evans PR, et al. Overview of the CCP4 suite and current developments. Acta Crystallogr D Biol Crystallogr. 2011;67:235-242.
254. Adams PD, Afonine PV, Bunkoczi G, Chen VB, Davis IW, Echols N, et al. PHENIX: a comprehensive Python-based system for macromolecular structure solution. Acta Crystallogr D Biol Crystallogr. 2010;66:213-221.
255. Emsley P, Lohkamp B, Scott WG, Cowtan K. Features and development of Coot. Acta Crystallogr D Biol Crystallogr. 2010;66:486-501.
256. McCoy AJ, Grosse-Kunstleve RW, Adams PD, Winn MD, Storoni LC, Read RJ. Phaser crystallographic software. J Appl Crystallogr. 2007;40:658-674.
257. Tomoo K, Mukai Y, In Y, Miyagawa H, Kitamura K, Yamano A, et al. Crystal structure and molecular dynamics simulation of ubiquitin-like domain of murine parkin. Biochim Biophys Acta. 2008;1784:1059-1067.
258. Petoukhov MV, Franke D, Shkumatov AV, Tria G, Kikhney AG, Gajda M, et al. New developments in the program package for small-angle scattering data analysis. J Appl Crystallogr. 2012;45:342-350.
259. Svergun D, Barberato C, Koch MHJ. CRYSOL - a Program to Evaluate X-ray Solution Scattering of Biological Macromolecules from Atomic Coordinates. J Appl Cryst. 1995;28:768-773.
260. Rambo RP, Tainer JA. Accurate assessment of mass, models and resolution by small-angle scattering. Nature. 2013;496:477-481.
261. Delaglio F, Grzesiek S, Vuister GW, Zhu G, Pfeifer J, Bax A. NMRPipe: a multidimensional spectral processing system based on UNIX pipes. J Biomol NMR. 1995;6:277-293.
262. Serniwka SA, Shaw GS. 1H, 13C and 15N resonance assignments for the human E2 conjugating enzyme, UbcH7. Biomol NMR Assign. 2008;2:21-23.
263. Tang MY, Vranas M, Krahn AI, Pundlik S, Trempe JF, Fon EA. Structure-guided mutagenesis reveals a hierarchical mechanism of Parkin activation. Nat Commun. 2017;8:14697.
264. Regnstrom K, Yan J, Nguyen L, Callaway K, Yang Y, Diep L, et al. Label free fragment screening using surface plasmon resonance as a tool for fragment finding - analyzing parkin, a difficult CNS target. PLoS One. 2013;8:e66879.
265. Beasley SA, Hristova VA, Shaw GS. Structure of the Parkin in-between-ring domain provides insights for E3-ligase dysfunction in autosomal recessive Parkinson's disease. Proc Natl Acad Sci U S A. 2007;104:3095-3100.
266. Wernimont A, Edwards A. In situ proteolysis to generate crystals for structure determination: an update. PLoS One. 2009;4:e5094.
267. Gheyi T, Rodgers L, Romero R, Sauder JM, Burley SK. Mass spectrometry guided in situ proteolysis to obtain crystals for X-ray structure determination. J Am Soc Mass Spectrom. 2010;21:1795-1801.
268. Derewenda ZS. Application of protein engineering to enhance crystallizability and improve crystal properties. Acta Crystallogr D Biol Crystallogr. 2010;66:604-615.

269. Cha SS, An YJ, Jeong CS, Kim MK, Lee SG, Lee KH, et al. Experimental phasing using zinc anomalous scattering. Acta Crystallogr D Biol Crystallogr. 2012;68:1253-1258.
270. Safadi SS, Shaw GS. Differential interaction of the E3 ligase parkin with the proteasomal subunit S5a and the endocytic protein Eps15. J Biol Chem. 2010;285:1424-1434.
271. Sakata E, Yamaguchi Y, Kurimoto E, Kikuchi J, Yokoyama S, Yamada S, et al. Parkin binds the Rpn10 subunit of 26S proteasomes through its ubiquitin-like domain. EMBO Rep. 2003;4:301-306.
272. Hristova VA, Beasley SA, Rylett RJ, Shaw GS. Identification of a novel Zn2+-binding domain in the autosomal recessive juvenile Parkinson-related E3 ligase parkin. J Biol Chem. 2009;284:14978-14986.
273. Choo YS, Zhang Z. Detection of protein ubiquitination. J Vis Exp. 2009.
274. Zheng N, Wang P, Jeffrey PD, Pavletich NP. Structure of a c-Cbl-UbcH7 complex: RING domain function in ubiquitin-protein ligases. Cell. 2000;102:533-539.
275. Narendra D, Tanaka A, Suen DF, Youle RJ. Parkin is recruited selectively to impaired mitochondria and promotes their autophagy. J Cell Biol. 2008;183:795-803.
276. Dawson TM, Dawson VL. The role of parkin in familial and sporadic Parkinson's disease. Mov Disord. 2010;25 Suppl 1:S32-39.
277. Ashrafi G, Schlehe JS, LaVoie MJ, Schwarz TL. Mitophagy of damaged mitochondria occurs locally in distal neuronal axons and requires PINK1 and Parkin. J Cell Biol. 2014;206:655-670.
278. Jin SM, Youle RJ. The accumulation of misfolded proteins in the mitochondrial matrix is sensed by PINK1 to induce PARK2/Parkin-mediated mitophagy of polarized mitochondria. Autophagy. 2013;9:1750-1757.
279. Ziviani E, Tao RN, Whitworth AJ. Drosophila parkin requires PINK1 for mitochondrial translocation and ubiquitinates mitofusin. Proc Natl Acad Sci U S A. 2010;107:5018-5023.
280. Gegg ME, Cooper JM, Chau KY, Rojo M, Schapira AH, Taanman JW. Mitofusin 1 and mitofusin 2 are ubiquitinated in a PINK1/parkin-dependent manner upon induction of mitophagy. Hum Mol Genet. 2010;19:4861-4870.
281. Tanaka A, Cleland MM, Xu S, Narendra DP, Suen DF, Karbowski M, et al. Proteasome and p97 mediate mitophagy and degradation of mitofusins induced by Parkin. J Cell Biol. 2010;191:1367-1380.
282. Okatsu K, Koyano F, Kimura M, Kosako H, Saeki Y, Tanaka K, et al. Phosphorylated ubiquitin chain is the genuine Parkin receptor. J Cell Biol. 2015;209:111-128.
283. Caulfield TR, Fiesel FC, Moussaud-Lamodiere EL, Dourado DF, Flores SC, Springer W. Phosphorylation by PINK1 releases the UBL domain and initializes the conformational opening of the E3 ubiquitin ligase Parkin. PLoS computational biology. 2014;10:e1003935.
284. Kazlauskaite A, Martinez-Torres RJ, Wilkie S, Kumar A, Peltier J, Gonzalez A, et al. Binding to serine 65-phosphorylated ubiquitin primes Parkin for optimal PINK1-dependent phosphorylation and activation. EMBO Rep. 2015.
285. Ordureau A, Heo JM, Duda DM, Paulo JA, Olszewski JL, Yanishevski D, et al. Defining roles of PARKIN and ubiquitin phosphorylation by PINK1 in mitochondrial quality control using a ubiquitin replacement strategy. Proc Natl Acad Sci U S A. 2015;112:6637-6642.
286. Sauve V, Lilov A, Seirafi M, Vranas M, Rasool S, Kozlov G, et al. A Ubl/ubiquitin switch in the activation of Parkin. EMBO J. 2015;34:2492-2505.

287. Kumar A, Aguirre JD, Condos TE, Martinez-Torres RJ, Chaugule VK, Toth R, et al. Disruption of the autoinhibited state primes the E3 ligase parkin for activation and catalysis. EMBO J. 2015;34:2506-2521.
288. Durcan TM, Kontogiannea M, Bedard N, Wing SS, Fon EA. Ataxin-3 deubiquitination is coupled to Parkin ubiquitination via E2 ubiquitin-conjugating enzyme. J Biol Chem. 2012;287:531-541.
289. Pao KC, Stanley M, Han C, Lai YC, Murphy P, Balk K, et al. Probes of ubiquitin E3 ligases enable systematic dissection of parkin activation. Nat Chem Biol. 2016;12:324-331.
290. Wallace DC. A mitochondrial paradigm of metabolic and degenerative diseases, aging, and cancer: a dawn for evolutionary medicine. Annu Rev Genet. 2005;39:359-407.
291. Seibler P, Graziotto J, Jeong H, Simunovic F, Klein C, Krainc D. Mitochondrial Parkin recruitment is impaired in neurons derived from mutant PINK1 induced pluripotent stem cells. J Neurosci. 2011;31:5970-5976.
292. Rakovic A, Shurkewitsch K, Seibler P, Grunewald A, Zanon A, Hagenah J, et al. Phosphatase and tensin homolog (PTEN)-induced putative kinase 1 (PINK1)-dependent ubiquitination of endogenous Parkin attenuates mitophagy: study in human primary fibroblasts and induced pluripotent stem cell-derived neurons. J Biol Chem. 2013;288:2223-2237.
293. Van Laar VS, Arnold B, Cassady SJ, Chu CT, Burton EA, Berman SB. Bioenergetics of neurons inhibit the translocation response of Parkin following rapid mitochondrial depolarization. Hum Mol Genet. 2011;20:927-940.
294. Cai Q, Zakaria HM, Simone A, Sheng ZH. Spatial parkin translocation and degradation of damaged mitochondria via mitophagy in live cortical neurons. Curr Biol. 2012;22:545-552.
295. Ashrafi G, Schwarz TL. PINK1- and PARK2-mediated local mitophagy in distal neuronal axons. Autophagy. 2015;11:187-189.
296. Gad H, Ringstad N, Low P, Kjaerulff O, Gustafsson J, Wenk M, et al. Fission and uncoating of synaptic clathrin-coated vesicles are perturbed by disruption of interactions with the SH3 domain of endophilin. Neuron. 2000;27:301-312.
297. Andersson F, Low P, Brodin L. Selective perturbation of the BAR domain of endophilin impairs synaptic vesicle endocytosis. Synapse. 2010;64:556-560.
298. Sundborger A, Soderblom C, Vorontsova O, Evergren E, Hinshaw JE, Shupliakov O. An endophilin-dynamin complex promotes budding of clathrin-coated vesicles during synaptic vesicle recycling. J Cell Sci. 2011;124:133-143.
299. Boucrot E, Ferreira AP, Almeida-Souza L, Debard S, Vallis Y, Howard G, et al. Endophilin marks and controls a clathrin-independent endocytic pathway. Nature. 2015;517:460-465.
300. Soukup SF, Verstreken P. EndoA/Endophilin-A creates docking stations for autophagic proteins at synapses. Autophagy. 2017;13:971-972.
301. Cao M, Wu Y, Ashrafi G, McCartney AJ, Wheeler H, Bushong EA, et al. Parkinson Sac Domain Mutation in Synaptojanin 1 Impairs Clathrin Uncoating at Synapses and Triggers Dystrophic Changes in Dopaminergic Axons. Neuron. 2017;93:882-896 e885.
302. Westphal CH, Chandra SS. Monomeric synucleins generate membrane curvature. J Biol Chem. 2013;288:1829-1840.
303. Duda DM, Olszewski JL, Schuermann JP, Kurinov I, Miller DJ, Nourse A, et al. Structure of HHARI, a RING-IBR-RING Ubiquitin Ligase: Autoinhibition of an Ariadne-Family E3 and Insights into Ligation Mechanism. Structure. 2013;21:1030-1041.

304. Stieglitz B, Rana RR, Koliopoulos MG, Morris-Davies AC, Schaeffer V, Christodoulou E, et al. Structural basis for ligase-specific conjugation of linear ubiquitin chains by HOIP. Nature. 2013;503:422-426.
305. Madegowda RH, Kishore A, Anand A. Mutational screening of the parkin gene among South Indians with early onset Parkinson's disease. J Neurol Neurosurg Psychiatry. 2005;76:1588-1590.
306. Iguchi M, Kujuro Y, Okatsu K, Koyano F, Kosako H, Kimura M, et al. Parkin-catalyzed Ubiquitin-Ester Transfer Is Triggered by PINK1-dependent Phosphorylation. J Biol Chem. 2013;288:22019-22032.
307. Shiba-Fukushima K, Arano T, Matsumoto G, Inoshita T, Yoshida S, Ishihama Y, et al. Phosphorylation of Mitochondrial Polyubiquitin by PINK1 Promotes Parkin Mitochondrial Tethering. PLoS Genet. 2014;10:e1004861.
308. Wauer T, Swatek KN, Wagstaff JL, Gladkova C, Pruneda JN, Michel MA, et al. Ubiquitin Ser65 phosphorylation affects ubiquitin structure, chain assembly and hydrolysis. EMBO J. 2014:pii: e201489847.
309. Zheng XD, Hunter T. Parkin mitochondrial translocation is achieved through a novel catalytic activity coupled mechanism. Cell Res. 2013;23:886-897.
310. Grenier K, McLelland GL, Fon EA. Parkin- and PINK1-Dependent Mitophagy in Neurons: Will the Real Pathway Please Stand Up? Front Neurol. 2013;4:100.
311. Grenier K, Kontogiannea M, Fon EA. Short Mitochondrial ARF Triggers Parkin/PINK1-Dependent Mitophagy. J Biol Chem. 2014;289:29519-29530.
312. Bingol B, Tea JS, Phu L, Reichelt M, Bakalarski CE, Song Q, et al. The mitochondrial deubiquitinase USP30 opposes parkin-mediated mitophagy. Nature. 2014;510:370-375.
313. Cornelissen T, Haddad D, Wauters F, Van Humbeeck C, Mandemakers W, Koentjoro B, et al. The deubiquitinase USP15 antagonizes Parkin-mediated mitochondrial ubiquitination and mitophagy. Hum Mol Genet. 2014;23:5227-5242.